UNIVERSITY OF CALIFORNIA,
IRVINE

Structural, Biochemical, and Biological Studies on Bacterial Nitric Oxide Synthase

DISSERTATION

submitted in partial satisfaction of the requirements
for the degree of

DOCTOR OF PHILOSOPHY

in Biological Sciences

by

Jeffrey K. Holden

Thesis Committee:
Professor Thomas L. Poulos, Chair
Professor Celia W. Goulding
Assistant Professor Jennifer A. Prescher

2015

DEDICATION

To

my wife and family

for their unconditional support

Failure is only the opportunity to begin again, this time more intelligently
- Henry Ford (1863 – 1947)

TABLE OF CONTENTS

LIST OF FIGURES

LIST OF TABLES

ACKNOWLEDGMENTS

I would like express my sincere gratitude to my supervisor, Professor Thomas L. Poulos, whose expertise, optimism, and patience provided the linchpin necessary to the success of my graduate career. Consistently, he encouraged me to pursue my own ideas and hypotheses. I was granted the opportunity to both fail and succeed and as a result I am a much better scientist. This work is also indebted to the many thought provoking conversations and scientific training provided by Dr. Huiying Li.

To my collaborators at Northwestern University, under the direction of Professor Richard Silverman, thank you for providing the chemical tools necessary to evaluate nitric oxide synthase inhibition. Their efforts made significant differences in advancing the field of bacterial nitric oxide synthase. This list of researchers includes Dr. Soosung Kang, Dr. Qing Jing, Dr. Maris Cinelli, and Dr. He Huang.

To my collaborators at University of California San Diego, Dr. Frederico Beasley and Professor Victor Nizet, thank you for excellent manuscript edits and highly significant contributions towards the microbiology studies required to further exploit the bacterial nitric oxide synthase as a viable drug target.

I am also indebted to the microbiology expertise of Dr. Manualla Rafatellu at University of California Irvine. Her suggestions for experimental design advanced my projects significantly. In addition, I am also very grateful for the shared resources between the Tenner, Tsai, and Goulding Labs at UC Irvine.

Last but not least thank you to my team of undergrads over the last several years. Your success has been my success and I am eternally grateful for all of your hard work, friendship, and personal growth as a mentor.

Curriculum Vitae

Jeffrey K. Holden

EDUCATION

University of California, Irvine, CA — September 2010 – April 2015
Ph.D. Student in Molecular Biology and Biochemistry
Dissertation Project 1: Evaluation and development of bacterial nitric oxide synthase inhibitors using biochemical assays, x-ray crystallography, and microbial studies
Dissertation Project 2: Engineering protein-protein interactions through covalent cross-links to isolate distinct conformations of multi-domained proteins
Advisor: Thomas L. Poulos, Ph.D.

Gonzaga University, Spokane, WA — August 2005 – May 2009
Bachelor of Science in Chemistry
Thesis: Biochemical and structural characterization of an allosteric binding site in the protein β-carbonic anhydrase

PUBLICATIONS

- **Holden, J.K.**, Li, H., Jing, Q., Kang, S., Richo, J.*****, Silverman, R. B., and Poulos, T.L. (2013) Structural and Biological Studies on Bacterial Nitric Oxide Synthase Inhibitors, *Proc. Natl. Acad. Sci. U.S.A.* 110, 18127-31
- **Holden, J.K.**, Lim, N.*****, and Poulos, T.L. (2014) Identification of Redox Partners and Development of a Novel Chimeric Bacterial Nitric Oxide Synthase for Structure Activity Analyses, *J. Biol. Chem.* 289, 29437-45
- **Holden, J.K.**, Kang, S., Hollingsworth, S.A., Li, H., Lim, N.*****, Chen, S.*****, Huang, H., Xue, F., Tang, W., Silverman, R.B., and Poulos, T.L. (2014) Structure-Based Design of Bacterial Nitric Oxide Synthase Inhibitors, *J. Med. Chem.* 58, 994-1004
- **Holden, J.K.**, Kang, S., Beasley, F.C., Cinelli, M.A., Li, H., Dejam, D.*****, Nizet, V., Silverman, R.B., Poulos, T.L. (2015) Nitric Oxide Synthase as a target for Methicillin Resistant Staphylococcus aureus, *in review at Cell Chemistry and Biology*.
- Hollingsworth, S.A[†], **Holden, J.K.**[†], Li, H., Poulos, T.L. (2015) Domain Interactions of Nitric Oxide Synthase Elucidated using Molecular Dynamics and Biochemical Assays, *in prep*. [†]Authors contributed equally
- **Holden, J.K**, Dejam, D.*, Kang, S., Silverman, R.B., Poulos, T.L. (2015) Inhibitor Bound Crystal Structures of Bacterial Nitric Oxide Synthase, *in prep*.

***** Mentored student

GRANTS AND AWARDS

University of California, Irvine, CA

- UC Irvine Associated Graduate Student Travel Award — Mar. 2015
- Extreme Science and Engin. Discovery Environ. — Jan. 2014 – Dec. 2015
  TG-MCB130001, Co-Investigator
- William Holcomb Scholarship — Jun. 2014

UC Irvine Graduate Honors Convocation

- American Society for Biochem. and Mol. Biology Travel Award — Apr. 2014

Gonzaga University, Spokane, WA

- American Institute of Chemists Outstanding Chemistry Senior Award — Apr. 2009
- Comprehensive Leadership Program — Apr. 2009
- Recognition for Leadership and Service by CA State Senator G. Romero — Mar. 2007

RESEARCH EXPERIENCE

PhD Student Jun. 2010 – Jun. 2015

School of Biosciences, University of California, Irvine

- Engineered and crystallized proteins to elucidate structural underpinnings that govern ligand binding
- Adapted and innovated biochemical assays for functional screening that are patent pending
- Identified and characterized drug targets while also collaborating in the design and synthesis of novel therapeutics
- Managed and directed collaborative research projects that resulted in multiple first author publications
- Promoted interdisciplinary approaches towards solving complex problems
- Stimulated undergraduate critical thinking and research as a mentor and teaching assistant

Research Assistant Aug. 2009 – May 2010

Department of Chemistry and Biochemistry, University of Colorado Boulder

- Collaborated with graduate students, post-doctoral researchers, and staff scientists as a rotation student
- Contributed towards the development of multiple biochemical, biophysical, and cell-based assays

Research Assistant Jun. 2007 – May 2009

Department of Chemistry, Gonzaga University, Spokane, WA

- Spearheaded undergraduate research in drug discovery and biochemistry
- Advanced protein purification protocols for undergraduate labs

LABORATORY TECHNIQUES

Molecular Biology and Protein Expression/Purification

- *Genetics and Microbiology:* Deletion/insertion of genes within bacteria and generation/maintenance of bacterial libraries
- *Cloning/PCR:* Primer design for site-directed mutagenesis and gene cloning using megawhop, In-Fusion cloning, and traditional cloning methods into bacterial expression vectors

- *Recombinant protein expression:* Optimized heterologous protein expression in *E. coli*
- *Protein purification:* Fab and enzyme purification using nickel affinity chromatography, ion exchange chromatography, hydrophobic exchange chromatography, size exclusion chromatography, and protein A chromatography
- SDS-page gel and western blot analysis of protein

Biophysical Techniques

- *Ligand binding:* analysis using dynamic scanning fluorimetry, difference spectroscopy, fluorescence spectroscopy and isothermal titration calorimetry
- *Kinetics:* steady state, enzyme-inhibition, and enzyme-product detection by HPLC
- Dynamic light scattering
- *Protein Crystallography:* high throughput protein crystal optimization using LabTech Mosquito and Art Robbins Gryphon, synchrotron x-ray diffraction, x-ray data processing and refinement using molecular replacement

Computational Skills

- Data processing on Linux system using CCP4 and Phenix programs
- High throughput *in silico* screening of ligands using GOLD and Autodock Vina
- Proficient in Microsoft Office (Word, Excel, PowerPoint, and Outlook) on Windows and Mac

POSTERS AND INVITED LECTURES

- **Holden, J.K.**, Kang, S., Silverman, R.B., Poulos, T.L. March 2015. Structure based drug design and targeted high-throughput screening to develop novel anti-MRSA drugs [oral presentation]. West Coast Protein Crystallography Workshop, Monterey, CA.
- **Holden, J.K.**, Kang, S., Silverman, R.B., Poulos, T.L. July 2014. Subtle Differences between NOS Active Sites Lends Towards the Development of a Bacterial NOS Specific Inhibitor [poster presentation]. The 28th Annual Symposium of The Protein Society, San Diego, CA.
- **Holden, J.K**, Lim, N., Li, H., Kang, S., Huang, H., Silverman, R.B., Poulos, T.L. June 2014. Exploiting the NOS Pterin Site for Structure Based Drug Design of Bacterial NOS Inhibitors [poster presentation]. Nitric Oxide – Nitrate/Nitrate Conference, Cleveland, OH.
- **Holden, J.K**., Li, H., Lim, N., Richo, J., Kang, S., Jing, Q., Silverman, R.B., Poulos, T.L. April 2014. Structural and Biological Characterization of NOS Inhibitors with Antimicrobial Properties [poster presentation]. American Society for Biochemistry and Molecular Biology Annual Meeting, San Diego, CA.
- **Holden, J.K.** April 2014. Characterization of a Novel Therapeutic Target for Combating MRSA and Anthrax [oral presentation]. Gonzaga University Biology Department, Spokane, WA.
- **Holden, J.K.** Li, H., Lim, N., Silverman, R.B., Meyskens, F.L., Poulos, T.L. November 2013. Targeting Nitric Oxide Synthase: Implications for Treating a Variety of Disease States [poster presentation]. Chao Family Comprehensive Cancer Annual Scientific Conference, Palm Springs, CA.

- **Holden, J.K.**, Li, H., Qing, J. Silverman, R.B., Poulos, T.L. March 2013. Bacterial NOS Inhibition: A Drug Discovery Approach for Development of a Novel Antibacterial [oral presentation]. West Coast Protein Crystallography Workshop, Monterey, CA.
- **Holden, J.K.** April 2009. Evaluation of the noncatalytic bicarbonate binding site in eubacterial carbonic anhydrase as a target for new drugs [oral presentation]. Gonzaga University Chemistry Department Thesis Seminar, Spokane, WA.
- **Holden, J.K.**, Cronk, J.D. April, 2008. Combating tuberculosis: Evaluation of the noncatalytic bicarbonate binding site in eubacterial carbonic anhydrase as a target for new therapeutic drugs [oral presentation]. Spokane Intercollegiate Research Conference, Spokane, WA.
- Fabrizzio, T., **Holden, J.K.**, Cronk, J.D. November 2007. Identification of a noncanonical binding site in β-carbonic anhydrase [poster presentation]. M.J. Murdock Undergraduate Research Conference, Salem, OR.

MENTORING EXPERIENCE

• Ziad Abdullatif	Undergraduate Student	Aug. 2014 – Jun. 2015
• Matthew Lewis	CMB Rotation Student	Aug. 2014 – Dec. 2014
• Dillon Dejam**	Undergraduate Student	Apr. 2014 – Jun. 2015
• Dail Chapman	CMB Rotation Student	Mar 2014 – Jun. 2014
• Nathan Lim	Undergraduate Student	Jan. 2012 – Jun. 2013
• Helen Pham	Undergraduate Student	Aug. 2012 – Mar. 2013
• Jerry Richo**	Undergraduate Student	Jan. 2012 – Jun. 2013
• Sarah Hightower	Bridges to Baccalaureate	May 2012 – Aug. 2012
• Steven Chen	Chao Cancer Center Student	May 2011 – Jun. 2012

** Received Undergraduate Research Award, $500

TEACHING EXPERIENCE

University of California, Irvine, CA

- Teaching Assistant, Molecular Biology Lecture and Lab Apr. 2014 – Jun. 2014
- Teaching Assistant, Biochemistry Lab Apr. 2014 – Jun. 2014
- Teaching Assistant, Biochemistry Lab Sep. 2013 – Dec. 2013
- Teaching Assistant, Intro. to Computational Biology Sep. 2013 – Dec. 2013
- Teaching Assistant, Advanced Biochemistry Lecture Jan. 2012 – Mar. 2012
- Teaching Assistant, Advanced Biochemistry Lab Jan. 2012 – Mar. 2012

University of Colorado, Boulder, CO

- Teaching Assistant, General Chemistry Lecture Aug. 2009 – May 2010
- Teaching Assistant, General Chemistry Lab Aug. 2009 – May 2010

Gonzaga University, Spokane, WA

- Teaching Assistant, Bio-analytical Chemistry Lab Jan. 2009 – May 2009
- Teaching Assistant, Biochemistry Lab Jan. 2008 – May 2008

ABSTRACT OF THE DISSERTATION

Structural, Biochemical, and Biological Studies on Bacterial Nitric Oxide Synthase

By

Jeffrey K. Holden

Doctor of Philosophy in Biological Sciences

University of California, Irvine, 2015

Professor Thomas L. Poulos, Chair

Nitric oxide synthase (NOS) is a heme-containing enzyme found in both mammals and select prokaryotes. Current evidence indicates NOS is only responsible for the generation of NO through the oxidation of L-Arg. Due to the critical signaling function of NO, NOS has emerged as an important therapeutic target as the over- or under-production of NO in mammals can lead to a variety of disease states. In sharp contrast, genetic and biochemical studies have demonstrated bacterial NO to protect gram-positive pathogens like *Staphyloccocus aureus* and *Bacillis anthracis* against oxidative and antibiotic stress. In order to first evaluate the protective functions afforded by bacterial NOS (bNOS), we identified several inhibitors that bind tightly to bNOS and demonstrated antimicrobial properties. These initial studies allowed for extensive crystallographic analyses in order to characterize inhibitor “hot-spots” and pharmacophores with improved bNOS inhibitor selectivity. Validation and characterization of these inhibitors also required development of new tools to assess bNOS inhibition. These tools include the utilization of bacterial redox partners we identified that support bNOS activity. More importantly, these tools allowed for the

development of new assays to rapidly identify potent NOS inhibitors. Together, these studies represent the first exploitation of bNOS as a therapeutic target and make significant contributions towards the continued development and characterization of bNOS inhibitors.

INTRODUCTION

Nitric oxide (NO) is a highly reactive, diatomic, free radical gas that is produced in plants, bacteria, and animals. Initially detected within biological systems as a product of bacterial denitrification[(1)], NO has also been classified as a critical signaling molecule in eukaryotes[(2)]. In fact, recognition of NO's important role within mammalian cells led to the 1998 Nobel Prize and resulted in a paradigm shift of how we understand cellular signaling. NO is a unique signaling molecule because it is charge neutral and toxic at high concentrations. Moreover, NO is unique because it functions within an organism by nitrosylating macromolecules, reacting with other free radicals, and coordinating to metal ions. Despite the ubiquitous presence of NO within the natural world only mammals and a select few bacteria produce NO enzymatically. The enzyme required for NO biosynthesis is known as nitric oxide synthase (NOS). For catalysis NOS requires the substrate L-Arg, a reduced pterin co-substrate and NADPH derived electrons. Oxidation of L-Arg to L-citrulline and NO occurs via intermediate N^{ω}-hydroxy-L-Arg, as shown in Figure 1.1.

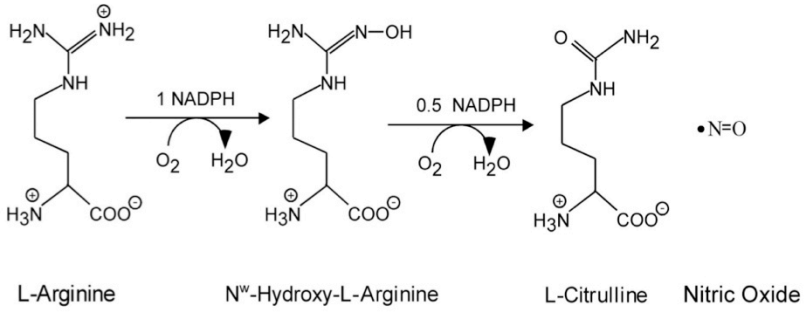

Figure I.1 NOS catalyzed oxidation of L-Arg to L-citrulline and NO via intermediate N^{ω}-hydroxy-L-Arg.

Biological Function of NOS

In mammals, NOS is found as one of three isoforms (inducible NOS = iNOS, endothelial NOS = eNOS, neuronal NOS = nNOS). Both eNOS and nNOS are commonly referred to as constitutive NOS because they are constitutively expressed in a given cell type. Activity of both constitutive NOS's is regulated by cellular calcium concentrations and binding of calmodulin. In sharp contrast, iNOS expression is transcriptionally controlled and it's activity is not regulated by cellular calcium levels[(3)]. Despite transcriptional and mechanistic controls to regulate the production of NO, an over or under-active NOS can lead to a wide variety of pathological conditions. Some of these pathological conditions include neurodegenerative diseases[(4)], septic shock[(5)] and tumor development[(6)]. Not surprisingly, there has been a longstanding interest in the development of therapeutics that regulate NOS activity[(7)]. For the Poulos and Silverman labs these efforts have led to the development of several nNOS inhibitors that have demonstrated to be very effective potential drugs for melanoma [(8)] and cerebral palsy[(9)].

With the advent of genomic sequencing, NOS genes have also been identified in some bacteria and archea species[(10)]. Current evidence indicates the function of bacterial NOS (bNOS) generated NO to vary amongst bacterial species. For example, *Deinococcus radiodurans* NOS is responsible for nitrosylating an atypical tRNA[(11)]. *D. radiodurans* NOS also binds a tryptophanyl tRNA synthetase and is activated upon binding to a tRNA synthetase[(12)]. Interestingly, this specific tryptophanyl tRNA synthetase is up-regulated following radiation damage[(13)] suggesting that *D. radiodurans* NOS may also play an important role in *D. radiodurans* stress response[(12)]. In the case of *Streptomyces turgidiscabies*, a plant pathogen notorious for being the causal agent of

potato scab disease, bNOS-generated NO is involved in production of the plant toxin thaxtomin[14]. Thaxtomin is a dipeptide produced by a nonribosomal peptide synthase required for pathogenicity[15]. Genetic studies have demonstrated the *S. turgidiscabies* NOS to be necessary for nitration of thaxtomin[16]. In the case of *Bacillus subtilis,* bNOS-NO has also been identified to function as a commensal molecule for *Caenorhabditis elegans*[17]. *C. elegans* utilizes *B. subtilis* as a food source and in turn acquires bacterial NO. Remarkably, the bacterial NO is evidenced to activate expression of several genes that work to extend the lifespan of *C. elegans*[17].

Recent microbial phenotypic studies in pathogens *Bacillus anthracis* and *St aureus* also indicate bacterial NO to function as a cytoprotective agent[18, 19]. These studies have clearly shown *Δno*s strains to be more susceptible to oxidative and antibiotics stress. Specifically, a *Δno*s strain of the highly drug resistant form of *S. aureus*, MRSA, was found to be less virulent and more prone to antibiotic clearance[20]. Between a series of gene deletion experiments and biochemical assays NO is currently hypothesized to act as effector molecule in *B. anthracis* and *S. aureus* via several mechanisms, as detailed in Figure 1.2. These mechanisms include nitrosylating catalase, nitrosylating the thioredoxins involved in Fenton chemistry, and nitrosylating antibacterials[10, 21]. Together, the protective mechanisms afforded by bacterial NO in pathogens *B. anthracis* and *S. aureus* implicate bNOS as an excellent antibacterial target. Not surprisingly co-treatment of NOS containing bacteria with NOS inhibitors was recently found to improve the efficacy of current antimicrobials[22, 23].

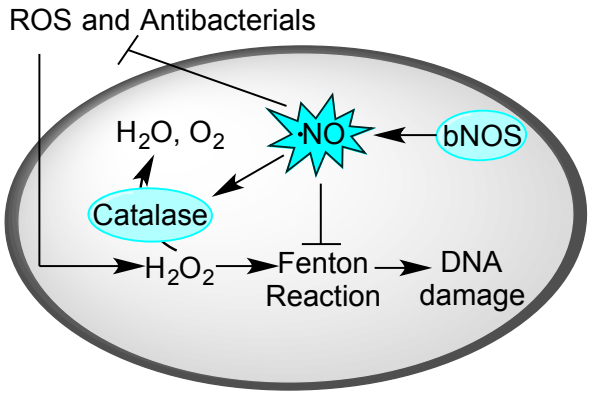

Figure I.2 A Cartoon image of a gram-positive bacterial cell and the protective mechanisms afforded by bNOS generated NO.

Structure of NOS

As a monoxygenase both the bacterial and mammalian NOS (mNOS) are active as dimers. Despite the structural homology between NOS oxygenase domains, bNOS and mNOS are quite different. Figure 1.3 shows the relationship between individual NOS monomers. The mNOS isoforms are multidomained enzymes. Each mNOS is composed of an oxygenase and reductase domain within a single polypeptide chain. At the dimer interface of mNOS is an N-terminal Zn^{2+} binding motif. The Zn^{2+} binding motif functions to facilitate dimerization and bind a Zn^{2+} ion. Moreover, the Zn^{2+} binding motif contributes several protein derived H-bonds to facilitate binding of the NOS co-substrate H_4B.

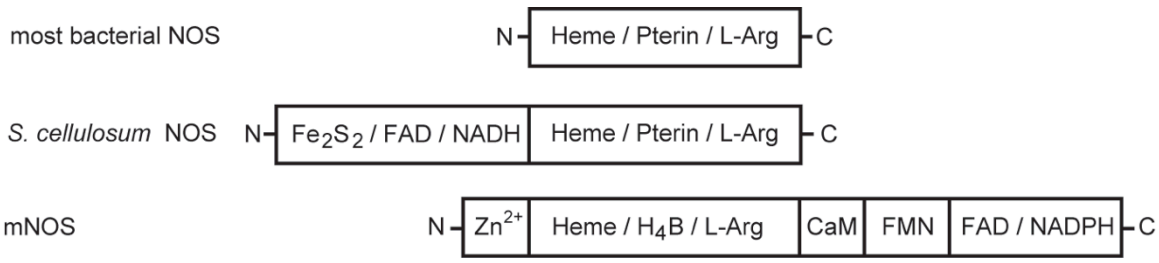

Figure 1.3 Domain organization of several representative NOS. Calmodulin binding sequence on mNOS is indicated as CaM.

The domain organization of mNOS also allows for the transfer of NADPH derived electrons from the flavin containing reductase domain to the oxygenase domain. Recent electron microscopy studies indicate mNOS to be highly dynamic in solution and the conformational equilibrium of NOS to be dependent on the binding of calmodulin[24]. Consequently, the exact pathway of electron transfer remains inconclusive, despite strong evidence that the reductase domain of one monomer is poised to transfer electrons to the oxygenase domain of the other monomer via a conserved tryptophan[25].

Since bNOS does not contain a reductase domain, bNOS must rely on external redox partners for electron transfer. This is similar to many bacterial P450s for which the physiological electron donors remain unknown. In the case of *B. subtilis* NOS considerable progress has been made toward the identification of bNOS redox partners. Between a series of bioinformatics and biochemical studies two flavodoxins and one ferredoxin reductase have been identified[26, 27]. Using a three-component reaction composed of ferredoxin reductase YumC and flavodoxin YkuN, *B. subtilis* NOS activity was detected in the presence of substrate and NADPH[27]. These observations led to the development of a chimera composed of *B. subtilis* NOS and redox partner YkuN. The bNOS chimera referred to as bBiDomain has proven a valuable tool for evaluating bNOS activity and inhibition[23, 27].

While current evidence suggests NOS activity requires the transfer of electrons from NADPH to the NOS oxygenase domain *via* FMN and FAD binding proteins/domains there is one atypical bNOS from *Sorangium cellulosum* that utilizes a covalently attached Fe_2S_2 cluster as a redox partner. Moreover, unlike mNOS, the *S.*

cellulosum[28] reductase domain is positioned at the N-terminus of the oxygenase domain. As far as we know *S. cellulosum* NOS is the only catalytically self-sufficient bNOS and the only NOS that contains a Fe_2S_2 cluster.

Enzymology of NOS

Conservation of key residues at NOS active sites suggests the mechanism of NOS catalyzed NO production to be conserved. The NOS active site is composed of a b-type heme axially ligated by a cysteine residue. Substrate L-Arg binds directly above the plane of the heme. A network of H-bonds between the guanidinium group of L-Arg and a conserved glutamic acid residue stabilizes binding (Figure 1.4). The binding affinity of L-Arg is also conserved, as all NOS isoforms bind L-Arg within a similar low micromolar range[27, 29].

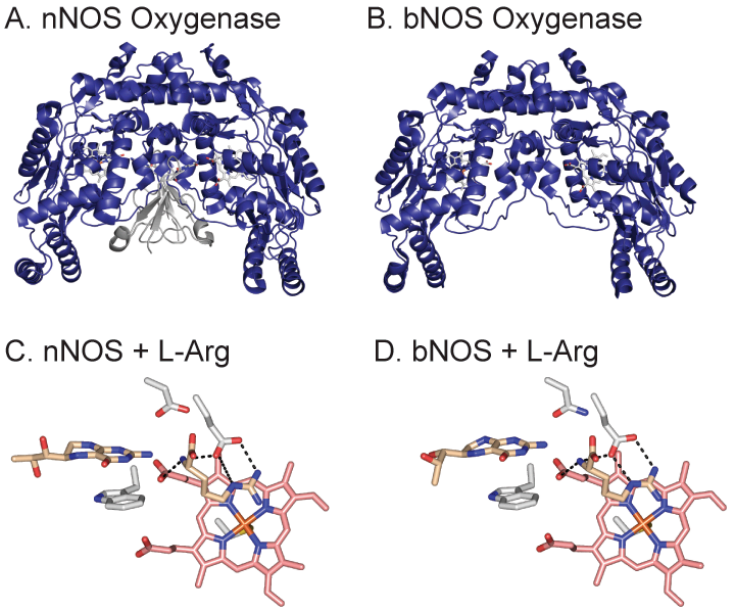

Figure I.4 A) Oxygenase domain of nNOS with Zn^{2+} binding motif colored silver. Oxygenase domain of *B. subtilis* NOS. NOS active sites are conserved in both C) nNOS (PDB 2G6K) and D) bNOS (PDB 2FC1). Both contain a heme coordinated by a protein derived cys residue. Above the plane of the heme is a conserved Glu that H-bonds the substrate L-Arg. H-bonds are shown as dashed black lines.

NO production is a two-step process at the NOS active site. In the first step, one atom of O_2 is added to the guanidinium group of L-Arg. This first step requires the transfer of two electrons to the heme in order to bind and activate O_2. Activation of O_2 is currently believed to result in formation of an oxy-ferryl species, also known as compound 1[(30)]. Formation of compound 1 is currently hypothesized to be mechanistically identical to P450's, another type of monooxygenase. Unlike most P450's, NOS undergoes a second round of oxygenation that requires an electron from a nearby pterin cofactor[(31, 32)]. In mammalian NOS, the pterin cofactor is 5,6,7,8-tetrahydrobiopterin (H_4B). Kinetic studies clearly demonstrate the reduced form of H_4B to be required for NOS activity[(33)]. Despite the strict requirement for a reduced pterin group, many NOS containing bacteria do not contain the biosynthetic machinery required to support H_4B biosynthesis. For this reason the physiologically relevant pterin cofactor of bNOS remains controversial. Current evidence suggests the ubiquitous pterin tetrahydrofolic acid to be a suitable co-substrate for bacterial NOS activity[(34)].

NOS Inhibitors

Unfortunately, the design and development of an isoform selective NOS inhibitor is not a trivial task. NOS inhibitor design is complicated by the high active site homology shared between NOS isoforms. Over the past decade a strong effort has been made to develop isoform selective NOS inhibitors[(35, 36)] with the earliest inhibitors designed to mimic L-Arg binding. These initial studies included L-Arg analogs, thioureus and amidines[(32)]. Subsequent generations of NOS inhibitors required the exploitation of amino acid differences near the active site. This approach has proven to provide the

linchpin necessary to facilitate the design of inhibitor selectivity. For example, the first selective nNOS inhibitors identified exploited electrostatic differences amongst mNOS isoforms at the carboxylate-binding site of L-Arg[37]. These electrostatic differences arise from the presence of an Asn residue that is present in iNOS and eNOS but is an Asp residue in nNOS.

In order to design an active site bNOS inhibitor that discriminates against the mNOS isoforms several key differences between the bNOS and mNOS must be considered. Similar to eNOS, bNOS also contains an Asn at the carboxylate-binding site. Unfortunately designing inhibitors that exploit the Asn would be detrimental if they also inhibited eNOS owing to the critical role eNOS plays in maintaining vascular tone and blood pressure[38]. A key difference that is suitable for inhibitor design is at the pterin co-substrate binding site. Since bNOS does not contain an N-terminal Zn^{2+} binding motif the pterin binding site is more solvent exposed. This results in weaker pterin binding affinity to bNOS[39] and a large cavity adjacent to the bNOS active site. Together these observations have led to the identification of several bNOS inhibitors that are able to bind the active site and displace the pterin co-substrate[22]. Further structure-based drug design efforts have also led to the generation of bNOS inhibitors that bind to both the active and pterin site[23].

Another key difference between mNOS and bNOS that has proven useful for the bNOS inhibitor design effort is the presence of an Ile (mammalian equivalent is a Val) adjacent to the O_2 binding site. While initial studies indicated that the Ile residue controls NO release rates[40], recent data also suggests the hydrophobic patch can facilitate inhibitor binding. These studies have not only led to modest improvements in bNOS

inhibitor potency and selectivity they have also provided the first evidence of bNOS inhibitors with anti-MRSA properties.

Moving Forward

Bacterial NO can be produced enzymatically or through denitrification. In several cases, the enzymatic production of NO by bNOS has shown to function as an important metabolite for pathogenicity. To address the role of bacterial NO in *bona fide* human pathogens *B. anthracis* and *B. subtilis* we evaluated the effect of NOS inhibitors on bacterial growth. This required using the model organism *B. subtilis* and generating a *Δnos* strain. Initial structure studies revealed the most potent inhibitors also displace the co-substrate pterin molecule.

To advance our understanding of bacterial NOS inhibition we identified redox partners that could facilitate bNOS activity. From these studies we developed a novel chimera that is catalytically self sufficient in the presence of a ferredoxin reductase and NADPH (Chapter 3). These studies provided the foundation for structure-based drug design of NOS inhibitors (Chapter 4) and a high throughput activity analysis that led to the identification of several lead candidates for bNOS inhibition (Chapter 5). Together these studies on bacterial NOS activity and inhibition provided new functional insights into the important role of NO within bacteria from the genus *Bacillus* and *S. aureus.* Moreover, structure based studies of inhibitor binding to bNOS has allowed us to elucidate important active site differences between NOS isoforms and provide a template for the continued design and development of selective bNOS inhibitors.

Chapter 1

Structural and biological studies on bacterial nitric oxide synthase

Summary

Nitric oxide (NO) produced by bacterial nitric oxide synthase (bNOS) functions as a cytoprotective agent against oxidative stress in *Staphylococcus aureus*, *Bacillus anthracis,* and *Bacillus subtilis*. The screening of several NOS-selective inhibitors has led to the discovery of two inhibitors with potential antimicrobial properties. These two compounds impede the growth of *B. subtilis* under oxidative stress while crystal structures show that each compound exhibits a unique binding mode. Both compounds serve as excellent leads for the future development of antimicrobials against bNOS-containing bacteria.

Introduction

NO is a highly reactive free radical produced by the hemethiolate monooxygenase nitric oxide synthase (NOS, mNOS = mammalian NOS, bNOS = bacterial NOS). NOS generates NO by oxidizing L-Arg and is found in both mammals and some bacteria. While mNOS is a multi-domain protein composed of both oxygenase and reductase domains, bNOS from the genus *Bacillus* and *Staphylococus* contains only an oxygenase domain. X-ray crystal structures determined for both bNOS and mNOS oxygenase domains reveals a near identical tertiary structure and active site

except that bNOS lacks the N-terminal fragment that contains the Zn^{2+} binding motif observed in mNOS[41].

In mammalian systems, NO functions as an essential signaling molecule and is involved in a variety of physiological functions ranging from blood pressure homeostasis to neural cell communication and host defense[42]. There are three mNOS isoforms: endothelial NOS (eNOS), inducible NOS (iNOS) and neuronal NOS (nNOS). Owing to the pathological consequences of the over or under production of NO[7, 43, 44], significant effort has been made toward the development and characterization of isoform selective mNOS inhibitors, which has resulted in the development of many unique inhibitors[35, 36].

In Gram-positive bacteria, bNOS produced NO has been found to modulate macromolecules by nitrosylation[12, 16], to function as a commensal molecule[17], to protect against oxidative stress[21], and to detoxify antimicrobials[19]. While the biological function of NO varies among bacterial organisms, the unique ability of NO to protect the pathogens *Staphyloccocus aureus* and *Bacillus anthracis* against oxidative and antibiotic-induced oxidative stress[19] by activation of catalase and by suppression of damaging Fenton chemistry[18, 21] implicates bNOS as a potential therapeutic target. Moreover, commonly used antibiotics for the treatment of Gram-positive pathogens—like beta-lactams and vancomycin—elicit antibacterial function by generation of reactive oxygen species[45]. Together, these data suggest that inhibition of bNOS will attenuate bacterial survival against antibiotic induced oxidative stress. Owing to the essential role NO plays in mammals, development of a bNOS-specific inhibitor ideally should take advantage of subtle differences between bNOS and mNOS. To do so first requires identification of NOS inhibitors that demonstrate antimicrobial-like properties within a

bacterial system under oxidative stress and characterization of the inhibitor-binding mode for future structure-based inhibitor development. The number of studies on the effects of inhibitors on bNOS has been limited to the finding that nonselective NOS inhibitor N^G-methyl-L-arginine generates greater sensitivity to H_2O_2-induced oxidative stress in *B. anthracis*[18]. Here we present results identifying NOS inhibitors that exhibit a dramatic decrease in bacterial viability in the presence of either an antimicrobial agent or H_2O_2 and present spectral and crystallographic studies on the binding of these inhibitors to *B. subtilis* NOS (bsNOS).

Results and Discussion

Effect of Oxidative Stress and NOS Inhibitor on *B. subtilis*

Bacterial oxidative stress was induced by addition of either H_2O_2 or the antimicrobial agent acriflavine (ACR). Direct comparison of *wt* and *Δnos B. subtilis* treated with ACR (Fig. 1.1) revealed the *Δnos B. subtilis* strain to have a decreased % survival in comparison to the untreated cells, as previously observed[19]. To identify NOS inhibitors that enhance the toxicity of oxidative stress on *wt B. subtilis* we utilized a library of inhibitors that were designed to target nNOS[35, 36]. Initially, we identified inhibitors that bound the bsNOS active site based on an imidazole displacement analysis outlined in Appendix I. From the NOS inhibitors identified to bind bsNOS we then screened 10 NOS inhibitors (data not shown) for the ability to delay *B. subtilis* growth in the presence of oxidative stress. From our initial screen, two NOS inhibitors, compounds **1** and **2 (**Fig. 1.2), were demonstrated to have antimicrobial-like properties with varying potencies. Further analysis revealed **2** significantly lowers the % survival of WT ACR and WT H_2O_2 treated cells (Fig. 1.1) and is more potent then **1**. We also tested

the non-selective NOS inhibitor L-NNA and found bacterial % survival to decrease in the presence of ACR. Interestingly, L-NNA has trivial effects on bacterial survival in the presence of H_2O_2, similar to **1** (Fig. 1.1).

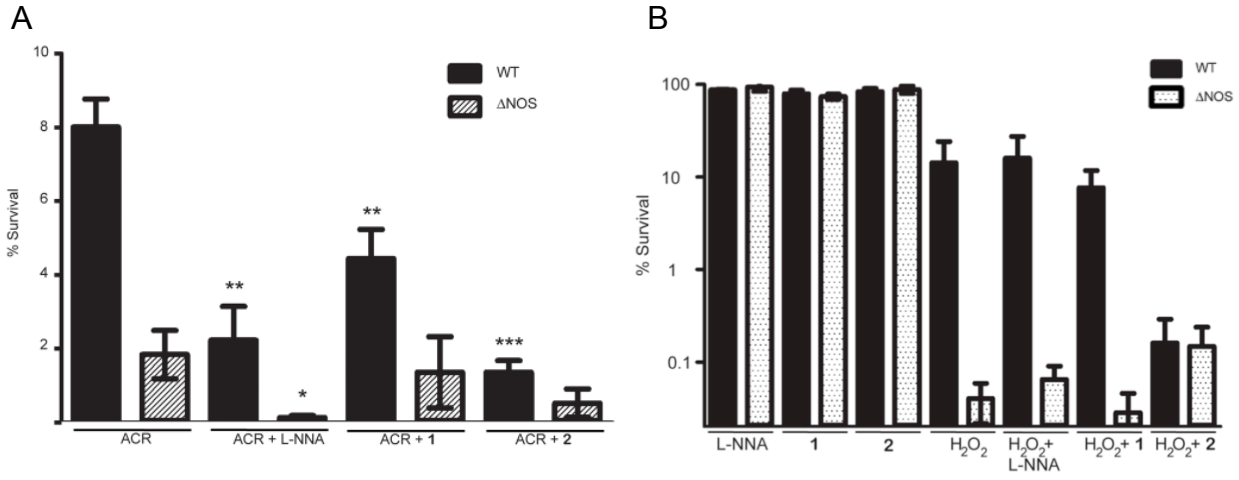

Figure 1.1 NOS inhibitors and their effect on *B. subtilis* survival. A) Bacterial survival of *B. subtilis* WT and *Δnos* strains decreases in the presence of 1.25 mM ACR and NOS inhibitors. The concentrations were 500 mM for L-NNA and **1** and 250 mM for **2** indicating that **2**+ACR is more effective and inhibiting growth at 250 mM inhibitor than L-NNA+ACR at 500 mM inhibitor. B) Bacterial survival of *B. subtilis* WT and *Δnos* strains also decreases in the presence of 2 mM H_2O_2, relative to untreated cells. Co-addition of NOS inhibitors and H_2O_2 results in a dramatic decrease in bacterial survival. Error bars represent the mean ± the SEM of at least three replicates, student's *t* test gives ***P < 0.001, **P < 0.01, *P < 0.05.

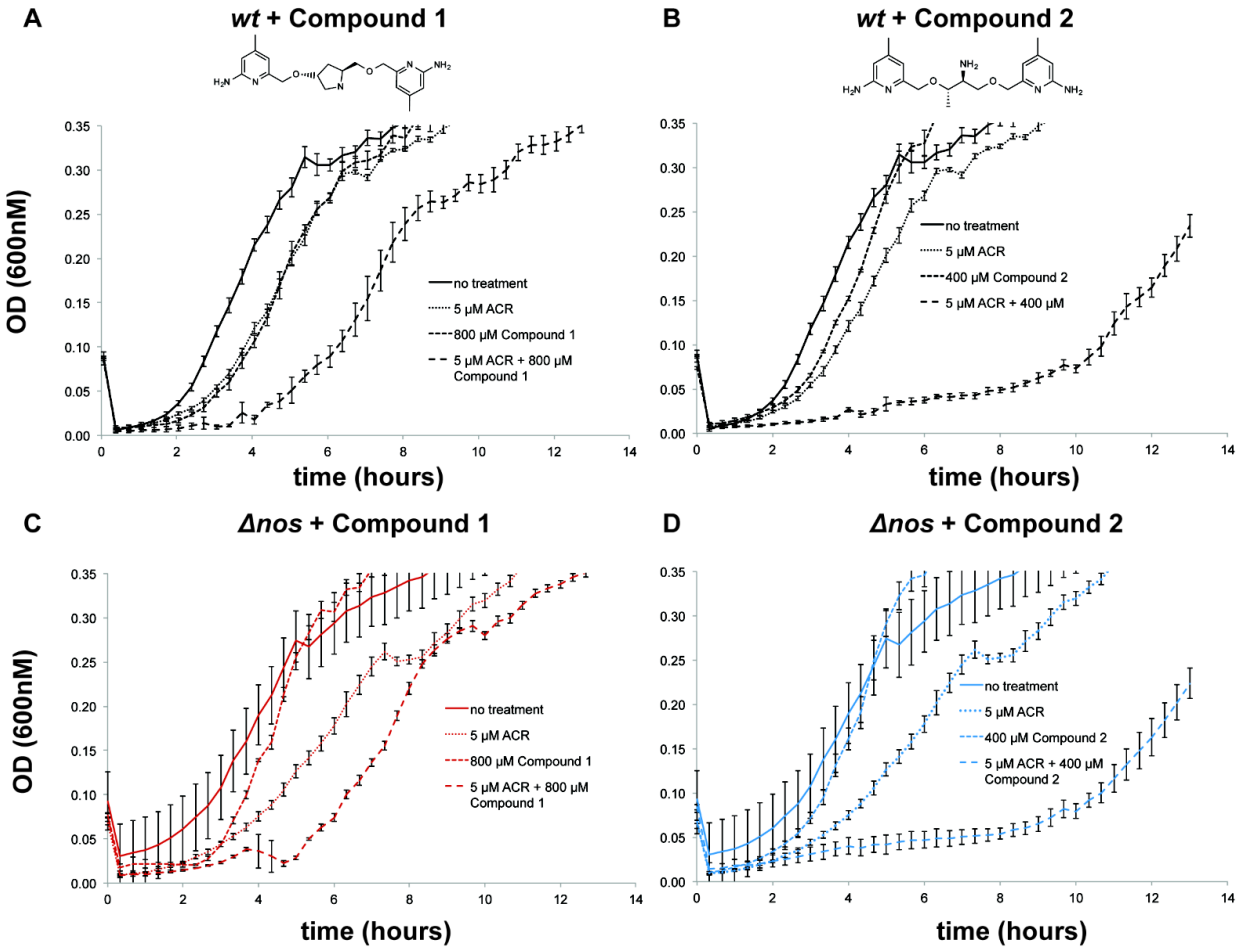

Figure 1.2. The effect of ACR and compounds **1** and **2** on bacterial growth in both *wt* and *Δnos B. subtilis*. Error bars represent the mean ± the SEM of three replicates.

From the above results it is clear that NOS inhibitors decrease the % survival of oxidatively stressed *B. subtilis*. To corroborate the additive effect of oxidative stress with NOS inhibitors on bacterial survival, *B. subtilis* growth was monitored over time in the presence of the antimicrobial agent ACR and/or NOS inhibitor (Fig. 1.2). Both untreated WT and *Δnos B. subtilis* growth curves revealed nearly identical growth rates. *B. subtilis* strains co-cultured with **1** or **2** demonstrated a slightly delayed growth but equal in both *wt* and *Δnos* cells relative to untreated cells. Most importantly, *Δnos* cells treated with ACR result in a dramatic shift in growth relative to WT treated with ACR. Moreover, cells co-treated with ACR and either **1** or **2** showed a severely delayed growth relative to the ACR treated cell. Compound **2** is the more potent inhibitor because it is more effective at 400 μM than **1** is at 800 μM (Fig. 1.2).

The effect of the more potent inhibitor, **2,** on *Δnos* suggests **2** to function promiscuously within *B. subtilis*. Based on the wild type results (Fig. 1.2B), we might have expected *Δnos* to exhibit the same growth pattern in the presence of ACR alone as wild type in the presence of ACR+**2**. This, however, is not the case. ACR does not inhibit *Δnos* growth to the extent one might have expected and the addition of **2**+ACR has a dramatic effect on growth (Fig. 1.2D). This suggests that **2** may be hitting some other non-NOS target or encouraging ACR mediated oxidative stress through a currently unknown mechanism. If the former, this hypothetical non-NOS target cannot be very important in WT *B. subtilis* since **1** and **2** have little effect on % survival (Fig 1.1B) and bacterial growth (Fig. 1.2) in the absence of oxidative stress. Therefore, a significant part of the ability of **1** and **2** to block bacterial growth in WT *B. subtilis* is

consistent with blocking NO production, which increases the susceptibility to antibiotic-induced oxidative stress[19].

Inhibitor Binding

The imidazole displacement shift from low- to high-spin was used to estimate the spectral dissociation constant, K_S [46] for bsNOS, eNOS, and nNOS (Table1.1). Both inhibitors bind to bsNOS with similar affinities to eNOS and nNOS with **2** being an especially good inhibitor. This correlates well with **2** being especially effective at inhibiting bacterial growth.

Table 1.1: Comparison of calculated K_S values at NOS active sites for L-Arg, **1** and **2**.

Ligand	bsNOS	eNOS	nNOS
L-Arg 1 K_S (μM)	0.8	1.0 [47]	0.72 [48]
L-NNA 1 K_S (μM)	1.3	0.1 [49]	0.04 [48]
Compound 1 K_S (μM)	4.4	2.1	0.1
Compound 2 K_S (μM)	1.1	1.7	0.4

Crystal Structures

X-ray data were collected on single crystals soaked in H_4B and NOS inhibitor (crystallographic tables can be found in Appendix II). bsNOS crystals contain one monomer of bsNOS per asymmetric unit, and the functional dimer is generated by the 2-fold crystallographic symmetry axis, as previously observed[50]. The C_α RMSD between the inhibitor bound crystal structures and the search model (PDB 2FBZ) for residues 2-137 and 147-363 are less then 0.36 Å; residues 138-146 were excluded because of sequence differences between our crystal structures and the search model. On the basis of the low RMSD, we were able to conclude surface mutations

E25A/E26A/E316A, predicted to lower surface entropy as outlined within Appendix I (page 99), did not affect the overall structure.

Electron density maps for both **1** and **2** clearly establish that the aminopyridine group is positioned on the distal face of the heme active site to hydrogen bond with the protein-derived Glu243 residue (Fig. 3A and 3B). In the bsNOS-**1** structure the pyrrolidine ring is positioned within 2.7 Å to H-bond to heme-propionate D. While the 2Fo-Fc map contoured at 1.5σ reveals density for the second aminopyridine group, the B-factors for this group are relatively high in comparison to the rest of the molecule, indicating less specific binding of the second aminopyridine group. As modeled, the amine on the second aminopyridine group is positioned within 3.1 Å of Asp220 for a potential H-bond (Fig. 1.3A). The second aminopyridine is also modeled as binding within a van der Waals contact radii of Tyr357. The cofactor H_4B also is present in the bsNOS-**1** crystal structure and is bound at the previously characterized bacterial pterin site[50, 51].

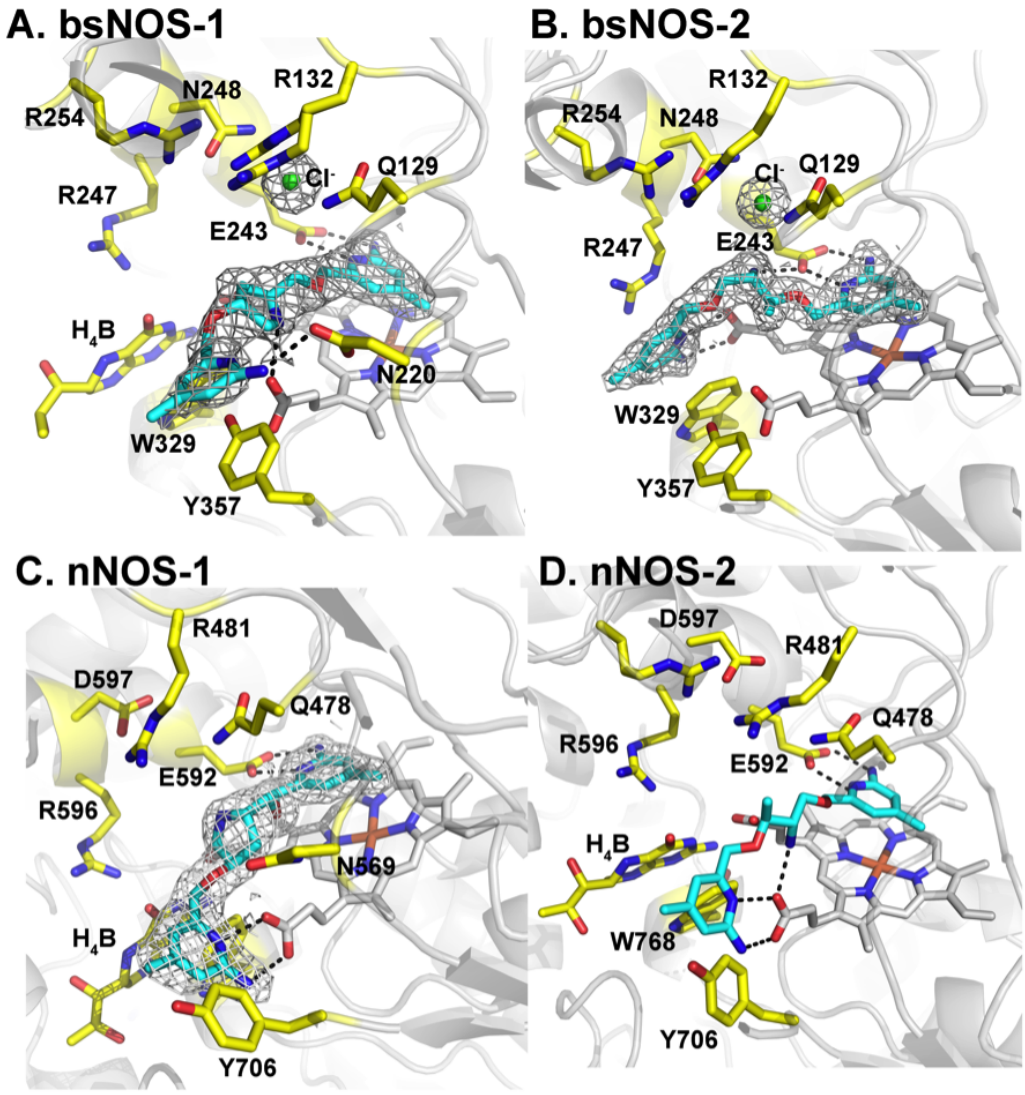

Figure 1.3. Active site structure of A) bsNOS-**1** complex with $2F_0$-F_c electron density map contoured at 1.5σ; B) bsNOS-**2** complex with $2F_0$-F_c electron density contoured at 1.0σ; C) *Rattus norvegicus* nNOS-**1** complex with the 2Fo-Fc electron density map contoured at 1.0s; D) nNOS-**2** complex. Important active site residues and H_4B are colored yellow. The inhibitors are colored cyan, chlorine anions are shown as green spheres, and the heme groups are displayed as white sticks.

Although **2** binds to Glu243 in a near identical orientation and position as **1**, the second aminopyridine group of **2** displaces the H_4B molecule to form two stabilizing H-bonds (2.8 Å and 2.9 Å) with heme propionate A (Fig. 1.3B). Unlike **1**, the electron density for **2** is well defined for the entire inhibitor. The improved electron density

corresponds to a lower K_S for **2**, 1.05 μM, compared to **1**, 4.44 μM. (Fig. 1.3). The binding mode of **2** is further stabilized by the cation-π interaction with the nearby Arg247, a H-bond (2.9 Å) between the primary amine and Glu243, and a H-bond (3.0 Å) between the primary amine and the heme propionate A (Fig. 1.3B).

Comparisons with nNOS and eNOS

A consistent finding in the bsNOS inhibitor crystal structures is the presence of a large solvent molecule located where the carboxyl group of the substrate, L-Arg, would be located. Modeling a Cl^- anion at this position accounts best for the electron density. In the eNOS-**2** structure there is an acetate ion located in approximately the same position. Electrostatic stabilization results from the nearby Arg254 and Arg132, both of which are conserved in eNOS and bsNOS (Fig. 1.3). However, nNOS has no anion at this position (Fig. 1.3D). This is very likely because bsNOS Asn248 (also Asn in eNOS) is replaced with Asp in nNOS. Asn248 is about 3.2 Å from the Cl^- anion, so an Asp at this position would result in weaker electrostatic stabilization of an anion.

The structures of **2** bound to eNOS and nNOS have been determined[(52)] but not to **1**, so we also determined the crystal structure of the nNOS-**1** complex (Fig. 1.3C). There are two major differences. First, the pyrrolidine ring in nNOS points “up” toward Asp597, while in bNOS the pyrrolidine ring points “down” toward heme propionate D. Second, Tyr706 is displaced in nNOS, which allows the second aminopyridine to H-bond with heme propionate D. Normally, this tyrosine H-bonds with heme propionate D, but we have observed in other double headed NOS inhibitors that this tyrosine readily moves to enable inhibitors to H-bond with heme propionate D, which happens more

often in nNOS than eNOS[35]. We also determined the structure of the eNOS-**1** complex (data not shown), and the main difference is that Tyr477 (corresponds to Tyr706 in nNOS) is not displaced. It, therefore, appears that Tyr706 is able to move more freely in nNOS than either eNOS or bsNOS. There are substantial sequence differences between NOS isoforms near Tyr706, but, unfortunately, several residues in this region are not well resolved in nNOS and eNOS electron density maps, so it is difficult to provide a structural basis for the observed enhanced susceptibility of Tyr706 to be displaced in nNOS.

Fig. 1.3D shows the nNOS-**2** complex. Here there is an even more dramatic difference. Relative to bsNOS, the inhibitor flips 180° in nNOS so that the aminopyridine that is situated near the active site Glu in bsNOS H-bonds with heme propionate D in nNOS, which requires movement of Tyr706. This enables the primary amino group in nNOS to H-bond with heme propionate D. We attribute this large difference in binding mode of **2** to the displacement of the H_4B cofactor in bsNOS but not in nNOS. The actual physiological cofactor in bsNOS remains an open question, but the binding of pterins to bsNOS is fairly weak, in the 10-20 μM range[39], compared to mNOS, which is in the nM range[31]. Therefore, H_4B is more easily displaced in bsNOS than in mNOS. As a result, inhibitors targeting the pterin binding pocket might be selective to bNOS over mNOS.

Conclusions

Although a previous study demonstrated a nonselective NOS inhibitor to render *B. anthracis* more susceptible to H_2O_2 induced oxidative stress[18], this is the first study

that illustrates the potential of NOS inhibitors to increase the killing efficacy of an antimicrobial. Of the limited number of NOS inhibitors we initially screened it is interesting that all compounds evaluated bind to bsNOS based on the measured K_s value but only two compounds were found to inhibit bacterial growth. Therefore, there is only a weak correlation between the ability to bind to bsNOS and to enhance the effect of antibiotic induced oxidative stress in blocking bacterial survival. One explanation for this is the better bioavailability of **1** and **2** relative to the other inhibitors we tested, although we cannot eliminate the possibility that these inhibitors affect bacterial growth by some other mechanism than by inhibiting bsNOS. The most important structural finding is that **2** is able to displace the H_4B cofactor in bsNOS but not mNOS. This observation therefore focuses attention towards the pterin site for future structure based inhibitor design targeting bNOS.

Chapter 2

Identification of Redox Partners and Development of a Novel Chimeric Bacterial Nitric Oxide Synthase for Structure Activity Analyses

Summary

Production of nitric oxide (NO) by nitric oxide synthase (NOS) requires electrons to reduce the heme iron for substrate oxidation. Both FAD and FMN flavin groups mediate the transfer of NADPH derived electrons to NOS. Unlike mammalian NOS's that contain both FAD and FMN binding domains within a single polypeptide chain, bacterial NOS is only composed of an oxygenase domain and must rely on separate redox partners for electron transfer and subsequent activity. Here we report on the native redox partners for *Bacillus subtilis* NOS (bsNOS) and a novel chimera that promotes bsNOS activity. By identifying and characterizing native redox partners we were also able to establish a robust enzyme assay for measuring bsNOS activity and inhibition. This assay was used to evaluate a series of established NOS inhibitors. Using the new assay for screening small molecules led to the identification of several potent inhibitors for which bsNOS-inhibitor crystal structures were determined. In addition to characterizing potent bsNOS inhibitors, substrate binding was also analyzed using isothermal titration calorimetry giving the first detailed thermodynamic analysis of substrate binding to NOS.

Introduction

Both mammals and select bacterial species oxidize L-Arg to L-citrulline and NO using nitric oxide synthase (NOS, mammalian NOS = mNOS, bacterial NOS = bNOS) as the enzyme catalyst. NO production by NOS requires electrons to be transferred from NADPH to the heme active site *via* redox partners. Between the three multidomain mNOS isoforms inducible NOS (iNOS), endothelial NOS (eNOS) and neuronal NOS (nNOS) electron transfer relies on calmodulin dependent interdomain protein-protein interactions[(53)] between the heme containing oxygenase domain and the NADPH/FAD/FMN containing reductase domain. In sharp contrast, bNOS from *Staphyloccocus aureus*, *Bacillus anthracis*, and *Bacillus subtilis* are only composed of an oxygenase domain and thus must rely on other redox partners[(54)].

Across species the biological function of NO is quite variable. In mammals, NO function ranges from neural communication to immune function and blood pressure homeostasis[(42)]. Recently, significant efforts have been made towards the development and characterization of isoform specific nNOS inhibitors to modulate the pathological effects of NO over-production by nNOS[(36)]. Much of this work has relied on characterizing the inhibitor structure-activity relationship for structure based drug design[(35)]. In gram-positive organisms NO function is diverse and varied across species[(41)]. Specifically bNOS generated NO renders the highly drug resistant pathogen *S. aureus* less sensitive to antibiotics[(19)]. Previously we identified and structurally characterized several non-specific bNOS inhibitors that improved the efficacy of an antimicrobial[(22)].

Initial kinetic analyses of bNOS relied on the mNOS reductase domain for electron transfer[34] or peroxide dependent oxidation of N-omega-hydroxy-L-arginine (NOHA)[51] in order to circumvent the requirement for native redox partners. In these experiments NO production was either indirectly quantified by the Griess reaction since NO is oxidized to nitrite/nitrate[55] or monitored by stop-flow analysis[34, 40]. Later identification of native flavodoxins that could support bNOS activity led to the development of a three-component reaction composed an *E. coli* derived ferredoxin reductase, *B. subtilis* derived flavodoxin YkuN (or YkuP) and *Bacillus subtilis* NOS (bsNOS)[26]. NO production was also measured using the three-component system by Griess reaction and electron transfer between YkuN and bsNOS was measured using stop-flow spectrophotometry[26]. While bsNOS activity could be measured in a reconstituted system, the relevance of using a heterologous ferredoxin reductase was unknown. More importantly, despite the advances made thus far to characterize NO production by a bNOS, a simple and rigorous assay for purposes of screening inhibitors against a bNOS has yet to be established.

In order to characterize and rapidly evaluate bNOS inhibitors for structure based drug design, it was essential to first develop a robust enzyme assay. To carry this out we first identified flavoproteins from *B. subtilis* that would support bsNOS activity. Since the flavodoxin YkuN was previously established as a redox partner for bsNOS[26], we hypothesized that electron transfer rates to YkuN would be improved using a *B. subtilis* derived reductase. In part because a blast search of the previously utilized *E. coli* ferredoxin/flavodoxin reductase (FLDR), for bsNOS activity, revealed no sequence homology to the *B. subtilis* proteome. This was not surprising because unlike the gram-

positive *B. subtilis* bacterium that have evolved the ability to produce NO, gram-negative *E. coli* does not contain a bNOS and thus has not evolved redox partners to support bNOS activity. Therefore, identification of a native redox system that promotes electron transfer from NAD(P)H to bsNOS would likely improve the flux of electrons to bsNOS for activity measurements.

Fortunately, a ferredoxin reductase from *B. subtilis*, YumC, has been previously identified and characterized[56, 57]. YumC shares high sequence homology to thioredoxin reductase but lacks the di-cysteine motif (CXXC) essential for thioredoxin function[56]. Interestingly, YumC also shares high sequence homology to another *B. subtilis* protein YcgT, a putative ferredoxin reductase, that is induced under nitrosative stress[58-60] and regulated by the ferric uptake regulator[61]. Unlike YumC, characterization of YcgT as a ferredoxin reductase has yet to be reported. Since YumC has previously been characterized as a redox partner to iron-sulfur ferredoxins[62], we elected to evaluate YumC as a potential redox partner to the flavodoxin YkuN.

To evaluate whether YumC and YkuN would support bsNOS activity, we report here several enzyme assays that confirm YumC to function as a native redox partner involved in bsNOS activity. Since substrate hydroxylation by bsNOS requires electron transfer and electron transfer between proteins is a distant dependent event[63], we anticipated that we could further improve bsNOS activity by engineering a bsNOS-YkuN chimera (bBiDomain), using a linker similar in length to mNOS. To this end, we found the chimera bBiDomain to support NO production at conditions in which the three-component reaction produced negligible amounts of NO. We also have used this new

assay to screen a series of potential bNOS inhibitors and have solved the crystal structure of a select few.

Results and Discussion

Cytochrome C Reduction by YkuN

Previous structural and biochemical analyses revealed YumC functions as a FAD-containing reductase[56, 57]. In order to compare the rates of electron transfer from either YumC or FLDR to the flavodoxin YkuN we monitored cyt-c reduction by YkuN since cyt-c is easily reduced by FMN containing flavodoxins[64]. As shown in Fig 2.1A, the rate of cyt-c reduction is dependent on the concentration of either YumC or FLDR with YumC reaching saturation at ≈600 nM while FLDR is unable to saturate YkuN. At saturation levels of YumC (≈600 nM) the rate of cyt-c reduction is ~20 fold faster than FLDR. This suggests that electron flux through YkuN is significantly improved when YumC is used as the reductase as compared to FLDR. The improved rates of electron transfer by YumC over FLDR also suggest that both YumC and YkuN function as native *B. subtilis* redox partners. This is also the first time YumC has been observed to reduce a flavodoxin. Since YumC now is established as a probable redox partner for multiple proteins in *B. subtilis* and is encoded by an essential gene[65], it is likely to play a necessary yet promiscuous role as a ferredoxin/flavodoxin reductase in supporting critical cellular redox processes.

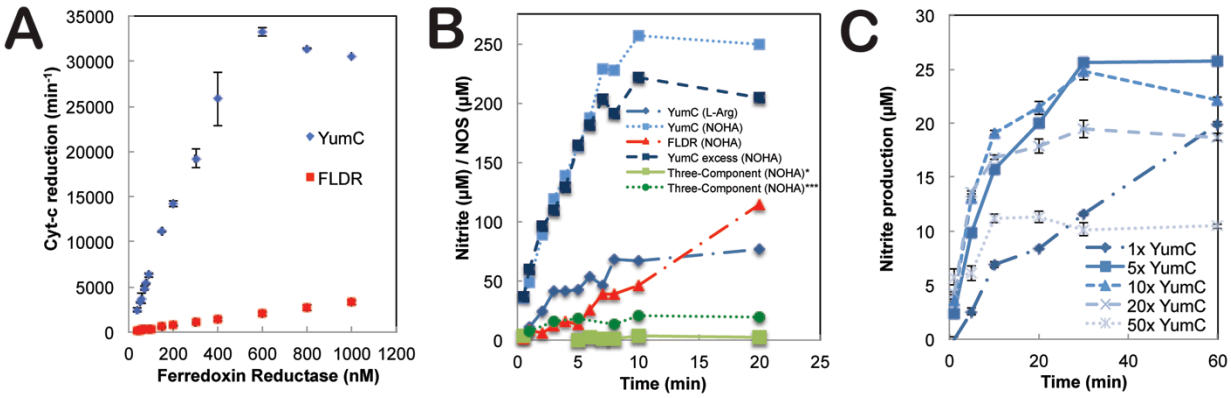

FIGURE 2.1. Catalytic activity of redox partners involved in bsNOS/bBiDomain production of NO. A) YumC more efficiently transfers electrons from NADPH to YkuN then FLDR based on cyt-c reductase activity. B) Time dependent production of NO, as measured by nitrite, is improved using a combination of bBiDomain and YumC. The substrate used, either NOHA or L-Arg is indicated for each trial. Reactions YumC (L-Arg), YumC (NOHA), FLDR (NOHA) were carried out with 0.1 μM bBiDomain and 1 μM YumC or FLDR as indicated. The three component reaction * was composed of 0.1 μM bsNOS, 0.1 μM YkuN and 1 μM YumC. Separately, the three component reaction *** was carried out with 1 μM bsNOS, 5 μM YkuN and 5 μM YumC. C) Stoichiometric ratio of YumC to bBiDomain influences activity over time. Error bars represent the SEM.

bsNOS and bBiDomain Activity

Based on previous experiments bsNOS mediated NO production requires YkuN and a flavodoxin reductase[(26)]. We confirmed that the three-component reaction utilizing YumC produces measurable quantities of NO oxidized nitrite over time (Fig 1B, indicated by ***) in the presence of substrate NOHA. In order to improve the production of bsNOS generated NO we chose to generate a catalytically self-sufficient system by fusing the N-terminal end of YkuN to the C-terminal end of bsNOS. This is similar to P450BM3 where the FMN/FAD reductase is fused to the C-terminal end of the P450[(66)]. The rate of the P450BM3 fatty acid hydroxylation using the individual modules is only 5% that of holo-P450BM3[(67)] thus illustrating that fusion of redox partners could well increase activity. Assuming the site of electron transfer to the NOS oxygenase domain is conserved across species we selected a linker length of 25 amino acids based on a

sequence alignment between mammalian NOS redox partners (Fig 2.2). The linker was composed of a GGGS motif and was chosen to promote flexibility and prevent proteolysis during expression and purification.

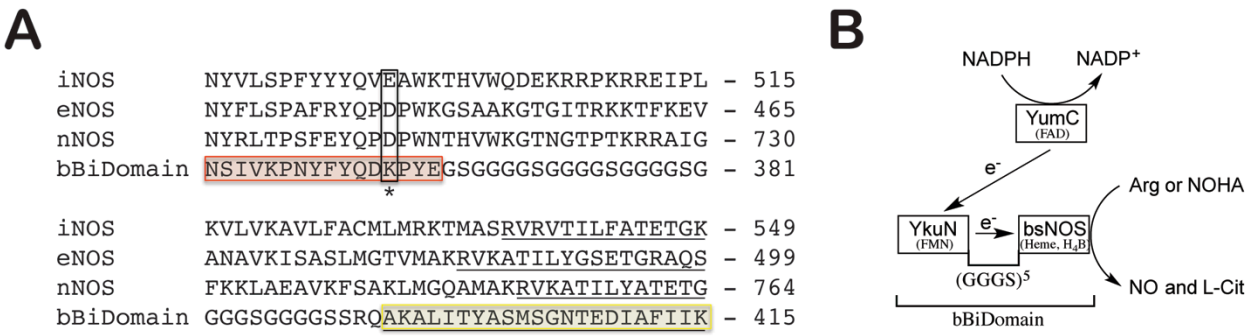

Figure 2.2 The chimera bBidomain contains a $(GGGS)^5$ linker. A) Partial protein sequence alignment of human iNOS, human eNOS, rat nNOS and bBiDomain. Sequences were manually aligned based on crystal structure comparison of oxygenase domain using the homologous residues indicated by (*) and the FMN binding domains are underlined. bBidomain oxygenase and FMN domain sequences are highlighted red and yellow, respectively. B) Model for electron transfer from NADPH to bBiDomain.

Similar to the three-component reaction, time dependent bBiDomain activity was evaluated using NADPH dependent nitrite formation from either NOHA or L-Arg (Fig 2.1B). Although L-Arg supported NO production, as measured by nitrite, the nitrite detected is less then half the amount produced by NOHA after 20 min. The bBiDomain dramatically improved bsNOS activity over the three-component system and is about 8-fold more active, as shown in Fig 2.1B. In addition, adding excess amounts of YkuN did not significantly alter bBiDomain activity (Fig 2.1B). This is expected since electron transfer from YumC to either free YkuN or the YkuN within bBidomain is not limiting and intramolecular electron transfer from YkuN to bsNOS in bBiDomain is much more efficient than with the free proteins. Electron transfer as a function of bBiDomain activity was also improved using YumC over FLDR as the ferredoxin reductase (Fig 2.1B). Thus, the combination of YumC and bBiDomain significantly improved NOS-like activity

and further corroborated the cyt-c assay results (Fig 2.1A) to provide additional support that YumC functions as a likely redox partner for YkuN to support bsNOS activity.

Interestingly, the ratio of YumC to bBidomain was critical for measuring bBiDomain activity (Fig 2.1C). Even though a 200 fold excess of YumC was required to saturate YkuN, as observed by cyt-c activity (Fig 2.1A), excess YumC clearly lowers the production of NO, as measured by nitrite concentration. This might be expected if the site for electron donation on YkuN from YumC and to the heme active site of bBiDomain is the same. At high concentrations of YumC, the amount of YumC-YkuN complex would increase thus limiting electron transfer to the bBiDomain active site.

NO Production and Inhibition of bBiDomain

In order to test the new assay for the ability to quickly and simply estimate inhibitor potency, we first tested the well-known NOS inhibitor N-omega-nitro-L-arginine (L-NNA). The reactions remained linear for the first 4 min and both reactions reached completion after about 10 min (Fig 2.3A). We next screened several commercial NOS inhibitors and previously identified bsNOS inhibitors **1** and **2** that we have shown exhibit antimicrobial properties (Fig 2.3B)[(22)]. These assays were carried out for 4 min prior to nitrite concentration being determined because we know from Fig 2.3A the reaction is still within the linear phase and thus is a direct measure of activity and inhibitor potency. While all inhibitors reduced NO production, both 7-NI and **2** stand out as the most potent. This is consistent with our previous findings where **2** was found to be superior to L-NNA in bacterial growth inhibition assays[(22)]. Moreover, these results show that a

single time point Griess determination of nitrite using bBiDomain can provide a high throughput method for screening bNOS inhibitors.

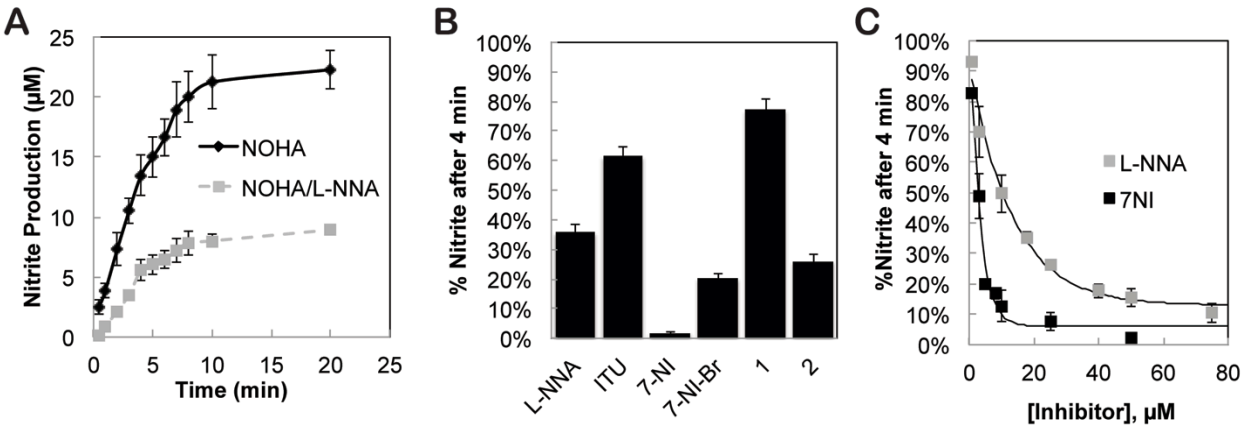

Figure 2.3 Time dependent bBiDomain activity and inhibition as measured by Griess reaction. A) Nitrite production remains linear in the first 4 min with bBiDomain and YumC at 100 nM and 1 μM, respectively. B) %Nitrite detected relative to no inhibitor after 4 min incubation at 35 °C with 30 μM inhibitor. C) %Nitrite detected as a function of inhibitor concentration for L-NNA and 7-NI. Error bars represent the SEM of three separate experiments for inhibitor concentration measured.

Similarly, we also demonstrated the single-time point measurements to be a useful approach for determining inhibitor IC_{50} by measuring the fraction of nitrite produced by bBiDomain as a function of inhibitor concentration (Fig 3C). IC_{50}'s for both L-NNA and 7-NI were evaluated and determined to be 10.2 μM and 2.7 μM, respectively. Interestingly, these data compare well with the previously determined mammalian NOS IC_{50}'s using separate and distinct enzyme assays (Table 2.1). Therefore, by utilizing a series of single time points as a function of inhibitor concentration we can determine accurate IC_{50}'s with bBiDomain and YumC.

Table 2.1 Comparison of NOS IC_{50} determined for L-NNA and 7-NI.

Ligand	bBiDomain	iNOS	eNOS	nNOS
L-NNA, IC_{50} (μM)	10.2	3.1[7]	0.35[7]	0.29[7]
		5.5[68]	7.04[68]	7.33[68]
7-NI, IC_{50} (μM)	2.7	9.7[7]	11.8[7]	8.3[7]
		20.0[69]		2.5[69]

Imidazole Displacement

To further evaluate ligand binding to the bsNOS active site we also measured the spectral binding constant, K_S, for each ligand (Table 2.2). All substrates/inhibitors evaluated were found to function as type I ligands in both bsNOS and bBiDomain and shift the heme iron from low-spin to high-spin. In the presence of 10 molar excess YkuN or by using bBiDomain to evaluate binding we consistently observed substrate/inhibitor binding in the low μM range, based on K_S. These data demonstrate that YkuN does not influence substrate/inhibitor binding to the heme active site. Interestingly, based on the K_s values for bsNOS, **2** binds about 4-fold better than **1** while based on the enzyme assays **2** is about a 13-fold better inhibitor than **1**. This pattern of K_s values giving less dramatic differences than the enzyme assay is consistent with the other inhibitors tested and we consider this reasonable agreement between the two methods given the complexity of the components required for the enzyme assay and that nitrite was measured at only a single time point.

Table 2.2 Chemical name and calculated K_S for substrate/inhibitor to active site of bsNOS, bsNOS in the presence of a 10 molar excess YkuN and bBiDomain. Error represents the error associated with the fit curve used to calculate the K_S. Values not determined (*n.d.*) are indicated.

Compound	Chemical Name	bsNOS	bsNOS + 10x YkuN	bBiDomain
		K_S, μM	K_S, μM	K_S, μM
L-Arg	(S)-2-Amino-5-guanidinopentanoic acid	0.8 ± 0.1[(22)]	6.5 ± 0.2	16 ± 2
NOHA	N-omega-hydroxy-L-arginine	3.2 ± 0.5	2.2 ± 0.1	13 ± 5
L-NNA	N-omega-nitro-L-arginine	1.3 ± 0.1[(22)]	4.9 ± 0.9	24 ± 7
L-NAME	N-omega-nitro-L-arginine methyl ester	66 ± 46	*n.d.*	*n.d.*
ITU	ethylisothiourea	9.3 ± 1.2	*n.d.*	*n.d.*
7-NI	7-nitroindazole	3.5 ± 0.4	6.8 ± 0.8	27 ± 4
7-NI-Br	3-bromo-7-nitroindazole	12 ± 1	*n.d.*	*n.d.*
1	6-({[(3R,5S)-5-{[(6-amino-4-methylpyridin-2-yl)methoxy]methyl}pyrrolidin-3-yl]oxy}methyl)-4-methylpyridin-2-amine	4.4 ± 0.1[(22)]	*n.d.*	*n.d.*
2	6,6'-{[(2S,3S)-2-aminobutane-1,3-diyl]bis(oxymethanediyl)} bis(4-methylpyridin-2-amine)	1.1 ± 0.1[(22)]	*n.d.*	*n.d.*

Ligand Bound Crystal Structures

Since both nitroindazole's and L-NNA are good bBiDomain inhibitors and structures of these inhibitors bound to a bacterial NOS have not previously been reported, we solved the crystal structures of these inhibitors bound to bsNOS (Fig 2.4 and Appendix II). Even though 7-NI-Br shares no structural similarity to L-Arg it is still able to bind at the active site and induce a spin shift (Table 2.2). The 7-NI-Br-bsNOS crystal structure was refined to 2.15 Å resolution with clear electron density for the

entire molecule (Fig 2.4A). Similar to previous mNOS crystal structures (Fig 2.4B), 7-NI-Br stacks parallel within a van der Waal's contact of the bsNOS heme group to form a hydrogen bond with the O carbonyl of Trp238 and NH of Met240 (Fig 2.4A). Also similar to mNOS, the active site Glu243 must assume a different rotomeric position. Unlike mNOS[70] the re-orientation of Glu243 toward the pterin binding site does not induce a significant conformational change in heme propionate A. Regardless, the bsNOS pterin site is distorted due to the re-orientation of Glu243 and a pterin molecule is not observed in the crystal structure. In mNOS the pterin is also displaced but a second 7-NI-Br molecule binds in the pterin site. We most likely do not observe a second 7-NI-Br in bsNOS because the pterin site in bsNOS is much larger and weakly binds pterins, in the 10-20 μM range[39], as compared to mNOS which binds pterins in the nanomolar range[31].

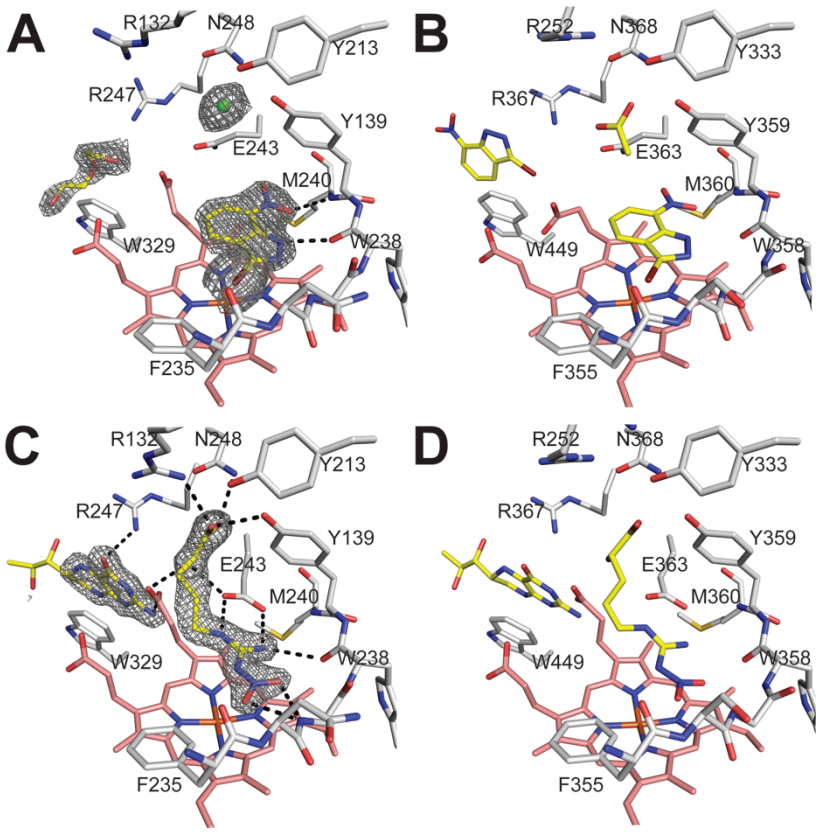

Figure 2.4 Inhibitor binding models of 7-NI-Br and L-NNA complexed to NOS active sites. Molecules bound near the active site are colored yellow and the active site residues are colored white with the heme shown in stick form and colored pink. A) The 2Fo-Fc map of 7-NI-Br bound to bsNOS active site and contoured to 1.5σ induces a conformational change in E243. Also observed in crystal structure is a PEG molecule and chloride ion. B) 7-NI-Br bound to eNOS (PDB 8NSE) reveals a near identical binding mode as observed in bsNOS except a second molecule of 7-Ni-Br forms a stacking interaction with W449 to occupy the H_4B co-substrate binding site. C) L-NNA binds to a network of active site hydrogen bonds and the 2Fo-Fc map of L-NNA is contoured at 2.0σ along with H_4B bound to pterin site and binds in a similar orientation to D) eNOS (PDB 1D0C).

We also solved and refined L-NNA bound bsNOS crystal structure to 1.72 Å (Fig 2.4C and Appendix II). The binding mode of L-NNA is similar to L-Arg and analogous L-NNA mNOS structures for which bsNOS utilizes Glu243 and the backbone atoms of both Met240 and Trp238 to H-bond the guanodinium group. Unlike L-Arg, the nitro group of L-NNA introduces new H-bonded interactions, as observed in mNOS

structures (Fig 2.4D) with Gly237 and Trp238 backbone atoms H bonding to the oxygen atoms of the nitro group[71]. The additional H-bond interactions result in a lower K_D, as compared to L-Arg, in mNOS systems[71]. The same pattern for L-NNA K_D likely holds true in bsNOS due to the high sequence similarity at the NOS active site across species and the observation that inhibitor binding modes are near identical.

L-Arg binding affinity

Further characterization of substrate binding to NOS active site was evaluated using isothermal titration calorimetry, as shown in Fig 2.5, and represents the first thermodynamic analysis for L-Arg binding to a NOS protein. Accurate determination of the L-Arg K_D was necessary for future inhibition studies that evaluate K_i using the Cheng-Prusoff equation[72], as is commonly done for mNOS[70]. The K_D of L-Arg to bsNOS was determined to be 5.6 ± 0.1 μM and is in close agreement with the *S. aureus* NOS K_D of 4.2 ± 0.2 μM determined by laser flash photolysis[73]. Compared to nNOS, which has an L-Arg K_M of 8.4 ± 2.7 μM[29], the bsNOS K_D is also within the same low μM range of mNOS This is not surprising since the mNOS and bsNOS active sites are nearly identical[41]. Moreover, L-Arg binding was also determined to be exothermic with a ΔH of -7.73 ± 0.02 kcal/mol at 25 °C. This thermodynamic result and additional characterization of L-Arg binding as enthalpically favored provides a better understanding for the thermodynamic considerations of future inhibitor based drug design.

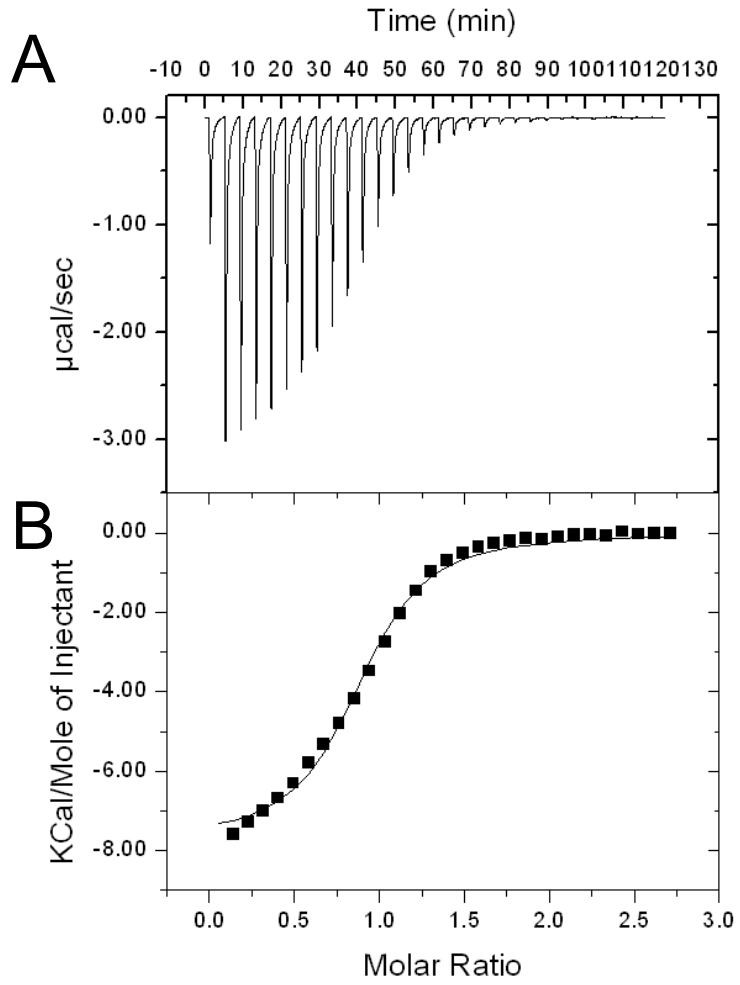

Figure 2.5. Isothermal titration calorimetry (ITC) data of L-Arg titrated into bsNOS in 50 mM KPi pH 7.4 at 25 °C. A) Raw ITC data plotted as heat generated versus time for one of three trials. B) Integrated and concentration normalized heat evolved for one of three trials at each injection. A one site model was used to generate the thermodynamic values for L-Arg binding K_D (or $1/K_A$) = 5.6 ± 0.1 µM, ΔH = -7.73 ± 0.02 kcal/mol and $T\Delta S$ = -0.047 ± 0.002 kcal/mol based on the average and SEM of three separate trials.

Conclusion

Between a series of recent gene knockout experiments and subsequent biological assays it is clear that bNOS functions in pathogenic bacteria to provide a protective barrier against reactive oxygen species and a variety of antibiotics[19-22]. Therefore, by inhibiting the enzymatic function of bNOS, it is plausible that we can

improve the efficacy of antibiotic treatments targeting pathogenic bacteria like *S. aureus* and *B. anthracis*. In order to first identify potential inhibitors of bNOS it was essential to develop a protein-based system in which ligand inhibition could be rapidly evaluated *in vitro*. Although previous studies have reported bNOS activity and rigorously characterized bNOS substrate catalysis[26, 34, 40, 51], this is the first study to utilize native redox partners for a bNOS and evaluate bNOS inhibition. Ultimately, this led us to the identification of YumC as a likely native redox partner for YkuN and the development of a novel chimera, bBiDomain, for activity analysis. In addition, this is also the first study to characterize the thermodynamics of substrate binding to a NOS protein and illustrates that detailed thermodynamic information can be obtained for ligand-bNOS interactions. While the calorimetric approach will not be useful for high throughput screening, a careful thermodynamic analysis of a select few tight binding inhibitors can provide important insights into the inhibitor design effort.

Chapter 3

Structure-Based Design of Bacterial Nitric Oxide Synthase Inhibitors

SUMMARY

Inhibition of bacterial nitric oxide synthase (bNOS) has the potential to improve the efficacy of antimicrobials used to treat infections by Gram-positive pathogens *Staphylococcus aureus* and *Bacillus anthracis*. However, inhibitor specificity toward bNOS over the mammalian NOS (mNOS) isoforms remains a challenge because of the near identical NOS active sites. One key structural difference between the NOS isoforms is the amino acid composition of the pterin cofactor binding site that is adjacent to the NOS active site. Previously we demonstrated that a NOS inhibitor targeting both the active and pterin sites was potent and functioned as an antimicrobial (Chapter 1, Holden *et al*, *Proc. Natl. Acad. Sci. U.S.A.* **2013**, 110, 18127). Here we present additional crystal structures, binding analyses, and bacterial killing studies of inhibitors that target both the active and pterin sites of a bNOS and function as antimicrobials. Together, these data provide a framework for continued development of bNOS inhibitors, as each molecule represents an excellent chemical scaffold for the design of isoform selective bNOS inhibitors.

INTRODUCTION

Structure-based drug design has played a key role in the development and

characterization of isoform selective mammalian nitric oxide synthase (mNOS) inhibitors[35, 36]. NOS, an enzyme responsible in mammals for the production of the essential signaling molecule NO, can also promote a variety of disease pathologies if production of NO is unregulated[74]. While structure-based inhibitor design efforts have largely focused on the three mNOS isoforms[35, 36], recent characterization of bNOS as an antibacterial target against Gram-positive pathogens *Staphylococcus aureus*[19, 20] and *Bacillus anthracis*[18] has promoted interest in the development of potent bNOS inhibitors. Between several bacterial gene deletion experiments and biological assays it is clear that bNOS functions in Gram-positive pathogens to provide a protective barrier against a variety of antibiotics, oxidative stress, and host antimicrobial peptides[18-21]. Recently, we demonstrated that the effectiveness of a common antimicrobial is significantly improved when *B. subtilis*, a non-pathogenic model organism for *B. anthracis*, is also treated with a NOS inhibitor[22] originally designed to selectively inhibit mammalian neuronal NOS (nNOS).

One of the major issues in the design of bNOS inhibitors is its structural similarity to mNOS isoforms. Avoiding the inhibition of endothelial NOS (eNOS) and inducible NOS (iNOS) is important given the role these mammalian isoforms play in regulating blood pressure[38] and in the immune host defense system,[75] respectively. Direct comparison of the mammalian and bacterial NOS structures/sequences reveals several key differences that could be exploited for a bNOS inhibitor design effort. The first key difference is between the domain architecture of the NOS isoforms. Each mNOS is a multi-domained protein composed of both a reductase and oxygenase domain whose activity is regulated by calmodulin. In sharp contrast, bNOS is only composed of an

oxygenase domain and is not regulated by calmodulin. Since bNOS is not covalently linked to its redox partners like mNOS, bNOS must utilize redox partners for activity[26, 27]. A second key difference is amino acid variances between the NOS active sites. For example, both bNOS and endothelial NOS (eNOS) have an Asn residue that directly interacts with the L-Arg substrate while this residue is Asp in nNOS and inducible NOS (iNOS). The active site Asp/Asn difference provided the initial structural underpinning for the design of nNOS selective inhibitors[37]. Despite this difference in electrostatics between bNOS and nNOS, inhibitors that target the Asn residue might be detrimental if they also inhibit the critical eNOS isoform. Additional active site differences in bNOS include His128 (mammalian equivalent is Ser) and Ile218 (mammalian equivalent is Val). The slightly bulkier Ile adjacent to the O_2 binding site has been shown to decrease the NO release rates in bNOS[50]. The last key difference between mNOS and bNOS is present at the pterin cofactor-binding site. Since bNOS lacks the N-terminal Zn^{2+} binding motif present in mNOS, the pterin binding site is more exposed in bNOS[50], resulting in weaker micromolar binding affinity in bNOS[39] vs. the stronger nanomolar affinity in mNOS[31]. While the physiologically relevant bNOS cofactor that binds to the bNOS pterin site remains unknown[41], inhibitors that target this site are an attractive avenue for structure-based drug design. These differences were first exploited by a NOS inhibitor that demonstrated antimicrobial properties against *B. subtilis*[22].

Since NOS inhibitors that bind both the active and pterin binding sites could allow for further design of bNOS inhibitor specificity, we report here on several NOS inhibitors (**1-7**) we identified by solving crystal structures that target both the active and pterin binding sites of *B. subtilis* NOS (bsNOS). From initial analysis of NOS inhibitors (**1-4**) we

were able to design and, in collaboration with the Silverman Lab at Northwestern University, synthesize two additional inhibitors (**5** and **6**) that also targeted the active and pterin binding sites. Further characterization of inhibition was carried out using inhibitor binding assays, enzyme assays, molecular dynamics simulations, and bacterial assays to provide a structural framework for the continued design of isoform-selective bNOS inhibitors that function as antimicrobials.

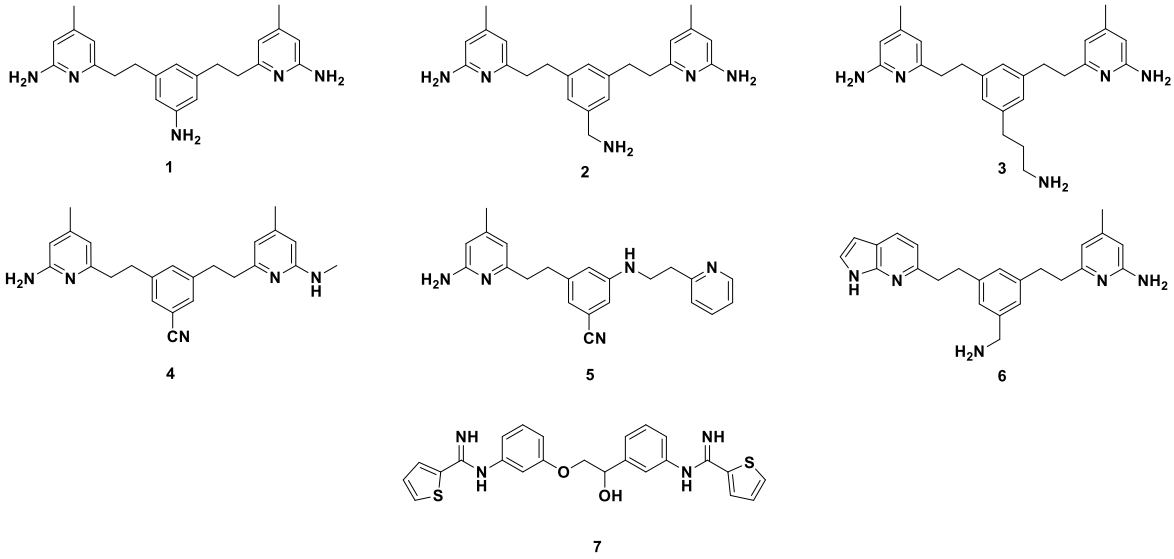

RESULTS AND DISCUSSION

Aminopyridine Inhibitor Binding

Although *S. aureus* is the primary target, we use non-virulent *B. subtilis* for routine screening. We also use *B. subtilis* NOS (bsNOS) for crystallography since bsNOS crystals diffract to much higher resolution than *S. auerus* NOS (saNOS) although the structures are nearly identical. The root-mean-square standard deviation of Cα atoms is 0.55 Å while 32 of 33 residues within 10 Å of the heme iron are identical. Therefore, structural insights gained from bsNOS are directly applicable to saNOS.

Inhibitors **1-3** were initially designed to target nNOS and the structures of nNOS-**1,2,3** have previously been reported[76, 77]. The structures of bsNOS with inhibitors **1**-**6** revealed that each compound interacts with the active site Glu-243 and heme propionate D through a series of H-bonds between the aminopyridine functional groups (Fig 3.1A-D and Appendix I). While **1** and **2** only differ in the amine substituent at the para-position of the aromatic ring linker, it is clear that linker composition between the aminopyridine groups dictates the orientation of the inhibitor and the rotameric position of Arg-247. For example, in **1** Arg-247 reorients to form a π-cation interaction with the aromatic ring of the linker. This alternative rotamer was also observed with **4**. In sharp contrast, the linkers of **2** and **3** are parallel to the heme group, and Arg-247 is observed in its native position. In the case of **2** the parallel orientation (relative to the heme group) of the aromatic ring within the linker is likely a result of the H-bond formed between the linker's primary amine and heme propionate A.

Considering that a cyano substituent within the linker of **4** results in a π-cation interaction with Arg-247 and a H-bond between heme propionate D and the aminopyridine functional group, we anticipated that inhibitor binding to the pterin site could be further improved by addition of a secondary amino group to form an additional H-bond with heme propionate D and the cyano conjugated ring to maintain the π-cation interaction with Arg-247. These observations led to the synthesis of **5**, whose linker unexpectedly adopted a parallel orientation to the heme group but maintained the π-cation interaction with Arg-247 (Fig 3.1E). To further improve inhibitor binding to the pterin site of bsNOS the Silverman lab synthesized **6**; the design of **6** was based on the crystal structure of **2**. The goal was to develop an inhibitor that formed a stable π-π

stacking interaction with Trp-329 by replacing one of the aminopyridine groups of **2** with a pyrrolopyridine. The pyrrolopyridine should also be able to H-bond with heme propionate D. As observed with **2**, compound **6** does indeed form a H-bond with the heme propionate and undergoes a π-π stacking interaction with Trp-329 as predicted from the modeling.

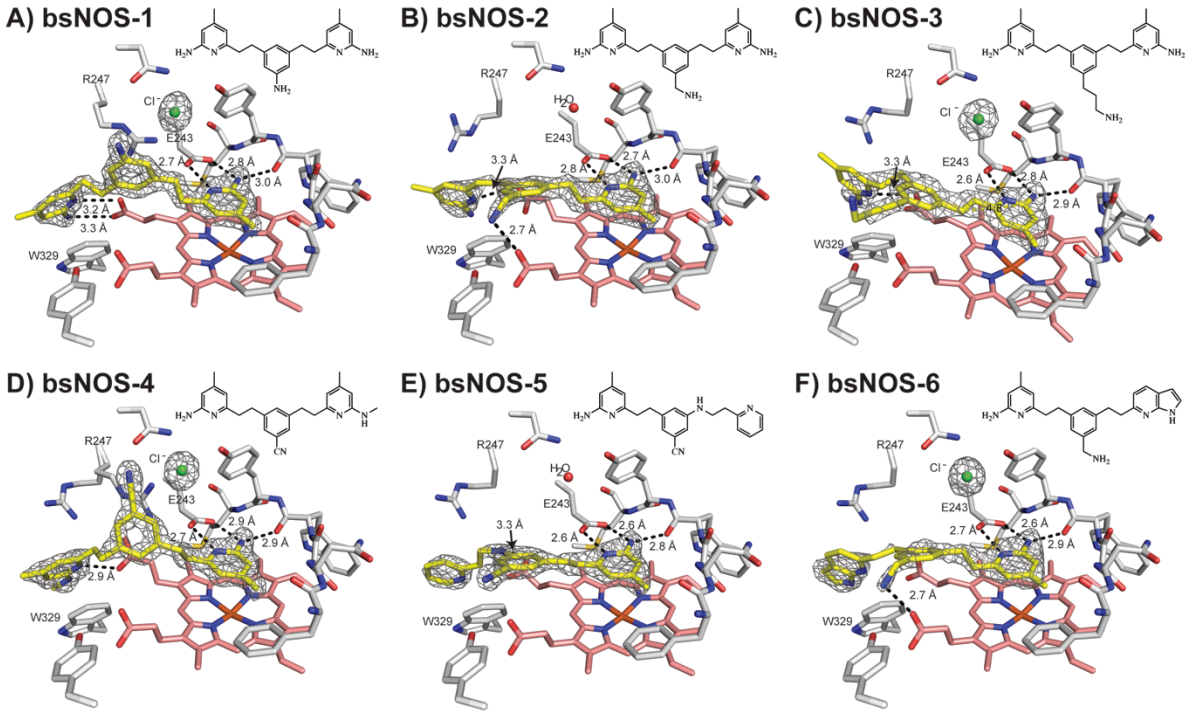

Figure 3.1. Active site view of bsNOS-inhibitor bound crystal structures with the inhibitor colored yellow, heme colored salmon, and select active site residues colored white. Inhibitor-protein H-bond distances are represented as black lines. The $2F_O$-F_C maps are shown for A) **1** contoured at 1.8σ, B) **2** contoured at 1.4σ, C) **3** contoured at 1.2σ, D) **4** contoured at 1.8σ, E) **5** contoured at 2.0σ and F) **6** contoured at 1.3σ.

To further characterize inhibitor binding at the NOS active site we measured the spectral binding constant, K_S, for each inhibitor to both bsNOS and iNOS. On the basis of the measured K_S for each inhibitor, binding to both bsNOS and iNOS was in the low

μM range (Table 3.1). In addition, we also measured K_S for bsNOS in the presence and absence of H_4B. We anticipated the K_S of inhibitors targeting the pterin site to increase in the presence of H_4B, as inhibitor binding would be weakened owing to competition with the pterin molecule. However, in the case of inhibitors that tightly bind to the pterin site, for example **1**, only a two-fold difference in binding was observed (Table 3.1), which we consider to be a negligible difference since the K_S of ligands L-NNA and NOHA—two ligands that do not bind to the pterin site—resulted in a 3.4 and 1.2 fold difference in binding, respectively. Another interpretation is that the binding affinity of **1** to the pterin site is significantly stronger than the binding affinity of H_4B and that **1** is able to easily displace H_4B. If this is true, for tight binders the K_S should remain unchanged in the presence or absence of H_4B. In contrast, for inhibitors that are transiently associated with the pterin site, as is observed with **5** and **6**, it is not surprising that we also observe a negligible change in K_S upon addition of H_4B owing to the weak non-covalent interactions observed at the pterin site. Regardless, from the crystal structures (Fig 3.1) it is apparent that **1-6** may serve as reasonable templates for future structure-based drug design against bNOS, as all molecules do bind to the pterin-binding site.

Table 3.1. Imidazole displacement assay used to calculate the spectral binding constants (K_S) in the absence (-) and presence (+) of 50 μM H_4B.

Compound	K_S (μM)		
	bsNOS (-H_4B)	bsNOS (+H_4B)	iNOS (+H_4B)
1	0.91 ± 0.08	1.9 ± 0.1	2.9 ± 0.4
2	15 ± 3	47 ± 2	33 ± 8
3	16 ± 1	19 ± 1	19 ± 4
4	12 ± 1	19 ± 2	6.1 ± 0.6
5	39 ± 2	34 ± 4	16 ± 6
6	10 ± 2	12 ± 4	21 ± 8
7	13 ± 2	80 ± 19	93 ± 77
N-omega-nitro-L-arginine (L-NNA)	1.32 ± 0.04[22]	4.4 ± 0.3	n.d.
N-omega-hydroxy-L-arginine (L-NOHA)	3.2 ± 0.5[27]	1.9 ± 0.1	n.d.

Thiophenecarboximidamide Inhibitor Binding

Thiophenecarboximidamide inhibitors are expected to exhibit improved pharmacological properties over aminopyridine inhibitors but form similar complexes with nNOS[77], so we investigated the binding of **7** to bsNOS. Similar to **1-6**, crystal structure analysis of **7** revealed that the inhibitor also bound at both the active and pterin sites (Fig 3.2A). Since **7** is an asymmetric inhibitor with both ends of **7** being composed of a thiophenecarboximidamide, we wanted to investigate in more detail the noncovalent interactions that allow for the unique binding mode and orientation of **7** to bsNOS. From the crystal structures we hypothesized that the inhibitor orientation observed in bsNOS-**7** resulted from the 3.2 Å H-bond formed with His-128 and/or the hydrophobic contact shared between Ile-218 and one of the inhibitor aromatic rings. The observation of a 3.2 Å H-bond between **7** and His-128 (Fig 3.2A) was of particular interest because the corresponding residue in mNOS is a Ser. Similarly, its feasible that the hydrophobic contact between Ile-218 and **7** would favor **7** to bind the aromatic ring

lacking a polar substituent to form better nonpolar interactions with the larger Ile-218 side chain. However, site directed mutagenesis of bsNOS revealed that neither the H128S (Fig 3.2B) nor the I218V mutants (Fig 3.2C) resulted in an alternative bsNOS-**7** binding mode. In fact, I218V-bsNOS resulted in a more stable H-bond, 2.7 Å vs. 3.3 Å for WT, with His-128. Together these data suggest that the binding mode of **7** results from the ability of **7** to bind in the pterin pocket in order for **7** to optimally interact with both the pterin and active sites, and this is likely observed in bsNOS because pterin binding is weak. The importance of **7** binding to the pterin site is evidenced by the 6-fold decrease in affinity in the presence of H_4B (Table 3.1).

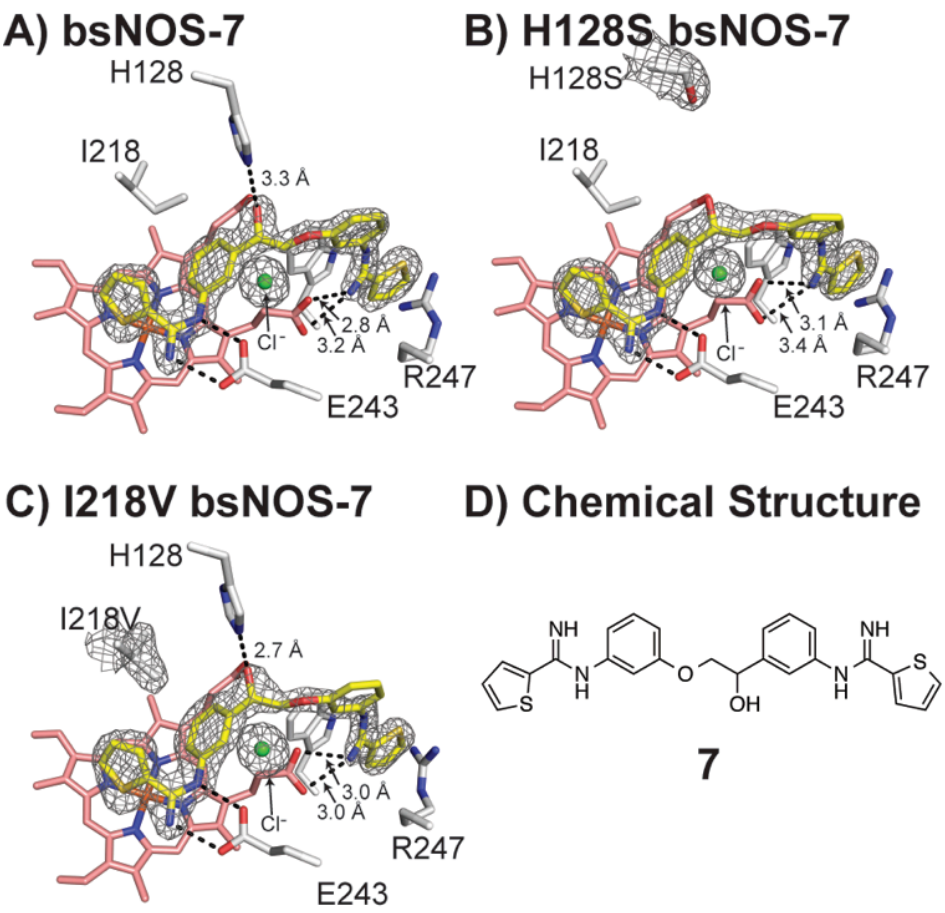

Figure 3.2. Neither His128 nor I218 provides binding specificity of **7** to bsNOS. A) WT bsNOS-**7** with $2F_O$-F_C map contoured at 2.0σ reveals a 3.3 Å H-bond interaction between His128 and the hydroxyl group of **7**. B) H128S-bsNOS-**7** crystal structure with $2F_O$-F_C map contoured at 1.5σ. C) I218V-bsNOS-**7** crystal structure with $2F_O$-F_C map contoured at 1.8σ. D) 2D chemical structure of **7**.

To further probe the binding mode of **7** to bsNOS and investigate the H-bond contribution of His-128 to the binding mode, we ran MD simulations for 25 ns. After allowing the system to equilibrate for 4.5 ns, the ligand was allowed to freely move. In both WT and H128S MD simulations **7** retains its interactions with the active site Glu-243 (Fig 3.3A) and is loosely bound to heme propionate D (Fig 3.3B), suggesting that the H-bond formed between **7** and Glu-243 is strong and the H-bond between **7** and

heme propionate D is weak. In fact, the bond distance between **7** and heme propionate D exceeded 3.5 Å for 96.4% of the bsNOS MD trajectory. Moreover, comparison of the MD trajectories for bsNOS and H128S-bsNOS suggests that the H-bond between **7** and His128 is also transient and does not contribute toward the binding mode of **7**. Distance measurements between the α-carbon of residue 128 and the hydroxyl group of **7** reveal His128 to function only by sterically restricting the movement of **7**, as the atom distances range from 2.6 Å to 7.6 Å for bsNOS-**7** and 4.7 Å to 10.7 Å for H128S-bsNOS-**7** (Fig 3.3C). This is not surprising as His is a much bulkier residue then Ser.

Interestingly, in both WT and H128S MD simulations, the thiophenecarboximidamide head group of **7** initially bound at the pterin site was observed to rotate in and out of the pterin pocket. This rotation of the thiophenecarboximidamide rendered the pterin-binding site temporarily solvent exposed. More specifically, direct measurement of the bond distance between heme propionate D and the imine of **7** throughout the MD simulation revealed the distance between heme propionate D and the imine of **7** to be non-uniform within each chain of the bsNOS dimer (Fig 3.3B). Together these data provide additional support that binding of **7** to the pterin site is relatively weak.

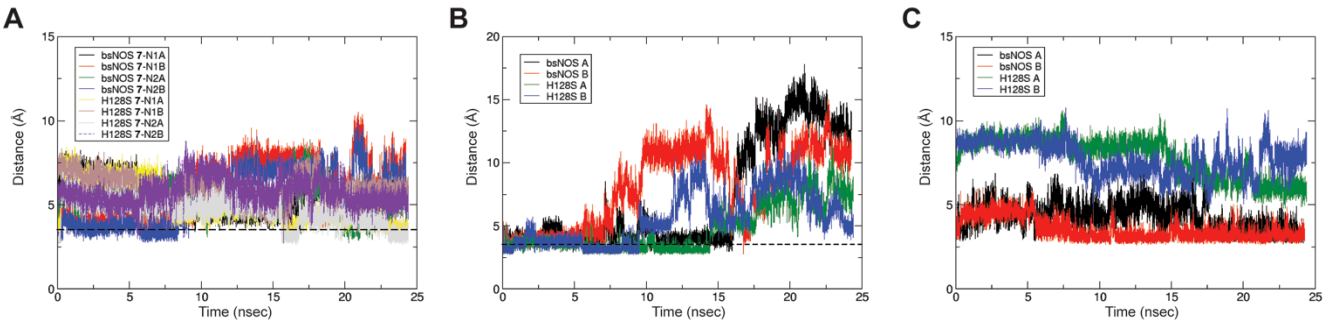

Figure 3.3 Molecular dynamics simulation of **7** bound to bsNOS and H128S-bsNOS reveals inhibitor is only tightly bound to active site Glu-243. A) The distance measured between active site Glu-243 and the imine group of **7** bound to the active site is constant over time. The dotted line indicates 3.5 Å. B) The distance measured between heme propionate D and the imine group bound to pterin site of **7** over time with the dotted line indicating a distance of 3.5 Å. C) The distance measured between the hydroxyl group of **7** and α-carbon of residue 128. Molecular dynamics simulations carried out by Scott Hollingsworth.

Inhibition-Activity Analysis

Both the aminopyridine and thiophenecarboximidamide based inhibitors bind and inhibit the three mNOS isoforms (Table 3.2). Considering **1-4** were originally designed to target nNOS, it is not surprising that **1-4** are good inhibitors of nNOS. Interestingly, a comparison of Ki's for **2** and **6**, with **6** having a bulkier pyrrolopyridine group then the aminopyridine present in **2**, suggests the bulkier pyrrolopyridine group lowers the specificity toward the mNOS isoforms. Specifically, the potency of **6** toward nNOS decreased > 4 fold as compared to the potency of **2** toward nNOS. Hence, the introduction of a bulkier group that also binds to the bNOS pterin site has the potential to lower inhibitor affinity to the mNOS isoforms.

Table 3.2. K_i values of inhibitors **1-7** with the mammalian NOS isoforms.

	Ki (nM)		
Inhibitor	rat nNOS	bovine eNOS	murine iNOS
1	85 *(76)*	4950 *(76)*	3400 *(76)*
2	53 *(45)*	11700 *(45)*	6310 *(45)*
3	540 *(45)*	12100 *(45)*	32500 *(45)*
4	196 ± 13	11806 ± 893	14410 ± 1227
5	1267 ± 45	1557 ± 136	12750 ± 1204
6	220 ± 17	52726 ± 482	7098 ± 482
7	819 *(78)*	10100 *(78)*	5200 *(78)*

With the use of the recently described bBiDomain and YumC system for bNOS activity/inhibition measurements, we also evaluated the potency of each inhibitor at varying concentrations using a single time point approach*(27)*. At all concentrations evaluated, **1** was the most potent with 49.2 ± 1.2% nitrite detected at an inhibitor concentration of 300 μM. The increased potency of **1**, compared to **2-7**, is likely because **1** is able to form two separate 3.3 Å H-bonds with heme propionate D (Fig 3.1A), which accounts for an additional 1-3 kcal/mol in binding energy. Unlike **1,** compounds **2-6** are unable to form a strong H-bond with the heme propionate D (Fig 3.1). On the basis of this limited data set, it is clear that formation of a strong H-bond with heme propionate D improves inhibitor potency for molecules that target the pterin site. Moreover, of the compounds evaluated here, it also is clear that inhibitor potency needs to be dramatically improved, as only one of these compounds lowered enzyme activity below 50% (Fig 3.4). The relatively weak potency observed might be the result of the inclusion of 50 μM H_4B in the enzyme assay, as these inhibitors must compete with H_4B. Moreover, because the physiological pterin group*(41)* and its concentration

within either *S. aureus* or *B. anthracis* is unknown, the actual *in vivo* potency may be substantially different from our *in vitro* results. Even so, the relative inhibitor potency of each inhibitor is a sufficient tool to guide inhibitor design. Regardless, improving the noncovalent protein-inhibitor interactions at the pterin-binding site will likely also improve inhibitor potency.

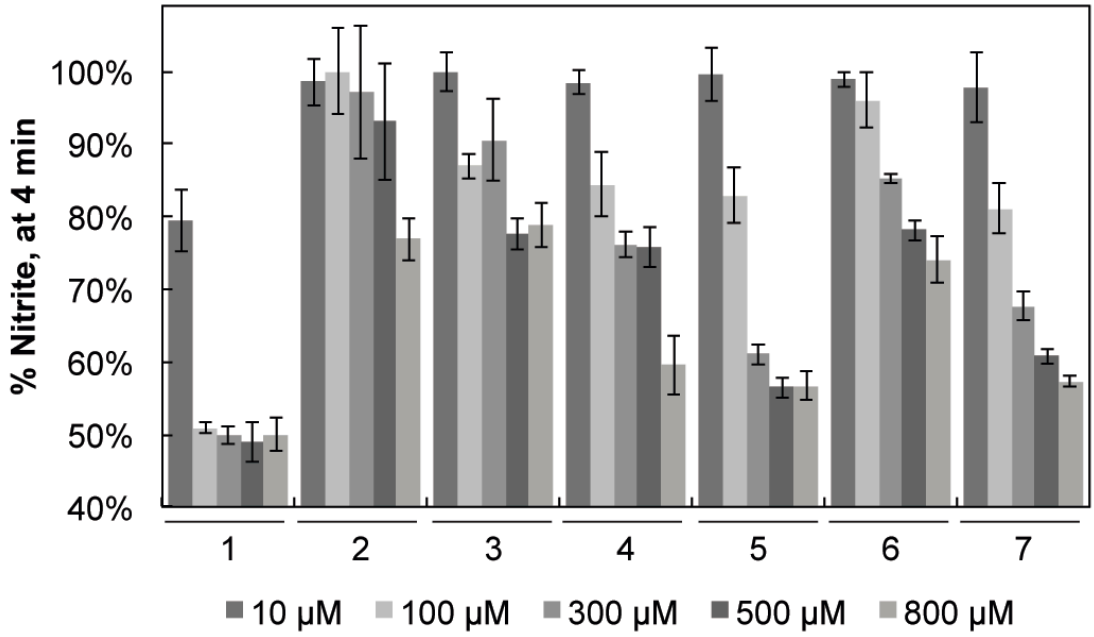

Figure 3.4 %Nitrite detected as a function of bBidomain activity in the presence of NOS inhibitors at varying concentrations. On the basis of a single time point analysis, **1** is the most potent bNOS inhibitor. Error bars represent the mean ± the SEM for three separate experiments.

Bacterial Growth Inhibition

We previously showed that some NOS inhibitors developed for selective inhibition of nNOS worked synergistically with the antibiotic acriflavine (ACR)[(22)], to inhibit the growth of *B. subtilis*. In the previous work there was a good correlation between the binding affinity of a NOS inhibitor to bsNOS and its ability to work synergistically with the antibiotic ACR in bacterial killing. We thus would expect inhibitor

1 to be especially effective at bacterial growth inhibition, and this indeed is the case (Fig. 3.5). Of the inhibitors tested, **1** is the most effective at working synergistically with ACR to block growth. With ACR alone bacterial growth is 23% of control. In the presence of inhibitor **1** growth is 36% of control, but together with ACR the inhibition is close to 99%, clearly indicating a strong synergistic effect. While the correlation between being an effective bsNOS and a bacterial growth inhibitor are strong, **2** is an outlier. Inhibitor **2** does not bind as tightly to bsNOS nor is it as effective at blocking bsNOS activity, but it is, nevertheless, a good inhibitor of bacterial growth. Given that both **1** and **2** can inhibit bacterial growth on their own suggests that these compounds block bsNOS to render the bacteria more susceptible to ACR but may also influence additional non-bsNOS target(s).

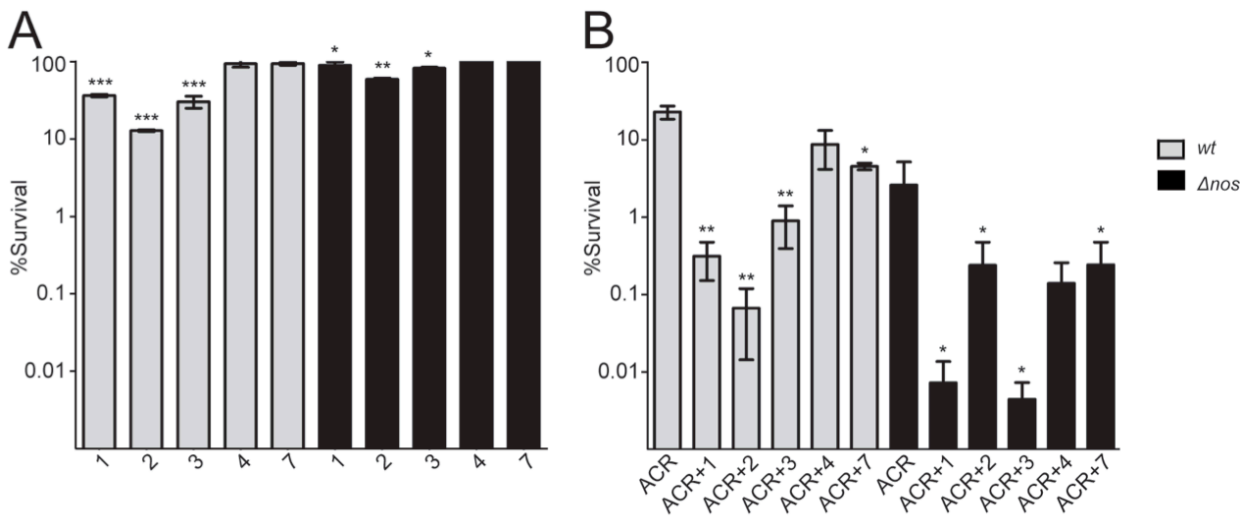

Figure 3.5 NOS inhibitors influence the %survival of *B. subtilis*. A) *B. subtilis* treated with NOS inhibitors. Significance calculated using the Student's t test between the measured CFU of *B. subtilis* treated with and without NOS inhibitors for each strain separately. B) Bacterial survival of *B. subtilis wt* and *Δnos* decreases in the presence of 800 μM ACR and 500 μM NOS inhibitors. Significance calculated for each strain separately using the Student's t test between the calculated % survival of ACR treated cells and % survival of ACR+NOS inhibitor treated cells. Error bars represent the mean ± the SEM of at least three replicates. Student's t test gives ***$p < 0.01$, **$p < 0.05$, *$p < 0.1$.

CONCLUSION

Although the physiological pterin cofactor for bNOS remains unknown, NO production by bNOS requires the presence of a pterin group[34]. Because of this strict pterin group requirement for activity and the significant differences in the pterin binding sites between mNOS and bNOS, inhibitors that target the pterin site may provide the key to unlocking the design and development of potent bNOS inhibitors. By taking a structure-based approach toward the identification of NOS inhibitors, we were able to identify several chemical scaffolds that inhibit bsNOS by binding to both the active and pterin sites. Several of these structures resulted in unexpected rotameric positions of active site residue Arg-247. These alternate rotameric positions will be important to consider for future structure-based drug design. Moreover, while the crystal structures and K_S analysis provide definitive support for each molecule binding at the active site, MD simulations suggest that the binding of **7** is transient and, therefore, weak. A particularly important observation is that aminopyridine inhibitors bind better than the pyrrolopyridine inhibitor even though both bind in the pterin pocket, form stacking interactions with Trp329, and H-bonds with the heme propionate. One might have expected the pyrrolopyridine to bind more tightly given the larger surface area that should form more extensive interactions with Trp329. However, a key difference between the aminopyridine group and the pyrrolopyridines is that the aminopyridine has a higher pKa than the pyrrolopyridine and is likely to be at least partially protonated and positively charged at neutral pH thus giving stronger interactions with the heme propionate. This underscores the importance of strong electrostatic interactions with the heme propionate relative to π stacking interactions. Further development of potent

bNOS inhibitors that work synergistically with antibiotics will thus require further modification of inhibitor scaffolds that take these lessons into account.

Chapter 4

Nitric Oxide Synthase as a Target for Methicillin Resistant *Staphylococcus aureus*

SUMMARY

Bacterial infections associated with methicillin-resistant *Staphylococcus aureus* (MRSA) are a major economic burden to hospitals and confer high rates of morbidity and mortality amongst those infected. Exploitation of novel therapeutic targets is thus necessary to combat MRSA infections. Here we report on the identification and characterization, including crystal structures, of two nitric oxide synthase (NOS) inhibitors that function as antimicrobials against MRSA. These data provide the first evidence that bacterial NOS (bNOS) inhibitors have the potential to work synergistically with antibiotic-induced oxidative stress to enhance MRSA killing. Crystal structures show that each inhibitor contacts an active site Ile residue in bNOS that is Val in the mammalian NOS isoforms. Mutagenesis studies show that the additional nonpolar contacts provided by the Ile in bNOS contributes to tighter binding of the bacterial enzyme.

Introduction

As bacterial pathogens continually acquire resistance to commonly used antibiotics, it has become clear that novel therapeutic strategies are required to combat serious infections[(79)]. In particular, there is an urgent need for the development of new pharmaceuticals that target methicillin-resistant *Staphylococcus aureus* (MRSA). MRSA, a Gram-positive pathogen resistant to common antibiotics like isoxazoyl penicillins and β-lactams[(80)], was first reported in 1961[(81)] and remains one of the most costly bacterial infections worldwide[(82)]. MRSA is a major threat to public health because

of the emergence of community-associated strains and their varying epidemiology[83]. In recent years, the threat of MRSA has been compounded by reports of strains resistant to vancomycin, as this agent is often considered the drug of last resort [84]. Characterization and exploitation of alternative bacterial drug targets will be essential for future management of MRSA infections.

Recent gene deletion experiments in *S. aureus*, *B. anthracis*, and *B. subtilis* have implicated bacterial nitric oxide synthase (bNOS) as a potential drug target, since this enzyme provides the bacterial cell a protective defense mechanism against oxidative stress and select antibiotics [18-20]. We recently provided an initial proof of principle regarding pharmacological targeting of bNOS, as growth of the nonpathogenic model organism *B. subtilis* was found to be severely perturbed in response to combination therapy with an active site NOS inhibitor and an established antimicrobial [22].

Design and development of a potent bNOS inhibitor against bone fide pathogens such as MRSA is complicated by the active site structural homology shared with the three mammalian NOS (mNOS) isoforms [50]: inducible NOS (iNOS), neuronal NOS (nNOS), and endothelial NOS (eNOS). It is especially important not to inhibit eNOS owing to the critical role eNOS plays in maintaining vascular tone and blood-pressure [38]. Selectivity over nNOS may represent less of an immediate problem, since many of the polar NOS inhibitors characterized thus far are not very effective at crossing the blood-brain barrier [36]. Recent structure-based studies suggest that bNOS specificity can be achieved through targeting the pterin-binding site [22, 23] as the bNOS and mNOS pterin binding sites are quite different.

To quickly identify potent bNOS inhibitors we screened a diverse set of NOS inhibitors (Fig. 4.1) using a novel chimeric enzyme recently reported for bNOS activity analysis [27]. From this high-throughput analysis we were able to identify two potent and chemically distinct bNOS inhibitors. Crystal structures and binding analyses of these inhibitors revealed both to bind a hydrophobic patch within the bNOS active site. Moreover, both of these compounds were found to possess antimicrobial activity against *S. aureus,* suggesting that these could represent viable new drug leads against this foremost human pathogen so frequently resistant to current antimicrobials.

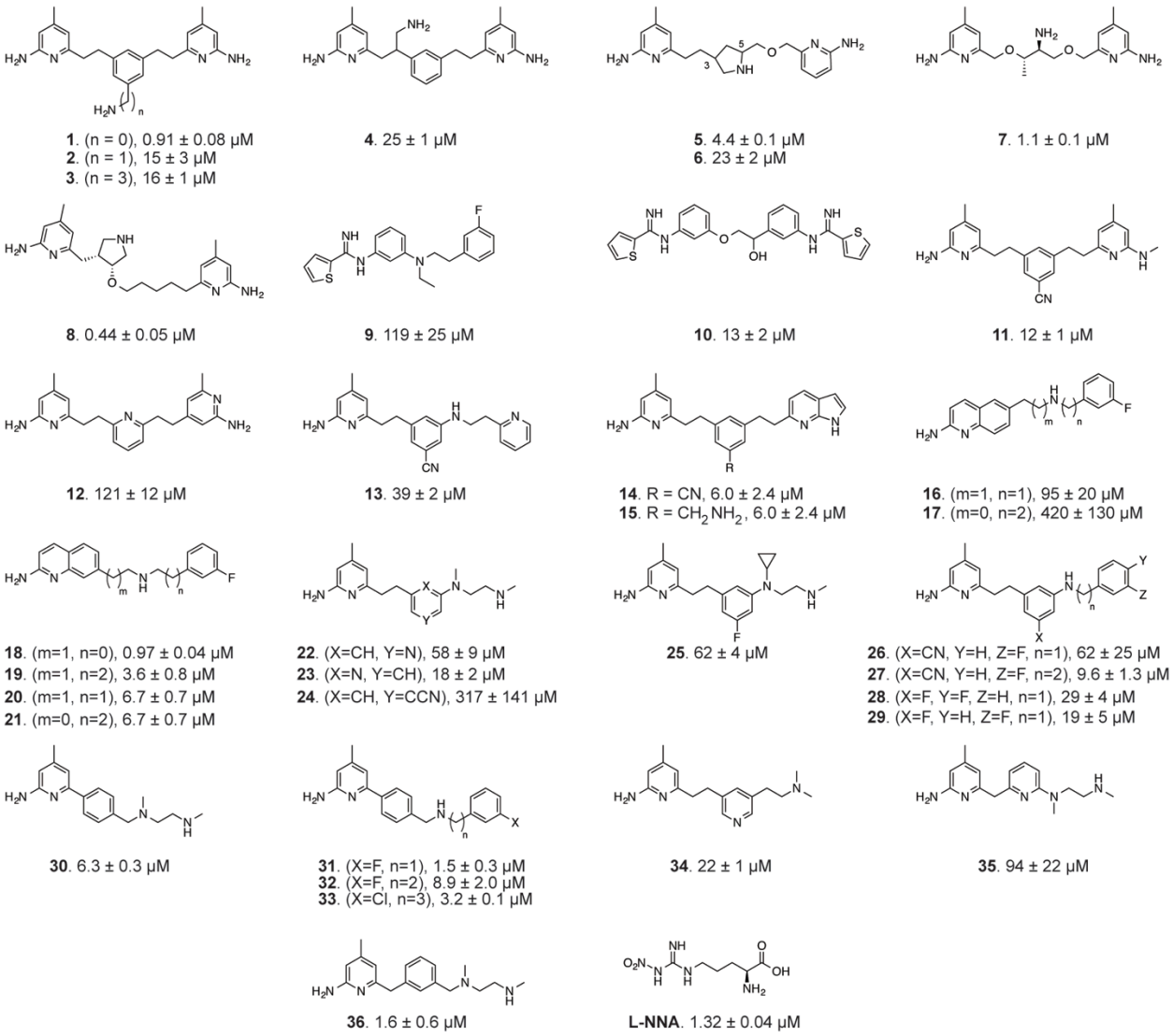

Figure 4.1 NOS inhibitor library used in this study. The spectral binding constants, K_S, are reported in μM for each inhibitor to bsNOS.

Results and Discussion

Identification of Potent bNOS Inhibitors

Rapid identification of molecular fragments that function as potent bNOS inhibitors is a key initial step toward the design and characterization of future bNOS inhibitors. To carry this out, we adapted a bNOS activity assay[(27)] to screen through a series of NOS inhibitors using a single time point approach (Fig 4.2). Concurrently, we

measured the K_S for each inhibitor using the imidazole displacement assay. While all inhibitors bound to *Bacillus subtilis* NOS (bsNOS) in the μM range, the most potent bsNOS inhibitors identified from the activity analysis were also calculated to have K_S values in the low μM to nM range. By using the single time point approach in combination with the imidazole displacement assay, we identified compounds that were both potent inhibitors and tight binders to the active site. Since L-NNA is an excellent inhibitor analog of the NOS substrate L-Arg, the potency of L-NNA at 40.9 ± 5.3 % nitrite (Fig 4.2) was established as an arbitrary threshold for identifying designer molecules with increased potency. Using L-NNA as a benchmark led us to classify several NOS inhibitors as potent bNOS inhibitors. This group includes three aminoquinoline inhibitors, two 6-benzyl aminopyridine inhibitors, and two aminopyridine inhibitors. Of the two aminopyridine inhibitors, **7** was previously described as a NOS inhibitor with antimicrobial properties [(22)]. Since we previously characterized the binding of aminopyridine inhibitors to bsNOS, we selected the most potent aminoquinoline and 6-benzyl-aminopyridine based inhibitors, **19** and **32**, respectively, for further analysis. Compounds **19** and **32** were also the two most potent inhibitors of the 37 NOS inhibitors evaluated using the bsNOS single time point analysis at 6.1% nitrite and 13.2% nitrite, respectively.

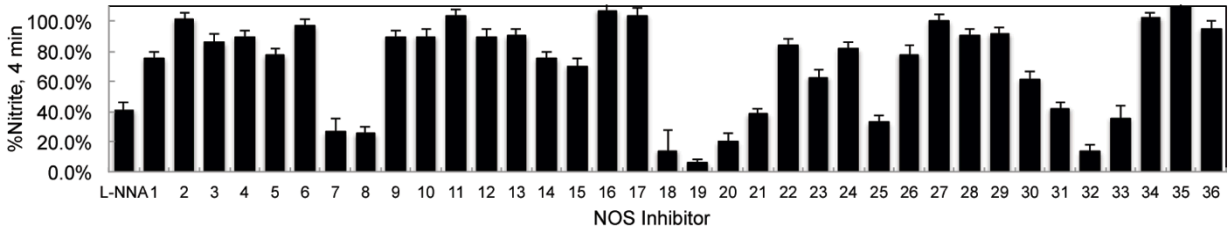

Figure 4.2 On the basis of a single time point analysis using the bBiDomain for bacterial NOS inhibition, NOS inhibitors have varying potency toward bacterial NOS. Nitrite concentrations were measured after a 4 min incubation. Error bars represent the average ± the SEM for three separate experiments.

Isoform Selectivity of NOS Inhibitors

Compounds **19** and **32** were next assayed separately against purified NOS isoforms at varying concentrations[27]. Even though the IC_{50}s for both mNOS and bsNOS were measured by complimentary methods, both methods allowed for an excellent comparison of inhibitor potency, as IC_{50} was used to calculate K_i using the Cheng-Prusoff equation [72]. From our K_i analysis (Table 4.1), it is clear that both **19** (269 nM) and **32** (1940 nM) function as potent bNOS inhibitors and demonstrate excellent selectivity over both iNOS and eNOS (Table 4.1). It is unclear whether cross-reactivity with nNOS expressed in neuronal tissues would represent an important limiting factor for these drugs during short course antibacterial therapy unless blood-brain penetration was high; indeed nNOS inhibition itself has been examined as a treatment for Parkinson's disease in the rat model [85].

Table 4.1 Inhibition of NOS isoforms by inhibitors **32** and **19**. The bBiDomain construct was used to evaluate inhibitor K_i against bsNOS.

Inhibitor	K_i bBiDomain (nM)	K_i nNOS (nM)	K_i iNOS (nM)	K_i eNOS (nM)
19	269	164	31900	7250
32	1940	525	6440	2870

To better understand the structural basis for inhibitor potency and selectivity we solved inhibitor bound crystal structures of **19** and **32** (Fig 4.3, Appendix II). While both compounds are chemically very different, both **19** and **32** bind to the active site Glu-243 through a series of H-bonds. In the case of nNOS inhibitor-bound crystal structures, the fluorinated-benzyl group of both **19** and **32** was observed to bind to a hydrophobic pocket adjacent to the heme propionate group. This hydrophobic pocket is composed of residues Leu-337 and Met-236 from the N-terminal Zn^{2+} binding motif and Tyr-706 (Figure 4.3). Unlike nNOS, bNOS does not contain an N-terminal Zn^{2+} binding motif and therefore does not contain an analogous hydrophobic pocket adjacent to the heme propionate. Despite slight differences in binding of the fluorinated-benzyl group, binding of **19** and **32** was observed in both NOS isoforms to be further stabilized by H-bonds between the secondary amine of each inhibitor and the heme propionate groups. Direct comparison of the bsNOS-**19** and the previously reported nNOS-**19**[(86)] structures revealed the binding mode of **19** to be unchanged between the two NOS isoforms. However, the binding mode in bsNOS was further stabilized by the hydrophobic contact between Ile-218 and the aminoquinoline group of **19**. Since Ile-218 is within van der Waals contact of **19** and the analogous residue in nNOS is Val-567, our data suggest that the slight differences in hydrophobicity between Ile and Val allow for improved binding of **19** to bsNOS.

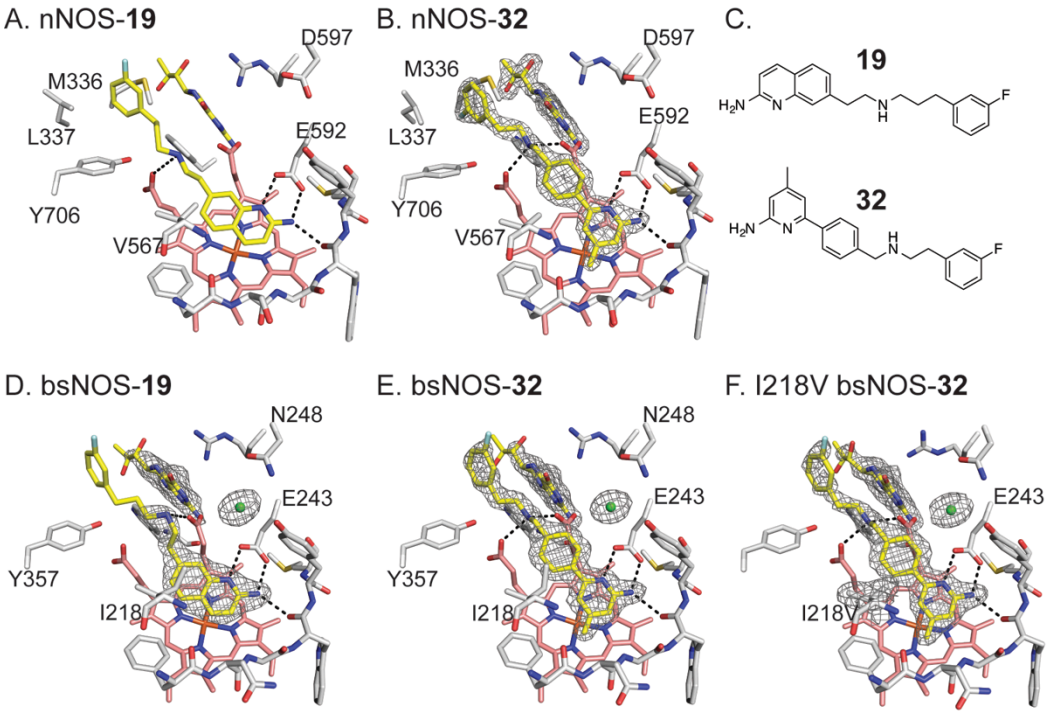

Figure 4.3 Inhibitor bound NOS crystal structures with select side chains colored white, heme group colored salmon, and both the active site inhibitor and H_4B molecule colored yellow. Both **19** and **32** bind to nNOS and bsNOS. In the nNOS structures (A and B) the fluorinated-benzyl group binds to a hydrophobic patch that is not present in bsNOS, adjacent to the heme propionate and composed of Y706, L337 and M336. At the NOS active sites both **19** and **32** bind in similar orientations to form a network of H bonds indicated by dashed lines. For the bsNOS structures, both **19** and **32** are within a hydrophobic contact of bsNOS I218. A) **19** bound to nNOS (PDB 4CAO). B) **32** bound to nNOS with the $2F_O$-F_C map contoured at 2.0σ. C) Chemical representations of **19** and **32**. D) **19** bound to bsNOS with the $2F_O$-F_C map contoured at 1.8σ. E) **32** bound to bsNOS with the $2F_O$-F_C map contoured at 1.8σ. F) **32** bound to I218V bsNOS with the $2F_O$-F_C map contoured at 1.8σ.

Similar to **19**, crystal structure analysis of **32** demonstrates the inhibitor-binding mode to be further stabilized by the hydrophobic contact between the inhibitor and Ile-218 (Fig 4.3C). In both the nNOS-**32** and I218V-bsNOS-**32** crystal structures, the inhibitor-binding mode of **32** is unchanged by the Ile/Val difference, as compared to WT bsNOS. To evaluate the contribution of Ile-218 to the inhibitor-binding mode we measured inhibitor binding using the imidazole displacement assay. From this analysis

we found the inhibitor binding of both **19** and **32** to be ~5-6 fold tighter to Ile-218 over I218V (Table 4.2). Between the crystal structures and binding assay results, our data suggest that the increased hydrophobicity of Ile-218 over the analogous mNOS Val residue improves inhibitor binding to bNOS. Considering that Ile-218 is conserved across all bNOS enzymes [(40)], future inhibitors designed to target bNOS should continue to exploit Ile-218 by using the scaffolds of **19** and **32**.

Table 4.2 Calculated K_S values by imidazole displacement for NOS ligands to bsNOS

Ligand	WT - K_S (μM)	I218V - K_S (μM)
L-Arg	4.8 ± 0.1[(40)]	2.0 ± 0.2[(40)]
19	3.6 ± 0.8	18 ± 2
32	8.9 ± 2.0	58 ± 4

Anti-MRSA Activity of NOS inhibitors

To evaluate the antibacterial potential of NOS inhibitors **19** and **32** on bacterial growth, we established a collaboration with the lab of Victor Nizet at UCSD who utilized the highly virulent CA-MRSA strain UAMS118 (*wt*) representative of the USA300 clonal linage and a previously engineered isogenic NOS deletion mutant [(20)]. Since previous experiments have shown bacterial *Δnos* strains to be more susceptible to H_2O_2-mediated killing [(18, 20, 22)], the Nizet group measured the effect of NOS inhibitors and H_2O_2 on *S. aureus* (Fig 4.4). The results both confirm previous findings that the *Δnos* strain is more susceptible to H_2O_2-mediated killing compared to the *wt* strain and further demonstrate that co-treatment of *S. aureus* with H_2O_2 and either **19** or **32** significantly increases the H_2O_2-mediated killing of the bacteria. Together these data suggest that survival of MRSA can be significantly lowered in the presence of oxidative stress when

a NOS inhibitor impairs bacterial NO production. These results are consistent with previous results indicating that blocking of NO signaling increases bacterial susceptibility to oxidative stress[21, 22] and indicate that **19** and **32** could perhaps function as antimicrobials to increase susceptibility to innate immune clearance. Furthermore, considering that many existing pharmaceutical antibiotics function through an oxidative mechanism [45], bNOS inhibitors like **19** and **32** could theoretically synergize to increase the killing efficiency of such agents. Despite the synergistic effect of NOS inhibitors and H_2O_2 on *S. aureus* survival, bacteria treated with **19** or **32** alone at 200 μM also showed reduced bacterial survival over time. The decreased survival observed for both *wt* and the *Δnos* strains as a result of **19** or **32** treatments implies that both molecules have additional off-target effects that further limit bacterial growth.

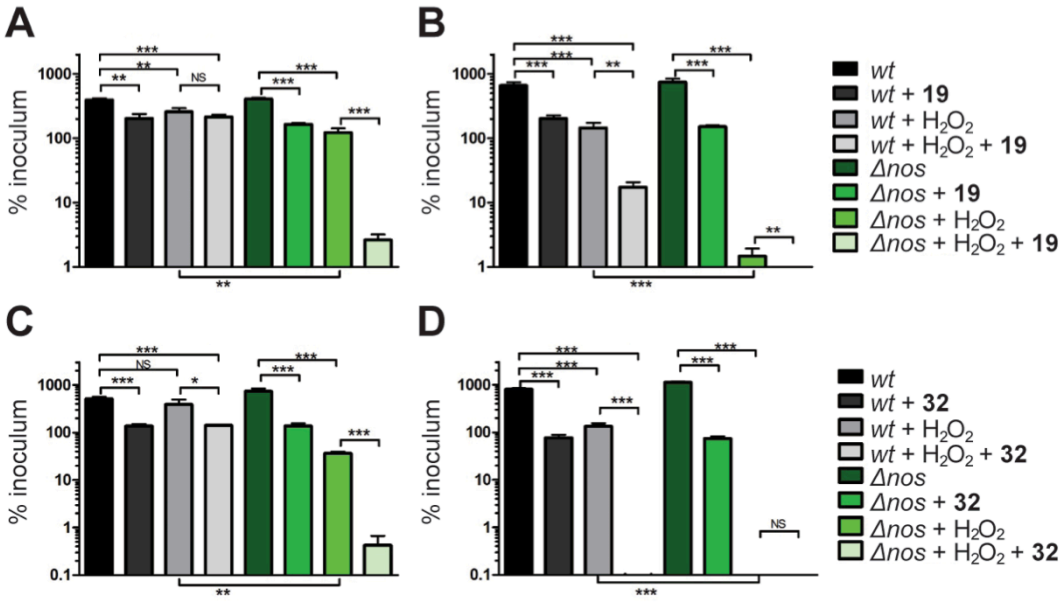

Figure 4.4 NOS inhibitors and peroxide work synergistically to eliminate *S. aureus* over time. Colonies of *S. aureus* observed after A) 30 min and B) 60 min exposure to 200 μM **19** and/or 5 mM H_2O_2. Similarly, *S. aureus* viability was also measured at C) 30 min and D) 60 min following exposure to 200 μM **32** and/or 5 mM H_2O_2. Error bars represent the mean ± SD of 3 replicates. Students *t* test gives ***P < 0.001, **P < 0.01 and *P < 0.05. The lab of Victor Nizet at UCSD performed these experiments.

Conclusion

Gene targeting experiments in pathogenic organisms including *B. anthracis* and *S. aureus* provided the basis for understanding bNOS function in mitigating antibiotic induced oxidative stress [(19-21)]. In earlier work, we found that a small number of inhibitors developed for selective nNOS inhibition also improved the efficacy of antimicrobials, suggesting that bNOS might be a viable drug target [(22)]. In the present study we sought to achieve two goals. The first was to identify bNOS-selective inhibitors with antimicrobial activity against the important human pathogen, MRSA. Of the many compounds screened two were found to bind well to bNOS and exhibit antimicrobial activity with selectivity over eNOS and iNOS. Selectivity over eNOS is more important since interfering with eNOS will adversely effect the critical role that eNOS derived NO plays in maintaining vascular tone and blood pressure [(38)]. The second goal was to use crystallography to identify subtle differences between the bNOS and mNOS active sites to exploit for future inhibitor design. Ile-218 (Val in mNOS) is one such potentially important difference. Previous work has shown Ile-218 to lower the off rate of NO [(40, 87)] and it is possible that Ile-218 also functions to trap inhibitors like **19** and **32** through hydrophobic contacts by limiting dissociation of the inhibitor-enzyme complex. Most interestingly, the I218V mutant binds the two inhibitors characterized in this study with about a 6-fold lower affinity than wild type, suggesting that Ile-218 functions to improve the inhibitor-protein association (K_A). Although this is a rather modest difference, we have also found that several NOS inhibitors more readily bind to the pterin site in bNOS [(88)]. Given the lower affinity of pterins for bNOS compared to mNOS, this is another important binding site difference between bNOS and mNOS. The Ile vs. Val active site

difference together with the larger structural differences in the pterin site are critical molecular features that could be exploited in future inhibitor design efforts.

Chapter 5

Inhibitor Bound Crystal Structures of Bacterial Nitric Oxide Synthase

Summary

Nitric oxide generated by bacterial nitric oxide synthase (NOS) increases the susceptibility of the gram-positive pathogen *Staphylococcus aureus* and *Bacillus anthracis* to oxidative stress including antibiotic-induced oxidative stress. Not surprisingly, NOS inhibitors also improve the effectiveness of antimicrobials. Development of potent and selective bacterial NOS inhibitors is complicated by the high active site sequence and structural conservation shared with the mammalian NOS isoforms. In order to exploit bacterial NOS for the development of new therapeutics, recognition of alternative NOS surfaces and pharmacophores suitable for drug binding is required. Here we report on a wide number of inhibitor bound bacterial NOS crystal structures to identify several compounds that interact with surfaces unique to the bacterial NOS. While binding studies indicate that these inhibitors weakly interact with the NOS active site, many of the inhibitors reported here provide a revised structural framework for the development of new antimicrobials that target bacterial NOS. In addition, mutagenesis studies reveal several key residues that unlock access to bacterial NOS surfaces that could provide the selectivity required to develop potent bacterial NOS inhibitors.

INTRODUCTION

NO is a critical signaling molecule produced by nitric oxide synthase (NOS). Dysregulation in NO signaling leads to a variety of pathophysiological conditions in

mammals. These conditions include—but are not limited to— neurodegeneration[4], septic shock[5], and tumor development[6]. Our group and others have focused on the development of competitive active site NOS inhibitors that both mitigate production of NO and demonstrate isoform selectivity for one of the three mammalian NOS isoforms: endothelial NOS (eNOS), inducible NOS (iNOS) or neuronal NOS (nNOS). In fact, several nNOS inhibitors have now been demonstrated to function as potential drugs for melanoma[8] and neurodegenerative diseases[9]. As a direct result of this previous work, a large and chemically diverse library of NOS inhibitors with varying potencies and specificity has been developed[35, 36].

With the advent of bacterial genome sequencing, bacterial NOS (bNOS) homologs have also been identified in several gram-positive bacteria. Current evidence indicates the role of bNOS to be varied amongst organisms ranging from nitrosylation of macromolecules[12, 14] to functioning as a commensal molecule[17] to enhancing pathogen virulence[20]. In pathogenic organisms *Bacillus anthracis* and *Staphylococcus aureus* gene deletion experiments first indicated bNOS to play an important role in ameliorating oxidative and antibiotic stress[18, 19, 21]. Recently, we also demonstrated that NOS inhibitors, originally designed to target nNOS, also function as antimicrobials in *Bacillus subtilis*[22, 23], a non-pathogenic model organism for *B. anthracis*. These studies were the first to demonstrate NOS inhibitors as improving the efficacy of antimicrobials. Therefore, the bNOS may serve as a useful therapeutic target for costly pathogens like *B. anthracis* and methicillin-resistant *S. aureus* that also utilize NO to mitigate oxidative and antibiotic stress.

Unfortunately, application of a generic NOS inhibitor for treatment of a gram-

positive infection would likely do more harm then good in humans. In order to exploit bNOS as a therapeutic target, specificity must be improved. Specificity against eNOS and iNOS is especially important, considering the essential role eNOS plays in maintaining blood-pressure homeostasis[89] and the important role iNOS plays in pathogen clearance[75]. Limiting eNOS specificity is further complicated by the fact that both bNOS and eNOS share a conserved Asn residue at the carboxylate-binding site of substrate L-Arg. The differences in electrostatics contributed by the Asn (Asp residue in nNOS and iNOS) have been useful for designing selective nNOS inhibitors[35, 37]. Recently, we also reported on several inhibitors with antimicrobial activity that targeted both the active and pterin binding sites of bNOS[23]. Since a co-substrate pterin group is required for NOS catalysis,[34] inhibitors that bind to both the active and pterin sites are an attractive option for limiting NO production. Further development of inhibitors that block pterin-binding represent one potential strategy for improving bNOS specificity since pterin binding affinity is drastically different between bNOS and mNOS, μM affinity[39] for bNOS vs. the nM affinity for mNOS[31].

In order to advance our understanding of the structural underpinnings that govern bNOS selectivity we report here over 30 different bNOS-inhibitor crystal structures. Additional characterization through mutagenesis and binding studies has led to the recognition of new hot spots that could prove useful towards future bNOS inhibitor design efforts. In particular, we identify a conserved Tyr near the active site that adopts an alternative rotameric position to make available a binding surface unique to the bacterial NOS.

RESULTS AND DISCUSSION

Sequence and Structure Based Differences Between NOS Isoforms

The design of selective bNOS inhibitors is difficult owing to the high sequence similarity among human NOS isoforms. In fact, saNOS shares in the range of 41-43% sequence identify with the human mNOS oxygenase domains; sequence conservation scored using Tcoffee[(90)]. At the active site alone, saNOS and nNOS share 8 out 10 residues within 5 Å of the native substrate L-Arg. The residue differences correspond to an Asn residue present at the L-Arg carboxylate binding site and an Ile residue that is positioned above the distal plane of the heme. Since eNOS also contributes an Asn residue at the L-Arg carboxylate binding site, inhibitors that target this electrostatic difference are not expected to be very selective. The second residue difference contributed by an Ile in bNOS is a Val in mNOS isoforms. Interestingly, the slightly bulkier Ile functions to lower NO release rates in bNOS.[(40)]

Fig. 1 presents structure-based sequence alignments between *B. subtilis* NOS (bsNOS) and mammalian NOS isoforms. Although the important pathogens *S. auerus* and *B. anthracis* are the therapeutic targets, we use *B. subtilis* NOS for our crystallographic studies since bsNOS crystals diffract to high resolution. Moreover, bsNOS and saNOS sequences are 98% conserved, based on a Tcoffee sequence alignment[(90)], hence bsNOS is a suitable model to study saNOS. The largest difference between the bacterial and mammalian NOS isoforms is the absence of an N-terminal Zn^{2+} binding motif in bNOS. The N-terminal Zn^{2+} binding motif is critical for dimerization in mammalian NOS isoforms and is absent in bNOS. Consequently, there is a large cleft at the dimerization interface that is a potential target for inhibitor design. This open

pocket encompasses the pterin cofactor binding site. Recently, several inhibitors were demonstrated to have a decreased selectivity for mNOS isoforms owing to the presence of a bulky pharmacophores that bound to the pterin site[(23)]. As shown in Fig 5.1, residues adjacent to the pterin site like R344 and S345 are unique to the bNOS, which indicates inhibitor design could be further improved to exploit these differences.

Near heme propionate group A there are additional residue differences (Fig 5.1) between NOS isoforms. Neither H128 nor K360 in *B. subtilis* are conserved in mNOS isoforms. Interestingly, H128 was recently implicated, through a molecular dynamics simulation, to limit the conformational dynamics of one specific inhibitor due to sterics[(23)]. Additional sequence differences are observed near bsNOS Y357 to include N354 and F356. Adjacent to Y357 is also the N-terminal Zn^{2+} binding motif. Hence inhibitors that bind to this region and not bind to the N-terminal Zn^{2+} binding motif may also serve as an excellent site for future structure-based inhibitor design.

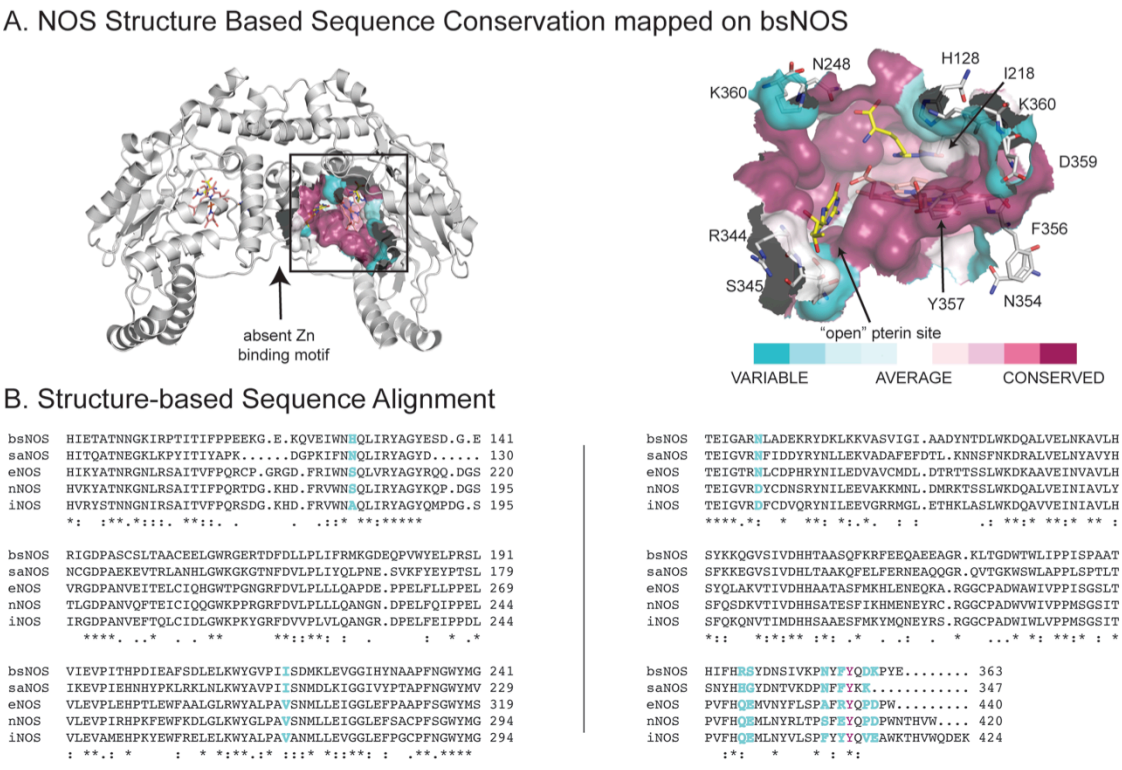

Figure 5.1 A) Crystal structure of bsNOS (PDB 4UQR) shown as a dimer with active site conservation colored using the consurf webserver[91, 92]. B) A partial sequence alignment of NOS isoforms based on a structural alignment using Chimera and crystal structures of bsNOS (PDB 4UQR), saNOS (PDB 1MJT), human eNOS (PDB 4D1O), human nNOS (PDB 4D1N) and human iNOS (PDB 3E7G). Residues identified on the bsNOS crystal structure in (A) are also colored in (B).

Inhibitor Binding

Imidazole displacement has proven to be an excellent assay for quantifying the spectral binding affinity (K_S) of NOS inhibitors based on the transition form an imidazole bound low spin iron-heme state to an inhibitor bound high spin state. As a first step towards characterization of inhibitor binding we analyzed 32 NOS inhibitors that have previously been characterized to bind mNOS isoforms. Consistent with previous results[22, 23], all inhibitors evaluated bind to bsNOS in the low μM range (Table 5.1).

Table 5.1 Comparison of inhibitor binding to bsNOS, using the imidazole displacement assay, indicates inhibitors studied here bind in the low μM range. Spectral binding constants that were not determined are indicated by *n.d.*

Inhibitor	K_S (μM)	Synthesis Reported	Inhibitor	K_S (μM)	Synthesis Reported
1	5.03 ± 0.04	*(76)*	**15**	18.3 ± 2.1	*(93)*
2	2.68 ± 0.12	*(76)*	**16**	*n.d.*	*(93)*
3	4.47 ± 0.36	*(77)*	**17**	22.3 ± 0.8	*(88)*
4	0.45 ± 0.05	*(94)*	**18**	62.14 ± 3.59	*(88)*
5	8.61 ± 0.50	*(77)*	**19**	99 ± 20	*(78)*
6	61.0 ± 3.5	*(95)*	**20**	17.8 ± 2.0	Not reported
7	237 ± 24	*(95)*	**21**	62.3 ± 7.6	*(78)*
8	18.7 ± 7.1	*(52)*	**22**	*n.d.*	*(78)*
9	37.9 ± 2.2	*(52)*	**23**	169 ± 31	*(96)*
10	*n.d.*	*(95)*	**24**	*n.d.*	*(96)*
11	23.3 ± 2.2	*(97)*	**25**	11.0 ± 0.8	*(96)*
12	25.6 ± 0.7	*(98)*	**26**	127 ± 44	*(78)*
13	50.46 ± 3.56	*(93)*	**27**	72.4 ± 8.9	*(99)*
14	57.6 ± 8.7	*(93)*	**28**	7.73 ± 0.43	*(96)*

Pterin Site Binding

NOS inhibitors that target the pterin site have previously been demonstrated to have antimicrobial properties against *B. subtilis* [(22, 23)]. Crystal structure analyses revealed two additional compounds, **5** and **15**, to interact with the pterin site. In the case of **5**, one of the aminopyridine groups displaces the pterin molecule in order to H-bond with heme propionate D (Figure 5.2). This binding motif has previously been observed in bNOS with inhibitors containing two aminopyridine groups[(22, 23)]. Identification of inhibitors that bind to the pterin site are interesting because the open cavity adjacent to the pterin binding site is unique to the bacterial NOS. Comparison of **5** binding to nNOS reveals the inhibitor to bind in a very different orientation (Fig 5.2C). In the case of nNOS-**5** the inhibitor interacts with heme propionate A by inducing an alternative

conformation in Y706. In several cases, potent nNOS inhibitors have been identified to bind heme propionate A by inducing an alternative conformation in a nearby Tyr[(100)]. For aminopyridine-based inhibitors the alternative rotameric position of Tyr results in a tight bi-furcated H-bond between the heme propionate and inhibitor. The alternative rotameric position of Tyr is further stabilized by a π-π stacking interaction between the Tyr residue and aminopyridine-based inhibitors. In nNOS **5** is likely not able to H-bond with heme propionate D because the binding affinity of H_4B is very tight[(31)]. Since binding of H_4B to bNOS is weak, **5** can more easily out compete H_4B.

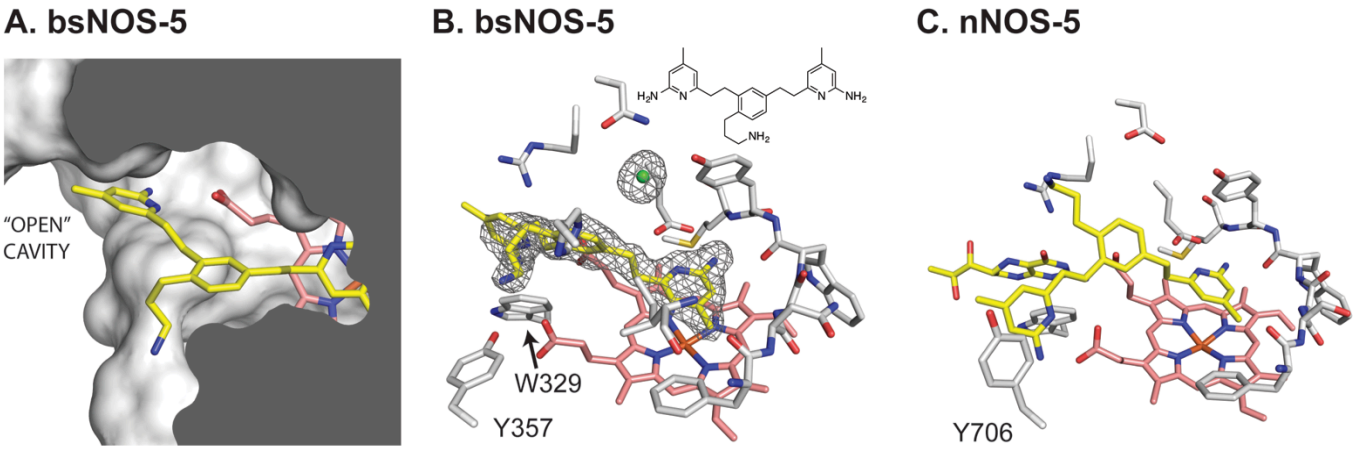

Figure 5.2 A) **5** bound to bsNOS with the aminopyridine group bound to the heme propionate and exposed to a solvent accessible surface that is unique to bNOS. B) Stick representation and 2Fo-Fc at 1.0σ of **5** bound to bsNOS. C) Stick representation of nNOS-**5** (PDB 4IMT). In all representation the heme group is colored salmon, ligands are colored yellow, and the protein residues are colored white.

In the case of **15**, inhibitor binding to bsNOS distorts the pterin binding site by inducing an alternative rotameric position in W329 (Fig 5.3A). Crystallographic refinement shows residual electron density consistent with an imidazole molecule forming a stacking interaction with W329. Direct comparison of the binding modes of **15** to bsNOS and nNOS are nearly identical (Fig 5.3A and 5.3B). In both cases, heme propionate D is in an atypical conformation with the carboxyl group pointing

perpendicular to the plane of the heme. This atypical conformation of heme propionate D induced by **15** binding is likely what leads to the alternative rotameric position of W329.

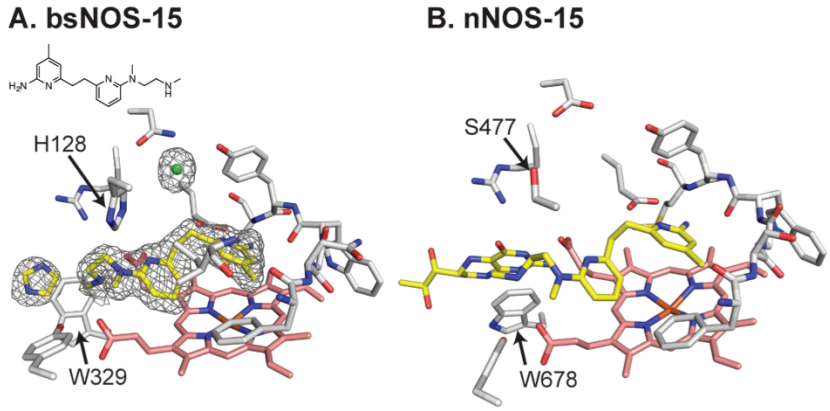

Figure 5.3 Inhibitor **15** binds in a near identical conformation to both A) bsNOS and B) nNOS. In the case of bsNOS-**15** a torque is applied to W329 and the pterin site is distorted. 2Fo-Fc maps for ligands are shown at 1.0σ.

Tyrosine Flipping Opens a Channel for bNOS Inhibitor Binding

A conserved tyrosine in all NOS isoforms H-bonds with heme propionate A. This tyrosine has previously been observed to occupy alternative rotameric positions in nNOS in order to accommodate inhibitors[(100)]. In several cases, including nNOS-**5** (Fig 5.2C), inhibitor potency and selectivity is enhanced by the propensity of nNOS Y706 to occupy alternative conformations due to the formation of two H-bonds with the heme propionate group[(100)]. This Tyr is conserved in bsNOS and also adopts alternative conformations in the presence of specific inhibitors. For example, in both bsNOS and nNOS **3** binds to heme propionate A through a bifurcated H-bond and a π-π stacking interaction between the conserved Tyr and aminopyridine group (Fig 5.4). Analogous binding interactions that result in a flipped Y357 in bsNOS are also observed for **2**, **11**,

12, and **1** (Appendix II). Moreover, these binding interactions lead to formation of a non-canonical surface that is unique to bNOS, labeled open binding surface in Fig 5.4. This surface is unique to bNOS owing to both the drastic differences in surface residues at this site (Fig 1) and the absent Zn^{2+} binding motif (Fig 5.4).

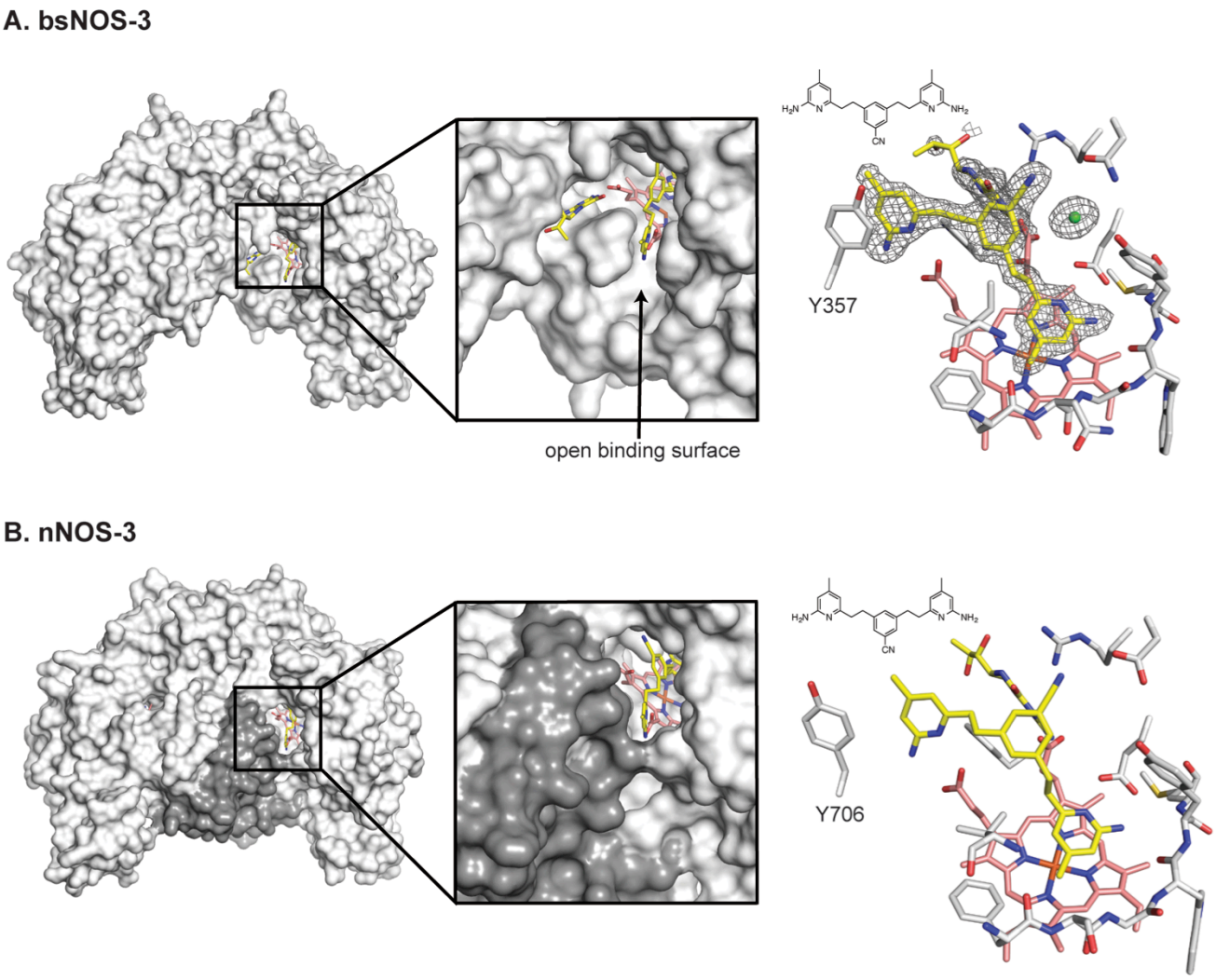

Figure 5.4 Inhibitor **3** induces a conformational change in both A) bsNOS Y357 and nNOS Y706. Rotation of Y357 in bsNOS opens access to a novel binding surface depicted in A. Surface representations of NOS oxygenase domains as dimers are colored white with the N-terminal Zn^{2+} motif colored grey. Heme groups are colored salmon and ligands ared colored yellow. The 2Fo-Fc map for bsNOS-3 is show at 1.0σ. The nNOS-**3** models were generated using PDB 4IMW.

To better understand the role of Tyr flipping and the H-bond shared between the NOS derived Tyr and the heme propionate group, we introduced mutation Y357F to bsNOS. Crystal structure analysis of Y357F with L-Arg, a ligand that does not induce Tyr flipping, revealed the rotameric position of Y357F to be near identical to the native Y357 (Fig 5.5). These data indicate that aside from the H-bond between Y357 and the heme propionate, there is an energetic barrier between alternative conformations of Y357. Consequently, the “flipped” rotameric position of Y357 can only be induced upon binding of specific ligands. This flipping requires an enthalpically favorable H-bond between the inhibitor and heme propionate groups to overcome the energetic barrier of an alternative rotameric conformation. These thermodynamic considerations are observed with the binding of inhibitor **4** (Fig 5.6). **4** is an inhibitor that induces a flipped out conformation in nNOS but not bsNOS (Fig 5.6A and 5.6B). However, the flipped conformation can be rescued in bsNOS by the introduction of Y357F (Fig 5.6C). Based on the crystal structures, it is clear that the orientation of **4** binding is controlled by H-bonds. More specifically, the binding of **4** to bsNOS is stabilized by a 3.3 Å H-bond between the pyrollidine ring and the carbonyl group of H_4B. However, the distance between the H_4B carbonyl group and the pyrollidine amine is extended to 3.7 Å in Y357 bsNOS-**4** in order to accommodate the two new H-bonds formed between **4** and heme propionate A.

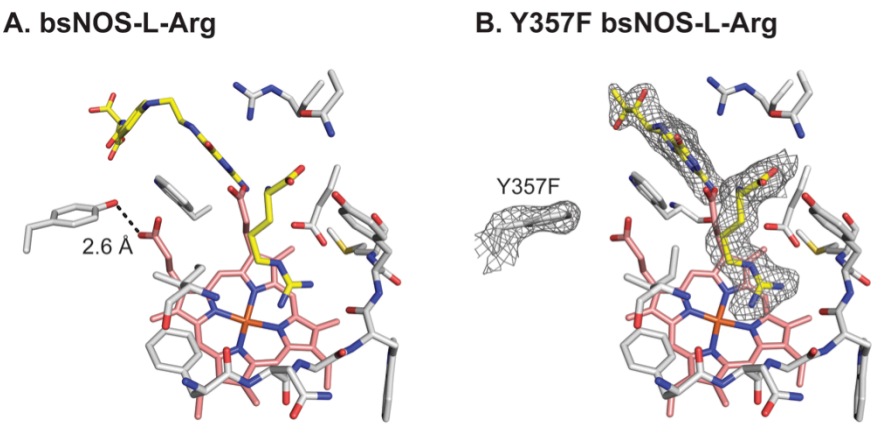

Figure 5.5 A) Active site view of L-Arg and tetrahydrofolate bound to bsNOS (redrawn from PDB 1M7V). B) Y357F bsNOS with L-Arg and H_4B bound and shown with 2Fo-Fc map contoured at 1.0σ. Protein residues of NOS active site are colored white, heme is colored salmon, and substrates are colored yellow.

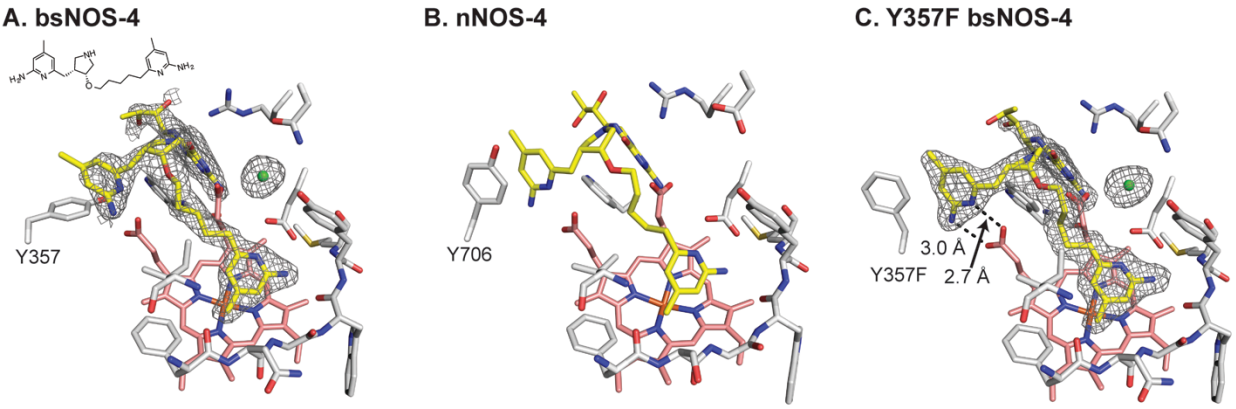

Figure 5.6 Inhibitor 4 bound to NOS active sites with substrates colored yellow, heme colored salmon, and protein residues colored white. A) 2Fo-Fc map contoured at 1.0σ for bsNOS-**4**. B) **4** binds to nNOS by coordinating to the heme propionate group. C) **4** binding to bsNOS is only able to coordinate heme propionate by introduction of mutation Y357F. 2Fo-Fc map of **4** is contoured at 1.0σ.

Thiophencarboximidamide Inhibitor Binding

Considerations for improving NOS inhibitor bioavailability has also led to the generation of thiophencarboximidamide based NOS inhibitors[(101)]. These inhibitors preserve a bifurcated H-bond with the active site Glu (Fig 5.7 and Appendix II).

Interestingly, in bNOS the conjugated ring system of this class of inhibitors forms a hydrophobic interaction with Ile218. Hence, molecules that utilize this scaffold may lead to improved binding to bNOS since the bNOS active site is slightly more hydrophobic then the mNOS active sites owing to the Ile/Val difference (Fig 5.1). Previous mutagenesis studies, however, have indicated that the binding mode of the benzyl substituted thiophencarboximidamide group to be unchanged by introduction of I218V in bsNOS[(23)]. This is not surprising since the benzyl portion of the inhibitor is a rigid.

The binding mode of several thiophencarboximidamide-based inhibitors characterized were found to bind uniquely to bsNOS. Due to the extended length of **24**, **23**, **25**, and **28** the inhibitors were able wrap around the active site (Fig 5.7 and Appendix II). This allows the molecules to access a surface on bsNOS that is not accessible to mNOS isoforms. Specifically, comparison of the binding modes for **24** in bsNOS and nNOS reveals one of the two thiophencarboximidamide groups to bind very differently in NOS isoforms. For nNOS one of the thiophencarboximidamide groups is unable to extend outside of the active site because the N-terminal Zn^{2+} binding motif sterically restricts the binding of **24** to the active site. Residues that sterically limit the binding of **24** include L337 and M336 (Fig 5.7B). In sharp contrast, **24** binds to bsNOS by extending outside the active site to interact with a surface adjacent to Y357 (Fig 5.7A). Despite this unique structural observation, it remains unclear if the extended conformation of **24** contributes to bsNOS binding affinity. Regardless, molecules like **24**, **23**, **25**, and **28** represent an interesting chemical scaffold that could be further improved upon to design inhibitors that exploit the residue differences on the surface of bNOS. Alternatively, addition of a bulky chemical group to a NOS inhibitor may also prove to be

a useful solution for improving specificity towards bNOS. As bulky pharmacophores would likely be unable to interact with the mNOS active sites owing to the steric crowding presented by the N-terminal Zn^{2+} binding motif.

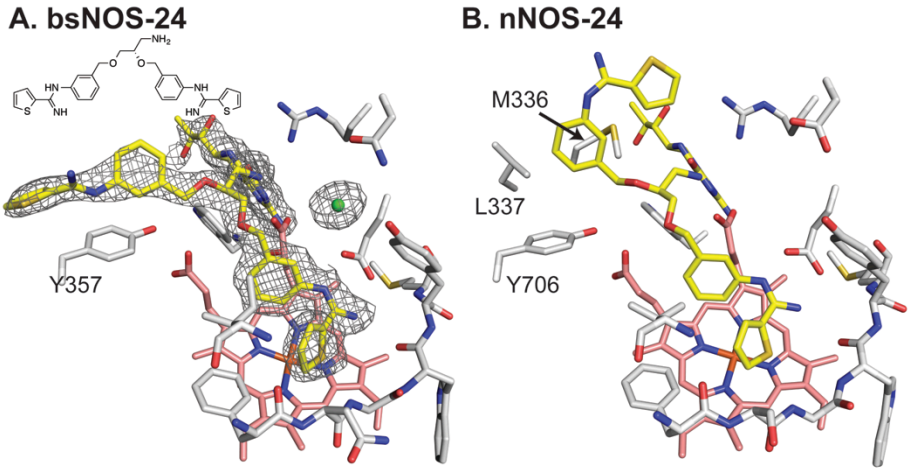

Figure 5.7 A) Binding mode of **24** to bsNOS is extended to accommodate binding on surface of protein outside of the active site. 2Fo-Fc map of **24**, H4B and active site chloride anion contoured at 1.0σ. B) **24** binding to nNOS is due to the partially blocked active site contributed by residues L337 and M336 (redrawn from PDB 4UPN).

CONCLUSION

The NOS inhibitor design effort has largely been aided by the structural characterization of NOS-inhibitor interactions[(35)]. These studies have been useful to provide a molecular understanding of residues that govern isoform selectivity and useful pharmacophores. Since the previous application of mNOS inhibitors to a bacterial system has proven to function as a potential antimicrobial target[(22, 23)], a renewed understanding of NOS isoform selectivity is needed to exploit the bNOS system. In order to further our understanding of bNOS inhibitor interactions we solved many bsNOS-inhibitor crystal structures. From our studies we identified an alternative rotameric position at Y357 induced upon ligand binding and several inhibitors that

exploit the pterin site. In previous studies we found that Y706 in nNOS (corresponds to Y357 in bsNOS) can also move to accommodate inhibitors while Tyr movement is much more restricted in eNOS. This might at first preclude targeting Y357 movement as a specific feature in bNOS drug design. However, a serious limitation in the use of these inhibitors for targeting nNOS for neurodegenerative diseases is poor blood brain barrier penetration, which is not an issue with anti-bacterials. The bNOS pterin site should provide another excellent target for selective bNOS inhibitors. Aminopyridine inhibitors are more readily able to displace pterin cofactors in bNOS than in the mammalian NOS isoforms very likely because the affinity for pterins is much weaker in bNOS. Future derivatization of inhibitors that exploit the pterin site and the flipping mechanism of Y357 could prove useful for engineering bNOS specificity as these molecules could easily exploit residues adjacent to the binding sites that are unique to bNOS.

Final Conclusions

Initial genetic studies established bNOS to play an important role in protecting pathogens *Staphylococcus aureus* and *Bacillus anthracis* against oxidative and antibiotic induced stress[17, 21]. Current evidence indicates bNOS functions to produce NO, of which, nitrosylates and modulates protective mechanisms that include activating a catalase and limiting damaging Fenton chemistry. Based on these observations it was our initial hypothesis that inhibition of bNOS would improve the efficacy of antibiotics, that function through an oxidative mechanism, to serve as a new antimicrobial target. Unfortunately, a synthetic route towards the design and development of a bNOS selective inhibitor was initially unclear as we were unaware of the structural underpinnings that governed bNOS selectivity over the mammalian NOS isoforms. Considering that the bNOS and mNOS active sites share a high degree of sequence homology, addressing selectivity issues would be of paramount importance moving forward in the exploitation of bNOS as a therapeutic target.

To evaluate our initial hypothesis we first established a model system using the nonpathogenic bacteria *Bacillus subtilis* to screen NOS inhibitors for antimicrobial properties. In the presence of other antimicrobials we identified several NOS inhibitors with excellent antimicrobial properties (Chapter 1). These studies served as the first proof-of-principle that NOS inhibitors can function as antimicrobials. More importantly, additional crystallographic studies provided the first structural understanding of bNOS inhibition and led to the important recognition that bNOS selectivity can be improved by targeting the pterin co-substrate binding site, of which is adjacent to the active site.

Despite an initial structural understanding of NOS inhibition, characterization of NOS inhibitors potency had yet to be reported. In order to characterize inhibitor potency we identified redox partners and developed a chimeric protein that proved useful for evaluating bNOS activity and inhibitor potency (Chapter 2). These new tools allowed us to first report on the structure-activity relationship of several NOS inhibitors in the bNOS system. More importantly, these new tools allowed us to adapt the new assays to a semi-high throughput screen and rapidly identify potent bNOS inhibitors (Chapter 4).

In collaboration with the Nizet Lab at UCSD we were able to screen several of the potent NOS inhibitors against the deadly pathogen methicillin resistant *S. aureus*. As previously observed in *B. subtilis* the bNOS inhibitors worked synergistically with antimicrobials to limit bacterial growth and provide additional support for the continued development of bNOS inhibitors. With selectivity in mind, we also collaborated with the Silverman Lab at Northwestern University to design inhibitors that selectively target both the bNOS active and pterin sites. Using structure based drug design approaches the inhibitors developed were found to bind at both the active and pterin sites of bsNOS and, most importantly, demonstrated a decreased affinity for the mammalian NOS isoforms and antimicrobial properties against *B. subtilis* (Chapter 3). Taking advantage of the large library of mammalian NOS inhibitors we have developed in collaboration with the Silverman group at Northwestern, further structural characterization of bNOS-inhibitor interactions also led to the recognition of several additional strategies for developing selective bNOS inhibitors (Chapter 5). Specifically, binding of bNOS inhibitors that exploit a conserved tyrosine allow for the inhibitors to access several surfaces that are unique to the bacterial NOS.

In short, we have identified and established several principles required to develop selective bNOS inhibitors using a combination of enzyme-activity studies, structural studies, and microbiological studies. Development of potent bNOS inhibitors requires exploiting the active site Ile-218 (Chapter 4) and the surface cavities adjacent to the active site; most notably the pterin co-substrate site. One re-occurring concern in our studies has been that bNOS inhibitors are toxic at the concentrations required to observe antimicrobial properties. In order to lower the toxicity of these compounds and improve the selectivity, inhibitors with higher rates of association and lower dissociation rates need to be developed. Furthermore, what remains to be shown is to what degree inhibitors lower bacterial concentrations of NO within a cell-based system. Continued studies on the bNOS system and development of bNOS inhibitors may serve as an important new resource in the fight against bacterial pathogens like *S. aureus* and *B. anthracis*.

References

1. Iwasaki, H., Matsubayashi, R., and Mori, T. (1956) Studies on Denitrification .2. Production of Nitric Oxide and Its Utilization in the N-N-Linkage Formation by Denitrifying Bacteria, *J Biochem-Tokyo 43*, 295-305.
2. Ignarro, L. J., Buga, G. M., Wood, K. S., Byrns, R. E., and Chaudhuri, G. (1987) Endothelium-derived relaxing factor produced and released from artery and vein is nitric oxide, *Proc. Natl. Acad. Sci. U.S.A. 84*, 9265-9269.
3. Nathan, C., and Xie, Q. W. (1994) Nitric oxide synthases: roles, tolls, and controls, *Cell 78*, 915-918.
4. Hunot, S., Boissiere, F., Faucheux, B., Brugg, B., Mouatt-Prigent, A., Agid, Y., and Hirsch, E. C. (1996) Nitric oxide synthase and neuronal vulnerability in Parkinson's disease, *Neuroscience 72*, 355-363.
5. Thiemermann, C. (1997) Nitric oxide and septic shock, *Gen. Pharmacol. 29*, 159-166.
6. Singh, S., and Gupta, A. K. (2011) Nitric oxide: role in tumour biology and iNOS/NO-based anticancer therapies, *Cancer Chemoth. Pharm. 67*, 1211-1224.
7. Alderton, W. K., Cooper, C. E., and Knowles, R. G. (2001) Nitric oxide synthases: structure, function and inhibition, *Biochem. J. 357*, 593-615.
8. Yang, Z., Misner, B., Ji, H., Poulos, T. L., Silverman, R. B., Meyskens, F. L., and Yang, S. (2013) Targeting nitric oxide signaling with nNOS inhibitors as a novel strategy for the therapy and prevention of human melanoma, *Antioxid. Redox. Sign. 19*, 433-447.
9. Ji, H., Tan, S., Igarashi, J., Li, H., Derrick, M., Martasek, P., Roman, L. J., Vasquez-Vivar, J., Poulos, T. L., and Silverman, R. B. (2009) Selective neuronal nitric oxide synthase inhibitors and the prevention of cerebral palsy, *Ann. Neurol. 65*, 209-217.
10. Gusarov, I., Starodubtseva, M., Wang, Z. Q., McQuade, L., Lippard, S. J., Stuehr, D. J., and Nudler, E. (2008) Bacterial nitric-oxide synthases operate without a dedicated redox partner, *J. Biol. Chem. 283*, 13140-13147.
11. Buddha, M. R., and Crane, B. R. (2005) Structure and activity of an aminoacyl-tRNA synthetase that charges tRNA with nitro-tryptophan, *Nat. Struct. Mol. Biol. 12*, 274-275.
12. Buddha, M. R., Keery, K. M., and Crane, B. R. (2004) An unusual tryptophanyl tRNA synthetase interacts with nitric oxide synthase in Deinococcus radiodurans, *Proc. Natl. Acad. Sci. U.S.A. 101*, 15881-15886.
13. Liu, Y., Zhou, J., Omelchenko, M. V., Beliaev, A. S., Venkateswaran, A., Stair, J., Wu, L., Thompson, D. K., Xu, D., Rogozin, I. B., Gaidamakova, E. K., Zhai, M., Makarova, K. S., Koonin, E. V., and Daly, M. J. (2003) Transcriptome dynamics of Deinococcus radiodurans recovering from ionizing radiation, *Proc. Natl. Acad. Sci. U.S.A. 100*, 4191-4196.
14. Johnson, E. G., Sparks, J. P., Dzikovski, B., Crane, B. R., Gibson, D. M., and Loria, R. (2008) Plant-pathogenic Streptomyces species produce nitric oxide synthase-derived nitric oxide in response to host signals, *Chem. Biol. 15*, 43-50.
15. Healy, F. G., Wach, M., Krasnoff, S. B., Gibson, D. M., and Loria, R. (2000) The txtAB genes of the plant pathogen Streptomyces acidiscabies encode a peptide

synthetase required for phytotoxin thaxtomin A production and pathogenicity, *Molecular microbiology 38*, 794-804.
16. Kers, J. A., Wach, M. J., Krasnoff, S. B., Widom, J., Cameron, K. D., Bukhalid, R. A., Gibson, D. M., Crane, B. R., and Loria, R. (2004) Nitration of a peptide phytotoxin by bacterial nitric oxide synthase, *Nature 429*, 79-82.
17. Gusarov, I., Gautier, L., Smolentseva, O., Shamovsky, I., Eremina, S., Mironov, A., and Nudler, E. (2013) Bacterial nitric oxide extends the lifespan of C. elegans, *Cell 152*, 818-830.
18. Shatalin, K., Gusarov, I., Avetissova, E., Shatalina, Y., McQuade, L. E., Lippard, S. J., and Nudler, E. (2008) Bacillus anthracis-derived nitric oxide is essential for pathogen virulence and survival in macrophages, *Proc. Natl. Acad. Sci. U.S.A. 105*, 1009-1013.
19. Gusarov, I., Shatalin, K., Starodubtseva, M., and Nudler, E. (2009) Endogenous nitric oxide protects bacteria against a wide spectrum of antibiotics, *Science 325*, 1380-1384.
20. van Sorge, N. M., Beasley, F. C., Gusarov, I., Gonzalez, D. J., von Kockritz-Blickwede, M., Anik, S., Borkowski, A. W., Dorrestein, P. C., Nudler, E., and Nizet, V. (2013) Methicillin-resistant Staphylococcus aureus bacterial nitric-oxide synthase affects antibiotic sensitivity and skin abscess development, *J. Biol. Chem. 288*, 6417-6426.
21. Gusarov, I., and Nudler, E. (2005) NO-mediated cytoprotection: instant adaptation to oxidative stress in bacteria, *Proc. Natl. Acad. Sci. U.S.A. 102*, 13855-13860.
22. Holden, J. K., Li, H., Jing, Q., Kang, S., Richo, J., Silverman, R. B., and Poulos, T. L. (2013) Structural and biological studies on bacterial nitric oxide synthase inhibitors, *Proc. Natl. Acad. Sci. U.S.A. 110*, 18127-18131.
23. Holden, J. K., Kang, S., Hollingsworth, S. A., Li, H., Lim, N., Chen, S., Huang, H., Xue, F., Tang, W., Silverman, R. B., and Poulos, T. L. (2015) Structure-based design of bacterial nitric oxide synthase inhibitors, *J. Med. Chem. 58*, 994-1004.
24. Campbell, M. G., Smith, B. C., Potter, C. S., Carragher, B., and Marletta, M. A. (2014) Molecular architecture of mammalian nitric oxide synthases, *Proc. Natl. Acad. Sci. U.S.A. 111*, E3614-3623.
25. Smith, B. C., Underbakke, E. S., Kulp, D. W., Schief, W. R., and Marletta, M. A. (2013) Nitric oxide synthase domain interfaces regulate electron transfer and calmodulin activation, *Proc. Natl. Acad. Sci. U.S.A. 110*, E3577-3586.
26. Wang, Z. Q., Lawson, R. J., Buddha, M. R., Wei, C. C., Crane, B. R., Munro, A. W., and Stuehr, D. J. (2007) Bacterial flavodoxins support nitric oxide production by Bacillus subtilis nitric-oxide synthase, *J. Biol. Chem. 282*, 2196-2202.
27. Holden, J. K., Lim, N., and Poulos, T. L. (2014) Identification of redox partners and development of a novel chimeric bacterial nitric oxide synthase for structure activity analyses, *J. Biol. Chem. 289*, 29437-29445.
28. Agapie, T., Suseno, S., Woodward, J. J., Stoll, S., Britt, R. D., and Marletta, M. A. (2009) NO formation by a catalytically self-sufficient bacterial nitric oxide synthase from Sorangium cellulosum, *Proc. Natl. Acad. Sci. U.S.A. 106*, 16221-16226.

29. Knowles, R. G., Palacios, M., Palmer, R. M., and Moncada, S. (1990) Kinetic characteristics of nitric oxide synthase from rat brain, *Biochem J 269*, 207-210.
30. Poulos, T. L. (2005) Structural biology of heme monooxygenases, *Biochem Bioph Res Co 338*, 337-345.
31. Tejero, J., and Stuehr, D. (2013) Tetrahydrobiopterin in nitric oxide synthase, *IUBMB Life 65*, 358-365.
32. Li, H. Y., and Poulos, T. L. (2005) Structure-function studies on nitric oxide synthases, *Journal of inorganic biochemistry 99*, 293-305.
33. Hurshman, A. R., Krebs, C., Edmondson, D. E., and Marletta, M. A. (2003) Ability of tetrahydrobiopterin analogues to support catalysis by inducible nitric oxide synthase: formation of a pterin radical is required for enzyme activity, *Biochemistry 42*, 13287-13303.
34. Adak, S., Aulak, K. S., and Stuehr, D. J. (2002) Direct evidence for nitric oxide production by a nitric-oxide synthase-like protein from Bacillus subtilis, *Journal of Biological Chemistry 277*, 16167-16171.
35. Poulos, T. L., and Li, H. (2013) Structural basis for isoform-selective inhibition in nitric oxide synthase, *Acc. Chem. Res. 46*, 390-398.
36. Silverman, R. B. (2009) Design of selective neuronal nitric oxide synthase inhibitors for the prevention and treatment of neurodegenerative diseases, *Acc. Chem. Res. 42*, 439-451.
37. Flinspach, M. L., Li, H., Jamal, J., Yang, W., Huang, H., Hah, J. M., Gomez-Vidal, J. A., Litzinger, E. A., Silverman, R. B., and Poulos, T. L. (2004) Structural basis for dipeptide amide isoform-selective inhibition of neuronal nitric oxide synthase, *Nat. Struct. Mol. Biol. 11*, 54-59.
38. Yamamoto, K., Shimamura, K., Sekiguchi, F., and Sunano, S. (2001) Effects of NG-nitro-L-arginine on the blood pressure of spontaneously hypertensive rats with different degrees of hypertension, *Clinical and experimental hypertension 23*, 533-544.
39. Crane, B. R., Sudhamsu, J., and Patel, B. A. (2010) Bacterial Nitric Oxide Synthases, *Annu. Rev. Biochem. 79*, 445-470.
40. Wang, Z. Q., Wei, C. C., Sharma, M., Pant, K., Crane, B. R., and Stuehr, D. J. (2004) A conserved Val to Ile switch near the heme pocket of animal and bacterial nitric-oxide synthases helps determine their distinct catalytic profiles, *J. Biol. Chem. 279*, 19018-19025.
41. Sudhamsu, J., and Crane, B. R. (2009) Bacterial nitric oxide synthases: what are they good for?, *Trends Microbiol 17*, 212-218.
42. Moncada, S., Palmer, R. M., and Higgs, E. A. (1991) Nitric oxide: physiology, pathophysiology, and pharmacology, *Pharmacol Rev 43*, 109-142.
43. Griffith, O. W., and Stuehr, D. J. (1995) Nitric oxide synthases: properties and catalytic mechanism, *Annual review of physiology 57*, 707-736.
44. Calabrese, V., Mancuso, C., Calvani, M., Rizzarelli, E., Butterfield, D. A., and Stella, A. M. (2007) Nitric oxide in the central nervous system: neuroprotection versus neurotoxicity, *Nature reviews. Neuroscience 8*, 766-775.
45. Kohanski, M. A., Dwyer, D. J., Hayete, B., Lawrence, C. A., and Collins, J. J. (2007) A common mechanism of cellular death induced by bactericidal antibiotics, *Cell 130*, 797-810.

46. Mcmillan, K., and Masters, B. S. S. (1993) Optical-Difference Spectrophotometry as a Probe of Rat-Brain Nitric-Oxide Synthase Heme-Substrate Interaction, *Biochemistry 32*, 9875-9880.
47. Berka, V., Chen, P. F., and Tsai, A. L. (1996) Spatial relationship between L-arginine and heme binding sites of endothelial nitric-oxide synthase, *J. Biol. Chem. 271*, 33293-33300.
48. Roman, L. J., Sheta, E. A., Martasek, P., Gross, S. S., Liu, Q., and Masters, B. S. (1995) High-level expression of functional rat neuronal nitric oxide synthase in Escherichia coli, *Proc. Natl. Acad. Sci. U.S.A. 92*, 8428-8432.
49. Martasek, P., Liu, Q., Liu, J., Roman, L. J., Gross, S. S., Sessa, W. C., and Masters, B. S. (1996) Characterization of bovine endothelial nitric oxide synthase expressed in E. coli, *Biochem Bioph Res Co 219*, 359-365.
50. Pant, K., Bilwes, A. M., Adak, S., Stuehr, D. J., and Crane, B. R. (2002) Structure of a nitric oxide synthase heme protein from Bacillus subtilis, *Biochemistry 41*, 11071-11079.
51. Bird, L. E., Ren, J., Zhang, J., Foxwell, N., Hawkins, A. R., Charles, I. G., and Stammers, D. K. (2002) Crystal structure of SANOS, a bacterial nitric oxide synthase oxygenase protein from Staphylococcus aureus, *Structure 10*, 1687-1696.
52. Jing, Q., Li, H., Chreifi, G., Roman, L. J., Martasek, P., Poulos, T. L., and Silverman, R. B. (2013) Chiral linkers to improve selectivity of double-headed neuronal nitric oxide synthase inhibitors, *Bioorg. Med. Chem. Lett. 23*, 5674-5679.
53. White, K. A., and Marletta, M. A. (1992) Nitric oxide synthase is a cytochrome P-450 type hemoprotein, *Biochemistry 31*, 6627-6631.
54. Adak, S., Bilwes, A. M., Panda, K., Hosfield, D., Aulak, K. S., McDonald, J. F., Tainer, J. A., Getzoff, E. D., Crane, B. R., and Stuehr, D. J. (2002) Cloning, expression, and characterization of a nitric oxide synthase protein from Deinococcus radiodurans, *Proc. Natl. Acad. Sci. U.S.A. 99*, 107-112.
55. Pufahl, R. A., Wishnok, J. S., and Marletta, M. A. (1995) Hydrogen peroxide-supported oxidation of NG-hydroxy-L-arginine by nitric oxide synthase, *Biochemistry 34*, 1930-1941.
56. Seo, D., Kamino, K., Inoue, K., and Sakurai, H. (2004) Purification and characterization of ferredoxin-NADP+ reductase encoded by Bacillus subtilis yumC, *Arch. Microbiol. 182*, 80-89.
57. Komori, H., Seo, D., Sakurai, T., and Higuchi, Y. (2010) Crystal structure analysis of Bacillus subtilis ferredoxin-NADP(+) oxidoreductase and the structural basis for its substrate selectivity, *Protein science : a publication of the Protein Society 19*, 2279-2290.
58. Moore, C. M., Nakano, M. M., Wang, T., Ye, R. W., and Helmann, J. D. (2004) Response of Bacillus subtilis to nitric oxide and the nitrosating agent sodium nitroprusside, *J. Bacteriol. 186*, 4655-4664.
59. Nakano, M. M. (2002) Induction of ResDE-dependent gene expression in Bacillus subtilis in response to nitric oxide and nitrosative stress, *J. Bacteriol. 184*, 1783-1787.

60. Reents, H., Munch, R., Dammeyer, T., Jahn, D., and Hartig, E. (2006) The Fnr regulon of Bacillus subtilis, *J. Bacteriol. 188*, 1103-1112.
61. Ollinger, J., Song, K. B., Antelmann, H., Hecker, M., and Helmann, J. D. (2006) Role of the Fur regulon in iron transport in Bacillus subtilis, *J. Bacteriol. 188*, 3664-3673.
62. Seo, D., Okabe, S., Yanase, M., Kataoka, K., and Sakurai, T. (2009) Studies of interaction of homo-dimeric ferredoxin-NAD(P)+ oxidoreductases of Bacillus subtilis and Rhodopseudomonas palustris, that are closely related to thioredoxin reductases in amino acid sequence, with ferredoxins and pyridine nucleotide coenzymes, *Biochim. Biophys. Acta 1794*, 594-601.
63. Gray, H. B., and Winkler, J. R. (2003) Electron tunneling through proteins, *Q Rev Biophys 36*, 341-372.
64. Simondsen, R. P., Weber, P. C., Salemme, F. R., and Tollin, G. (1982) Transient kinetics of electron transfer reactions of flavodoxin: ionic strength dependence of semiquinone oxidation by cytochrome c, ferricyanide, and ferric ethylenediaminetetraacetic acid and computer modeling of reaction complexes, *Biochemistry 21*, 6366-6375.
65. Kobayashi, K., Ehrlich, S. D., Albertini, A., Amati, G., Andersen, K. K., Arnaud, M., Asai, K., Ashikaga, S., Aymerich, S., Bessieres, P., Boland, F., Brignell, S. C., Bron, S., Bunai, K., Chapuis, J., Christiansen, L. C., Danchin, A., Debarbouille, M., Dervyn, E., Deuerling, E., Devine, K., Devine, S. K., Dreesen, O., Errington, J., Fillinger, S., Foster, S. J., Fujita, Y., Galizzi, A., Gardan, R., Eschevins, C., Fukushima, T., Haga, K., Harwood, C. R., Hecker, M., Hosoya, D., Hullo, M. F., Kakeshita, H., Karamata, D., Kasahara, Y., Kawamura, F., Koga, K., Koski, P., Kuwana, R., Imamura, D., Ishimaru, M., Ishikawa, S., Ishio, I., Le Coq, D., Masson, A., Mauel, C., Meima, R., Mellado, R. P., Moir, A., Moriya, S., Nagakawa, E., Nanamiya, H., Nakai, S., Nygaard, P., Ogura, M., Ohanan, T., O'Reilly, M., O'Rourke, M., Pragai, Z., Pooley, H. M., Rapoport, G., Rawlins, J. P., Rivas, L. A., Rivolta, C., Sadaie, A., Sadaie, Y., Sarvas, M., Sato, T., Saxild, H. H., Scanlan, E., Schumann, W., Seegers, J. F., Sekiguchi, J., Sekowska, A., Seror, S. J., Simon, M., Stragier, P., Studer, R., Takamatsu, H., Tanaka, T., Takeuchi, M., Thomaides, H. B., Vagner, V., van Dijl, J. M., Watabe, K., Wipat, A., Yamamoto, H., Yamamoto, M., Yamamoto, Y., Yamane, K., Yata, K., Yoshida, K., Yoshikawa, H., Zuber, U., and Ogasawara, N. (2003) Essential Bacillus subtilis genes, *Proc. Natl. Acad. Sci. U.S.A. 100*, 4678-4683.
66. Narhi, L. O., and Fulco, A. J. (1986) Characterization of a catalytically self-sufficient 119,000-dalton cytochrome P-450 monooxygenase induced by barbiturates in Bacillus megaterium, *J. Biol. Chem. 261*, 7160-7169.
67. Sevrioukova, I., Truan, G., and Peterson, J. A. (1997) Reconstitution of the fatty acid hydroxylase activity of cytochrome P450BM-3 utilizing its functional domains, *Arch. Biochem. Biophys. 340*, 231-238.
68. Boer, R., Ulrich, W. R., Klein, T., Mirau, B., Haas, S., and Baur, I. (2000) The inhibitory potency and selectivity of arginine substrate site nitric-oxide synthase inhibitors is solely determined by their affinity toward the different isoenzymes, *Mol. Pharmacol. 58*, 1026-1034.

69. Wolff, D. J., and Gribin, B. J. (1994) The inhibition of the constitutive and inducible nitric oxide synthase isoforms by indazole agents, *Arch. Biochem. Biophys. 311*, 300-306.
70. Xue, F., Fang, J., Delker, S. L., Li, H., Martasek, P., Roman, L. J., Poulos, T. L., and Silverman, R. B. (2011) Symmetric double-headed aminopyridines, a novel strategy for potent and membrane-permeable inhibitors of neuronal nitric oxide synthase, *J. Med. Chem. 54*, 2039-2048.
71. Raman, C. S., Li, H., Martasek, P., Southan, G., Masters, B. S., and Poulos, T. L. (2001) Crystal structure of nitric oxide synthase bound to nitro indazole reveals a novel inactivation mechanism, *Biochemistry 40*, 13448-13455.
72. Cheng, Y., and Prusoff, W. H. (1973) Relationship between the inhibition constant (K1) and the concentration of inhibitor which causes 50 per cent inhibition (I50) of an enzymatic reaction, *Biochem. Pharmacol. 22*, 3099-3108.
73. Chartier, F. J., and Couture, M. (2007) Interactions between substrates and the haem-bound nitric oxide of ferric and ferrous bacterial nitric oxide synthases, *Biochem J 401*, 235-245.
74. Vallance, P., and Leiper, J. (2002) Blocking NO synthesis: How, where and why?, *Nat. Rev. Drug Discov. 1*, 939-950.
75. Bogdan, C. (2001) Nitric oxide and the immune response, *Nat. Immunol. 2*, 907-916.
76. Delker, S. L., Xue, F., Li, H., Jamal, J., Silverman, R. B., and Poulos, T. L. (2010) Role of zinc in isoform-selective inhibitor binding to neuronal nitric oxide synthase, *Biochemistry 49*, 10803-10810.
77. Huang, H., Li, H., Martasek, P., Roman, L. J., Poulos, T. L., and Silverman, R. B. (2013) Structure-guided design of selective inhibitors of neuronal nitric oxide synthase, *J. Med. Chem. 56*, 3024-3032.
78. Huang, H., Li, H., Yang, S., Chreifi, G., Martasek, P., Roman, L. J., Meyskens, F. L., Poulos, T. L., and Silverman, R. B. (2014) Potent and selective double-headed thiophene-2-carboximidamide inhibitors of neuronal nitric oxide synthase for the treatment of melanoma, *J. Med. Chem. 57*, 686-700.
79. Talbot, G. H., Bradley, J., Edwards, J. E., Gilbert, D., Scheld, M., and Bartlett, J. G. (2006) Bad bugs need drugs: An update on the development pipeline from the Antimicrobial Availability Task Force of the Infectious Diseases Society of America, *Clinical Infectious Diseases 42*, 657-668.
80. Loomba, P. S., Taneja, J., and Mishra, B. (2010) Methicillin and Vancomycin Resistant S. aureus in Hospitalized Patients, *Journal of global infectious diseases 2*, 275-283.
81. Jevons, M. P., Rolinson, G. N., and Knox, R. (1961) Celbenin-Resistant Staphylococci, *Brit Med J 1*, 124-&.
82. Diekema, D. J., Pfaller, M. A., Schmitz, F. J., Smayevsky, J., Bell, J., Jones, R. N., Beach, M., and Grp, S. P. (2001) Survey of infections due to Staphylococcus species: Frequency of occurrence and antimicrobial susceptibility of isolates collected in the United States, Canada, Latin America, Europe, and the Western Pacific region for the SENTRY Antimicrobial Surveillance Program, 1997-1999, *Clinical Infectious Diseases 32*, S114-S132.

83. Stefani, S., Chung, D. R., Lindsay, J. A., Friedrich, A. W., Kearns, A. M., Westh, H., and MacKenzie, F. M. (2012) Methicillin-resistant Staphylococcus aureus (MRSA): global epidemiology and harmonisation of typing methods, *International journal of antimicrobial agents 39*, 273-282.
84. Gardete, S., and Tomasz, A. (2014) Mechanisms of vancomycin resistance in Staphylococcus aureus, *The Journal of clinical investigation 124*, 2836-2840.
85. Yuste, J. E., Echeverry, M. B., Ros-Bernal, F., Gomez, A., Ros, C. M., Campuzano, C. M., Fernandez-Villalba, E., and Herrero, M. T. (2012) 7-Nitroindazole down-regulates dopamine/DARPP-32 signaling in neostriatal neurons in a rat model of Parkinson's disease, *Neuropharmacology 63*, 1258-1267.
86. Cinelli, M. A., Li, H., Chreifi, G., Martasek, P., Roman, L. J., Poulos, T. L., and Silverman, R. B. (2014) Simplified 2-aminoquinoline-based scaffold for potent and selective neuronal nitric oxide synthase inhibition, *J. Med. Chem. 57*, 1513-1530.
87. Whited, C. A., Warren, J. J., Lavoie, K. D., Weinert, E. E., Agapie, T., Winkler, J. R., and Gray, H. B. (2012) Gating NO Release from Nitric Oxide Synthase, *J. Am. Chem. Soc. 134*, 27-30.
88. Holden, J. K., Kang, S., Beasley, F. C., Cinelli, M. A., Li, H., Roy, S. G., Dejam, D., Edinger, A. L., Nizet, V., Silverman, R. B., and Poulos, T. L. (2015) Nitric Oxide Synthase as a Target for Methicillin-Resistant Staphylococcus aureus.
89. Forstermann, U., and Sessa, W. C. (2012) Nitric oxide synthases: regulation and function, *Eur. Heart J. 33*, 829-837, 837a-837d.
90. Notredame, C., Higgins, D. G., and Heringa, J. (2000) T-Coffee: A novel method for fast and accurate multiple sequence alignment, *Journal of molecular biology 302*, 205-217.
91. Celniker, G., Nimrod, G., Ashkenazy, H., Glaser, F., Martz, E., Mayrose, I., Pupko, T., and Ben-Tal, N. (2013) ConSurf: Using Evolutionary Data to Raise Testable Hypotheses about Protein Function, *Isr. J. Chem. 53*, 199-206.
92. Pettersen, E. F., Goddard, T. D., Huang, C. C., Couch, G. S., Greenblatt, D. M., Meng, E. C., and Ferrin, T. E. (2004) UCSF chimera - A visualization system for exploratory research and analysis, *J. Comput. Chem. 25*, 1605-1612.
93. Kang, S., Li, H., Tang, W., Martasek, P., Roman, L. J., Poulos, T. L., and Silverman, R. B. (2015) 2-Aminopyridines with a Truncated Side Chain to Improve Human Neuronal Nitric Oxide Synthase Potency and Selectivity.
94. Huang, H., Ji, H., Li, H., Jing, Q., Labby, K. J., Martasek, P., Roman, L. J., Poulos, T. L., and Silverman, R. B. (2012) Selective monocationic inhibitors of neuronal nitric oxide synthase. Binding mode insights from molecular dynamics simulations, *J. Am. Chem. Soc. 134*, 11559-11572.
95. Jing, Q., Li, H., Fang, J., Roman, L. J., Martasek, P., Poulos, T. L., and Silverman, R. B. (2013) In search of potent and selective inhibitors of neuronal nitric oxide synthase with more simple structures, *Bioorg. Med. Chem. 21*, 5323-5331.
96. Jing, Q., Li, H., Roman, L. J., Martasek, P., Poulos, T. L., and Silverman, R. B. (2014) Combination of chiral linkers with thiophenecarboximidamide heads to

improve the selectivity of inhibitors of neuronal nitric oxide synthase, *Bioorg. Med. Chem. Lett. 24*, 4504-4510.
97. Jing, Q., Li, H., Roman, L. J., Martasek, P., Poulos, T. L., and Silverman, R. B. (2014) An Accessible Chiral Linker to Enhance Potency and Selectivity of Neuronal Nitric Oxide Synthase Inhibitors, *ACS Med. Chem. Lett. 5*, 56-60.
98. Kang, S., Tang, W., Li, H., Chreifi, G., Martasek, P., Roman, L. J., Poulos, T. L., and Silverman, R. B. (2014) Nitric oxide synthase inhibitors that interact with both heme propionate and tetrahydrobiopterin show high isoform selectivity, *J. Med. Chem. 57*, 4382-4396.
99. Silverman, R. B. W., IL, US), Huang, He (Chicago, IL, US), Jing, Qing (Morton Grove, IL, US). (2014) Thiophene-2-carboximidamide Based Selective Neuronal Nitric Oxide Inhibitors, Northwestern University (Evanston, IL, US), United States.
100. Li, H., Jamal, J., Delker, S., Plaza, C., Ji, H., Jing, Q., Huang, H., Kang, S., Silverman, R. B., and Poulos, T. L. (2014) The mobility of a conserved tyrosine residue controls isoform-dependent enzyme-inhibitor interactions in nitric oxide synthases, *Biochemistry 53*, 5272-5279.
101. Huang, H., and Silverman, R. B. (2013) Recent advances toward improving the bioavailability of neuronal nitric oxide synthase inhibitors, *Curr. Top. Med. Chem. 13*, 803-812.
102. Anagnostopoulos, C., and Spizizen, J. (1961) Requirements for Transformation in Bacillus Subtilis, *J. Bacteriol. 81*, 741-746.
103. GueroutFleury, A. M., Frandsen, N., and Stragier, P. (1996) Plasmids for ectopic integration in Bacillus subtilis, *Gene 180*, 57-61.
104. Kunst, F., Ogasawara, N., Moszer, I., Albertini, A. M., Alloni, G., Azevedo, V., Bertero, M. G., Bessieres, P., Bolotin, A., Borchert, S., Borriss, R., Boursier, L., Brans, A., Braun, M., Brignell, S. C., Bron, S., Brouillet, S., Bruschi, C. V., Caldwell, B., Capuano, V., Carter, N. M., Choi, S. K., Cordani, J. J., Connerton, I. F., Cummings, N. J., Daniel, R. A., Denziot, F., Devine, K. M., Dusterhoft, A., Ehrlich, S. D., Emmerson, P. T., Entian, K. D., Errington, J., Fabret, C., Ferrari, E., Foulger, D., Fritz, C., Fujita, M., Fujita, Y., Fuma, S., Galizzi, A., Galleron, N., Ghim, S. Y., Glaser, P., Goffeau, A., Golightly, E. J., Grandi, G., Guiseppi, G., Guy, B. J., Haga, K., Haiech, J., Harwood, C. R., Henaut, A., Hilbert, H., Holsappel, S., Hosono, S., Hullo, M. F., Itaya, M., Jones, L., Joris, B., Karamata, D., Kasahara, Y., Klaerr-Blanchard, M., Klein, C., Kobayashi, Y., Koetter, P., Koningstein, G., Krogh, S., Kumano, M., Kurita, K., Lapidus, A., Lardinois, S., Lauber, J., Lazarevic, V., Lee, S. M., Levine, A., Liu, H., Masuda, S., Mauel, C., Medigue, C., Medina, N., Mellado, R. P., Mizuno, M., Moestl, D., Nakai, S., Noback, M., Noone, D., O'Reilly, M., Ogawa, K., Ogiwara, A., Oudega, B., Park, S. H., Parro, V., Pohl, T. M., Portelle, D., Porwollik, S., Prescott, A. M., Presecan, E., Pujic, P., Purnelle, B., Rapoport, G., Rey, M., Reynolds, S., Rieger, M., Rivolta, C., Rocha, E., Roche, B., Rose, M., Sadaie, Y., Sato, T., Scanlan, E., Schleich, S., Schroeter, R., Scoffone, F., Sekiguchi, J., Sekowska, A., Seror, S. J., Serror, P., Shin, B. S., Soldo, B., Sorokin, A., Tacconi, E., Takagi, T., Takahashi, H., Takemaru, K., Takeuchi, M., Tamakoshi, A., Tanaka, T., Terpstra, P., Togoni, A., Tosato, V., Uchiyama, S., Vandebol, M., Vannier, F., Vassarotti, A., Viari, A., Wambutt, R., Wedler, H., Weitzenegger, T., Winters, P., Wipat, A.,

Yamamoto, H., Yamane, K., Yasumoto, K., Yata, K., Yoshida, K., Yoshikawa, H. F., Zumstein, E., Yoshikawa, H., and Danchin, A. (1997) The complete genome sequence of the gram-positive bacterium Bacillus subtilis, *Nature 390*, 249-256.
105. Li, H., Shimizu, H., Flinspach, M., Jamal, J., Yang, W., Xian, M., Cai, T., Wen, E. Z., Jia, Q., Wang, P. G., and Poulos, T. L. (2002) The novel binding mode of N-alkyl-N'-hydroxyguanidine to neuronal nitric oxide synthase provides mechanistic insights into NO biosynthesis, *Biochemistry 41*, 13868-13875.
106. Raman, C. S., Li, H., Martasek, P., Kral, V., Masters, B. S., and Poulos, T. L. (1998) Crystal structure of constitutive endothelial nitric oxide synthase: a paradigm for pterin function involving a novel metal center, *Cell 95*, 939-950.
107. Lawson, R. J., von Wachenfeldt, C., Haq, I., Perkins, J., and Munro, A. W. (2004) Expression and characterization of the two flavodoxin proteins of Bacillus subtilis, YkuN and YkuP: biophysical properties and interactions with cytochrome P450 BioI, *Biochemistry 43*, 12390-12409.
108. Stuehr, D. J., and Ikeda-Saito, M. (1992) Spectral characterization of brain and macrophage nitric oxide synthases. Cytochrome P-450-like hemeproteins that contain a flavin semiquinone radical, *J. Biol. Chem. 267*, 20547-20550.
109. Goldschmidt, L., Cooper, D. R., Derewenda, Z. S., and Eisenberg, D. (2007) Toward rational protein crystallization: A Web server for the design of crystallizable protein variants, *Protein science : a publication of the Protein Society 16*, 1569-1576.
110. Derewenda, Z. S. (2004) Rational protein crystallization by mutational surface engineering, *Structure 12*, 529-535.
111. Otwinowski, Z., and Minor, W. (1997) Processing of X-ray diffraction data collected in oscillation mode, *Method. Enzymol. 276*, 307-326.
112. Battye, T. G., Kontogiannis, L., Johnson, O., Powell, H. R., and Leslie, A. G. (2011) iMOSFLM: a new graphical interface for diffraction-image processing with MOSFLM, *Acta. Crystallogr. D 67*, 271-281.
113. Kabsch, W. (2010) Xds, *Acta. Crystallogr. D 66*, 125-132.
114. Evans, P. (2006) Scaling and assessment of data quality, *Acta. Crystallogr. D 62*, 72-82.
115. Mccoy, A. J., Grosse-Kunstleve, R. W., Adams, P. D., Winn, M. D., Storoni, L. C., and Read, R. J. (2007) Phaser crystallographic software, *J. Appl. Crystallogr. 40*, 658-674.
116. Schuttelkopf, A. W., and van Aalten, D. M. (2004) PRODRG: a tool for high-throughput crystallography of protein-ligand complexes, *Acta. Crystallogr. D 60*, 1355-1363.
117. Emsley, P., Lohkamp, B., Scott, W. G., and Cowtan, K. (2010) Features and development of Coot, *Acta. Crystallogr. D 66*, 486-501.
118. Murshudov, G. N., Vagin, A. A., and Dodson, E. J. (1997) Refinement of macromolecular structures by the maximum-likelihood method, *Acta. Crystallogr. D 53*, 240-255.
119. Adams, P. D., Mustyakimov, M., Afonine, P. V., and Langan, P. (2009) Generalized X-ray and neutron crystallographic analysis: more accurate and complete structures for biological macromolecules, *Acta. Crystallogr. D 65*, 567-573.

120. Martasek, P., Miller, R. T., Roman, L. J., Shea, T., and Masters, B. S. (1999) Assay of isoforms of Escherichia coli-expressed nitric oxide synthase, *Methods Enzymol. 301*, 70-78.
121. Miranda, K. M., Espey, M. G., and Wink, D. A. (2001) A rapid, simple spectrophotometric method for simultaneous detection of nitrate and nitrite, *Nitric Oxide-Biol Ch 5*, 62-71.
122. Salard-Arnaud, I., Stuehr, D., Boucher, J. L., and Mansuy, D. (2012) Spectroscopic, catalytic and binding properties of Bacillus subtilis NO synthase-like protein: comparison with other bacterial and mammalian NO synthases, *Journal of inorganic biochemistry 106*, 164-171.

APPENDIX I

Bacterial Strains

B. subtilis 168 was obtained from American Type Culture Collection (23857) and made competent by the Spizizen method[(102)]. NOS deletion vector, pTPJH046, was synthesized by Genscript to contain a spectinomycin resistance gene, adapted from pDG1728[(103)], flanked by two 400 BP fragments upstream and downstream of *nos* (*yflM*). *B. subtilis Δnos* was engineered by transforming pTPJH046 and selecting for spectinomycin resistance, as previously reported[(21)]. Double recombination was checked by colony PCR. Spectinomycin was used at 100 μg/mL.

Effect of Oxidative Stress and NOS inhibitor on *B. subtilis*

B. subtilis wt and *Δnos* were grown to an OD_{600} ~ 1.0 and diluted to OD_{600} = 0.6. Cell stocks were treated with either nonselective NOS inhibitor N^{ω}-nitro-L-arginine (L-NNA), compound **1,** or compound **2** at 500 μM, 500 μM, and 250 μM, respectively, and either H_2O_2 or ACR at 2 mM and 1.25 mM, respectively, for 30 min at 30 °C. Cells were serially diluted in M9 minimal media, plated on LB agar (with 0.5% glucose) and plates were incubated overnight at 37 °C. Colony forming units (CFU) were counted the following day and % survival was calculated. For the *B. subtilis* growth assays *wt* and *Δnos* strains were grown in LB media to an OD_{600} ~ 1.0 and diluted into LB media until OD_{600} = 0.28. The OD_{600} = 0.28 cell stocks were then diluted 30 fold into a 96 well plate containing fresh LB media. Cells were pre-treated with NOS inhibitors **1** and **2** for 5 min, at 800 μM and 400 μM, respectively. ACR then was added to a final concentration of 5 μM, and growth was monitored at 600 nm for 14 h at 28 ºC using a plate reader.

Cloning and Mutagenesis

The *B. subtilis* NOS sequence was obtained from GenBank[(104)]. The DNA sequence was codon optimized for bacterial expression, synthesized, and cloned into a pET28a vector (Novagen) using the NdeI and XhoI restriction sites by GenScript. Site directed mutagenesis was carried out using the QuikChange Lightning Site-Directed Mutagenesis Kit (Stratagene) to introduce surface mutations E25A/E26A/E316A. Active site mutations H128S and I218V were introduced separately using PfuTrubo (Agilent) on bsNOS expression vector containing sERP mutations E24A/E25A/E316A.

Cloning of yumC Gene—The *yumC* gene was PCR amplified from chromosomal DNA of *B. subtilis* (ATCC 23857) using primers YumC-NdeI-F (5' – cgccatatgcgagaggatacaaaggtttatgatattacaattatag – 3') and YumC-XhoI-R (5' – cggctcgagttatttatttttcaaaaagacttgttgagtgaagagg – 3'). The PCR product was digested with restriction enzymes NdeI and XhoI, gel purified and ligated into pET28a (Novagen) using the NdeI and XhoI restriction sites to generate pJH085.

Cloning of ykuN—The *B. subitilis* YkuN protein sequence was obtained from Genbank[(104)]. The DNA sequence was then codon optimized for *E. coli* expression, synthesized, and ligated into pET21a vector (Novagen) using the NdeI and XhoI restriction sites by Genewiz to generate pJH060.

FLDR—The *E. coli* ferredoxin $NADP^+$ reductase encoded plasmid was kindly provided by Dr Michael Waterman (Univ. Southern Calif.) and subcloned into pET28a (Novagen) using the NdeI and XhoI restriction sites to generate overexpression plasmid pJH063.

Cloning of bBiDomain—*A* linker encoding the $(GGGS)^5$ sequence, synthesized by Genewiz, was ligated into the BamH1 and SalI restriction sites of pET28a (Novagen)

to generate the primary shuttle vector pJH045. DNA encoding bsNOS from [22] was PCR amplified and ligated into the shuttle vector pJH045 using NdeI and BamH1 restriction sites to generate the secondary shuttle vector pJH067. YkuN DNA was also PCR amplified and ligated into pJH067 using the SalI and XhoI restriction sites to produce pJH070.

Protein Expression and Purification

B. subtilis NOS (bsNOS) was expressed and purified as previously reported[50]. Heme domains of nNOS and eNOS were also expressed and purified as previously reported[105, 106].

YumC containing expression plasmid pJH085 was transformed into chemically competent BL21 DE3 (Invitrogen) *E. coli* and expressed as previously reported[56]. YumC containing cell pellets were re-suspended and lysed by microfluidics in buffer containing 50 mM KPi (pH 7.4), 100 mM NaCl, 5 μM FAD and 10 mM imidazole. Cell lysate was loaded onto a Ni-NTA agarose (Qiagen) column and washed with buffer containing 50 mM KPi (pH 7.4), 200 mM NaCl, 5 μM FAD and 18 mM imidazole. YumC was then eluted off the Ni-NTA column using 50 mM KPi (pH 7.4), 10 mM NaCl, 5 μM FAD and 200 mM imidazole. The eluted YumC was then diluted 10 fold into 50 mM KPi (pH 7.4) and loaded onto a Q sepharose column that was pre-equilibrated in 50 mM KPi (pH 7.4). The Q sepharose column was washed with buffer containing 50 mM KPi (pH 7.4) and 10 mM NaCl. YumC was eluted with buffer contaiing 50 mM KPi (pH 7.4) and 200 mM NaCl. Protein was concentrated and further purified over an Superdex 75 column, using an AKTA FPLC (G.E. Life Sciences), in buffer containing 50 mM KPi (pH

7.4), 5% (v/v) glycerol, and 5 μM FAD. YumC purity was checked by SDS-page gel analysis and concentration was calculated using the BCA assay kit (Pierce).

Expression of YkuN using plasmid pJH060 was followed as previously reported[107]. Cells containing YkuN were purified as described for YumC except purification buffers contained 5 μM FMN instead of FAD.

FLDR expression plasmid pJH063 was transformed into chemically competent BL21 DE3 (Invitrogen) *E. coli* and plated on kanamycin containing LB agar plates. Starter cultures from individual colonies were grown for 8 hrs and used to inoculate 1 L LB media at 37 °C and shaken overnight at 200 RPM. The following morning cultures were induced at 25 °C with 1 mM IPTG, 3 μM riboflavin and shaking was lowered to 80 RPM. Bacterial cultures were harvested 24 hrs post induction. FLDR was purified as described for YkuN.

Expression of bBiDomain also followed the previous bsNOS expression protocol [22] except 3 μM riboflavin and 1 mM 5-aminolevulinic acid (Biosynth International Inc.) were added at the time of induction to improve cofactor biosynthesis. The bBiDomain and bsNOS concentrations were determined from the 444 nm ferrous-CO complex absorption using a molar extinction coefficient of 76 $mM^{-1}cm^{-1}$[108].

Crystallization

Crystals of bsNOS belonging to space group $P2_12_12$ were grown by vapor diffusion at 22 ºC. Initial crystals were obtained by mixing an equal volume of the crystallization reservoir and bsNOS at 25 mg/mL in 25 mM Tris pH 7.6, 150 mM NaCl, 1 mM DTT. The reservoir was composed of 60 mM Bis-Tris methane/40 mM citric acid pH

7.6 and 20% (v,v) polyethylene glycol (PEG) 3350. Crystal quality was further improved by introduction of surface entropy mutants E25A/E26A/E316A identified using the sERP server[109]. Each glutamate was selected for mutation as a residue predicted to facilitate crystal packing [110] and as a residue that did not contribute a stabilizing non-covalent interaction with nearby residues. Crystals of the E25A/E26A/E316A bsNOS were then seeded into an equal volume drop of reservoir containing 60 mM Bis-Tris methane/40 mM citric acid pH 7.6, 15% (v,v) PEG 3350, 1.9% (v/v) 1-propanol and protein containing E25A/E26A/E316A bsNOS at 18 mg/mL in 25 mM Bis-Tris methane pH 7.6, 150 mM NaCl, 1% (v/v) glycerol, 1% (w/v) PEG 3350, 1 mM DTT, and 500 μM imidazole. Enzyme-inhibitor-H_4B complex crystals were prepared during the cryoprotection with 23% (v/v) glycerol by soaking at inhibitor and H_4B concentrations of 7-10 mM and 2 mM, respectively, for 3-6 h. The heme domain of eNOS and nNOS were prepared and crystallized as described[105, 106, 111].

Data Collection and Structure Determination

High-resolution data were collected at the Stanford Synchrotron Radiation Lightsource (SSRL) beamline 7-1. Data frames were indexed and integrated using either HKL2000[111], MOSFLM[112] , or XDS[113]. Data was scaled using either Aimless[114] or HKL2000[111]. Initial phases were determined by molecular replacement using Phaser[115] with the PDB entry 2FBZ as the search model for bsNOS inhibitor bound structures. Inhibitor topology files were constructed using the online program PRODRG[116], protein and inhibitor were modeled in Coot[117] and refined using

REFMAC[118] and PHENIX[119]. Water molecules were added and checked by REFMAC and COOT, respectively.

Enzyme Assays

Cytochrome C Reduction—Horse heart cytochrome c (cyt-c) reduction assays were performed at room temperature and cyt-c reduction was monitored at 550 nM using a Cary 3E UV-visible spectrophotometer. The assays were carried out in 25 mM KPi (pH 7.4), 1 μM FMN, 1 μM FAD, 40 μM horse heart cytochrome c (Affymetrix USB), 5 nM YkuN, and varying amounts of either FLDR or YumC. Individual reactions were initiated with 100 μM NADPH and the steady-state oxidation of cyt-c reduction was calculated as previously described using $\Delta\varepsilon_{550}$ = 21 $mM^{-1}cm^{-1}$[120].

NO mediated Nitrite Production by a Three-Component Reaction—Reactions were carried out at 35 °C in a buffered solution composed of 25 mM KPi (pH 7.4), 100 mM NaCl, 10 U/mL SOD, 10 U/mL catalase, 5 μM FMN, 5 μM FAD, 50 μM H_4B and 200 μM NOHA. To the buffered solution bsNOS, YkuN, and YumC were also added. Protein concentrations evaluated for NO mediated nitrite production using a three-component reaction included 0.1 μM bsNOS, 0.1 μM YkuN and 1 μM YumC. In addition, the three-component reaction was also evaluated with 1 μM bsNOS, 5 μM YkuN and 5 μM YumC. Reactions were initiated by addition of NADPH at a final concentration of 400 μM and quenched by thermal denaturation at 100 °C for 10 min. Excess NADPH was consumed by adding 10 U/mL lactate dehydrogenase and 150 mM sodium pyruvate. Reactions were aliquoted to a 96-well microplate and mixed in a 1:1 ratio with Griess reagents as previously described [121] with the exception that nitrate was not reduced to nitrite. Nitrite

concentrations were determined from a standard curve of nitrite solutions based on absorbance at 548 nm.

NO mediated Nitrite Production by bBiDomain—Reactions were carried out using the buffered solution reported for the three-component reaction. The bBiDomain reactions included 100 nM bBiDomain and either YumC or FLDR at 1 μM; except for reactions in which YumC concentrations were varied. For inhibition assays, inhibitors were added at 30 μM. Similar to the three-component reaction, bBiDomain reactions were initiated with NADPH at a final concentration of 400 μM, quenched by thermal denaturation and analyzed by Griess reaction.

IC_{50} Determination—Reactions were run analogous to bBiDomain activity assays except inhibitors were included at varying concentrations. Nitrite concentration was measured 4 min after NADPH addition by the Griess reaction. Percent activity was calculated based on the fraction of nitrite detected at a specific inhibitor concentration as compared to no inhibitor. In order to calculate the IC_{50} the data were fit to a curve using SigmaPlot version 10.0 (Systat Software, Inc., www.sigmaplot.com). IC_{50} was calculated from the line of best fit.

Ligand Binding

Isothermal Titration Calorimetry—A VP-ITC titration calorimeter instrument (GE Healthcare) was used to measure L-Arg binding to bsNOS. L-Arg was prepared in 50 mM KPi (pH 7.4) and protein samples were exchanged into 50 mM KPi (pH 7.4) using Superdex 75 (G.E. Life Sciences). All samples were degassed under vacuum at -30 mm Hg for about 20 min. The sample cell was filled with 118.14 μM bsNOS and the injection

syringe contained 3.0 mM L-Arg. All experiments were performed in triplicate at 25 °C using 30 injections at a reference power of 10 µcal/sec, stirring speed of 307 rpm and a 240 s time delay between injections. The first injection volume was set at 3 µL and the remaining 29 injections were set to 5 µL. Heat measured for each injection was integrated and the data were fit to a one-to-one binding mode using Origin 7.0 (OriginLab Corporation).

Imidazole Displacement—Coordination of imidazole to the heme iron generates a low spin spectrum with a Soret peak at 430 nm. NOS inhibitors displace the imidazole ligand and shift the heme to high-spin, resulting in a Soret maximum at 395 nm. This provides a convenient method for estimating the spectral dissociation constant, K_s[48, 122]. High spin ligands were titrated into a cuvette containing 2 µM NOS, 1 mM imidazole, 50 mM Tris pH 7.6 and 100 µM dithiothreitol. An apparent K_s ($K_{s,app}$) was calculated based on a non-linear regression analysis using Sigmaplot version 10.0 (Systat Software, Inc., San Jose California, USA, www.sigmaplot.com) using **Eq. 1**, $A_{395} - A_{430} = \frac{B_{\max} \cdot [I]}{K_{S,app} + [I]}$. Assuming K_d of imidazole for bsNOS to be 384 µM[40], for nNOS to be 160 µM[46], and for eNOS to be 150 µM[47], the K_S was calculated as previously reported[48]. In chapter 2, additional imidazole displacement assays using bsNOS and YkuN were composed of 2 µM and 20 µM protein. For trials that included H_4B, H_4B was added at 50 µM.

Appendix II

Table A.1 Data collection, processing and refinement statistics of the NOS inhibitor complexes reported in Chapter 1.

PDB Code	bsNOS-1 4LWB	bsNOS-2 4LWA
Data Collection		
Space group	$P2_12_12$	$P2_12_12$
Cell dimensions		
a, b, c (Å)	80.3, 95.1, 62.7	80.6, 95.0, 63.0
α, β, γ (°)	90, 90, 90	90, 90, 90
Resolution (Å)	50-2.15 (2.19-2.15)	50-2.06 (2.1-2.06)
R_{merge}	0.133 (0.581)	0.076 (0.259)
$I / \sigma I$	17.9 (2.3)	26.5 (3.8)
Completeness (%)	99.55 (99.02)	99.49 (95.48)
Redundancy	5.6 (3.9)	5.4 (4.5)
Refinement		
Resolution (Å)	43.90-2.15	49.71-2.06
No. reflections	25354	29114
R_{work}	0.185 (0.300)	0.165 (0.201)
R_{free}	0.233 (0.333)	0.202 (0.245)
No. of atoms	3241	3283
protein	2949	2941
ligand	105	99
water	187	243
B-factors		
protein	45.3	33.7
ligand/ion	54.9	31
water	47.2	38.7
R.m.s deviations		
Bond lengths (Å)	0.015	0.013
Bond angles (°)	2.17	2.1

*Values in parentheses are for highest-resolution shell.

Table A.1 *Continued*

PDB Code	eNOS-1 4LUW	nNOS-1 4LUX
Data Collection		
Space group	$P2_12_12_1$	$P2_12_12_1$
Cell dimensions		
a, b, c (Å)	58.1, 106.6, 156.8	51.8, 110.9, 164.7
α, β, γ (°)	90, 90, 90	90, 90, 90
Resolution (Å)	50-2.25 (2.29-2.25)	50-1.86 (1.89-1.86)
R_{merge}	0.069 (0.613)	0.066 (0.581)
$I / \sigma I$	19.4 (1.9)	24.2 (1.7)
Completeness (%)	98.92 (96.90)	99.23 (98.82)
Redundancy	3.6 (3.5)	4.0 (4.0)
Refinement		
Resolution (Å)	44.07-2.25	39.01-1.86
No. reflections	46580	80292
R_{work}	0.184 (0.295)	0.180 (0.315)
R_{free}	0.233 (0.331)	0.212 (0.362)
No. of atoms	6941	7326
protein	6438	6682
ligand	207	181
water	296	463
B-factors		
protein	44.2	40.7
ligand/ion	44.5	33.3
water	27.2	27.6
R.m.s deviations		
Bond lengths (Å)	0.016	0.015
Bond angles (°)	1.62	1.45

*Values in parentheses are for highest-resolution shell.

Table A.2 Data collection, processing and refinement statistics of the NOS inhibitor complexes reported in Chapter 2.

PDB Code	bsNOS-L-NNA 4UQR	bsNOS-7NI-Br 4UQS
Data Collection		
Wavelength (Å)	1.127092	0.91837
Space group	$P2_12_12$	$P2_12_12$
Cell dimensions		
a, b, c (Å)	80.61, 94.82, 62.89	80.42, 94.53, 63.23
α, β, γ (°)	90 90 90	90 90 90
Unique Reflections	50723	26866
Resolution (Å)	61.41 - 1.72 (1.75 - 1.72)	49.70 - 2.15 (2.21 - 2.15)
R_{merge}	0.064 (0.555)	0.196 (0.720)
R_{pim}	0.045 (.509)	.080 (.429)
$CC_{1/2}$	0.998 (0.812)	0.992 (0.827)
$I / \sigma I$	12.5 (1.9)	7.4 (1.3)
Completeness (%)	97.9 (94.2)	99.8 (99.5)
Multiplicity	4.4 (3.6)	5.7 (3.5)
Refinement		
Resolution (Å)	50.00 - 1.72	50.00 - 2.15
No. reflections	42876	24931
R_{work}	0.1681	0.2286
R_{free}	0.199	0.2831
No. of atoms	3402	3144
macromolecule	2949	2941
ligand	123	64
water	329	138
B-factors		
macromolecule	28.5	53.2
ligand/ion	30.9	44.4
solvent	34.9	50.5
R.m.s deviations		
Bond lengths (Å)	0.012	0.019
Bond angles (°)	1.77	2.05

*Values in parentheses are for highest-resolution shell.

Table A.3 Data collection, processing and refinement statistics of the NOS inhibitor complexes reported in Chapter 3.

PDB Code	bsNOS-1 4D3J	bsNOS-2 4D3I
Data Collection		
Wavelength (Å)	1.000000	1.000000
Space group	$P2_12_12$	$P2_12_12$
Cell dimensions		
a, b, c (Å)	80.62 95.01 62.77	80.52 94.94 63.49
α, β, γ (°)	90 90 90	90 90 90
Total Observations	230276 (11686)	122521 (9449)
Unique Observations	56580 (2868)	29389 (2258)
Resolution (Å)	37.11 - 1.67 (1.73 - 1.67)	44.14 - 2.09 (2.15 - 2.09)
R_{merge}	0.037 (1.118)	0.131 (0.882)
R_{PIM}	0.032 (0.951)	0.101 (0.690)
$CC_{1/2}$	0.999 (0.591)	0.991 (0.674)
$I / \sigma I$	17.74 (1.1)	5.2 (1.1)
Completeness (%)	99.79 (99.77)	99.7 (99.8)
Multiplicity	4.1 (4.1)	4.2 (4.2)
Wilson B-factor	26.54	28.44
Refinement		
Resolution (Å)	1.67	2.09
No. reflections	56494	29338
R_{work}	0.1648	0.1674
R_{free}	0.1884	0.2199
No. of atoms	3399	3280
macromolecules	2951	2949
ligands	106	85
solvent	342	246
Average B-factor	31.9	40.5
macromolecule	30.8	40.1
ligands	30.8	41.9
solvent	41.1	44.6
Ramachandran favored (%)	98	96
Ramachandran outliers (%)	0	0.28
R.m.s deviations		
Bond lengths (Å)	0.007	0.008
Bond angles (°)	1.17	1.24

*Values in parentheses are for highest-resolution shell.

Table A.3 *Continued*

PDB Code	bsNOS-3 4D3K	bsNOS-4 4D3M
Data Collection		
Wavelength (Å)	0.97684	1.000000
Space group	$P2_12_12_1$	$P2_12_12$
Cell dimensions		
a, b, c (Å)	80.97 94.55 125.12	80.38 95.70 63.07
α, β, γ (°)	90 90 90	90 90 90
Total Observations	358403 (14500)	244251 (8510)
Unique Observations	63764 (4312)	50162 (2562)
Resolution (Å)	49.51 - 2.02 (2.07 - 2.02)	52.66 - 1.74 (1.77 - 1.74)
R_{merge}	0.053 (0.108)	0.082 (0.396)
R_{PIM}	0.031 (0.094)	0.052 (0.357)
$CC_{1/2}$	0.999 (0.990)	0.997 (0.867)
$I / \sigma I$	21.6 (8.5)	10.6 (2.3)
Completeness (%)	99.7 (97.2)	99.3 (94.8)
Multiplicity	5.6 (3.4)	4.9 (3.3)
Wilson B-factor	20.36	20.89
Refinement		
Resolution (Å)	2.017	1.74
No. reflections	63603	49954
R_{work}	0.1718	0.1668
R_{free}	0.1987	0.1878
No. of atoms	6740	3318
macromolecules	5873	2949
ligands	167	87
solvent	700	282
Average B-factor	28	28.3
macromolecule	26.8	27.9
ligands	30.5	23.6
solvent	37.5	34.5
Ramachandran favored (%)	97	97
Ramachandran outliers (%)	0.14	0
R.m.s deviations		
Bond lengths (Å)	0.004	0.007
Bond angles (°)	1.03	1.218

*Values in parentheses are for highest-resolution shell.

Table A.3 *Continued*

PDB Code	bsNOS-5 4D3N	bsNOS-6 4D3O
Data Collection		
Wavelength (Å)	1.000000	1.000000
Space group	$P2_12_12$	$P2_12_12$
Cell dimensions		
a, b, c (Å)	79.70 93.54 62.30	79.85 93.45 62.48
α, β, γ (°)	90 90 90	90 90 90
Total Observations	226474 (10117)	211092 (9519)
Unique Observations	34237 (2377)	37512 (2303)
Resolution (Å)	49.09 - 1.96 (2.01 - 1.96)	49.21 - 1.90 (1.94 - 1.90)
R_{merge}	0.144 (0.347)	0.141 (0.346)
R_{PIM}	0.082 (0.289)	0.078 (0.268)
$CC_{1/2}$	0.995 (0.915)	0.991 (0.868)
$I / \sigma I$	7.4 (2.4)	8.9 (3.0)
Completeness (%)	99.9 (99.3)	99.4 (95.7)
Multiplicity	6.6 (4.3)	5.6 (4.1)
Wilson B-factor	27.21	19.22
Refinement		
Resolution (Å)	2.13	1.90
No. reflections	26698	36318
R_{work}	0.1525	0.1666
R_{free}	0.2014	0.2077
No. of atoms	3285	3357
macromolecules	2944	2946
ligands	100	89
solvent	241	322
Average B-factor	34.6	28.9
macromolecule	34.2	27.9
ligands	32.6	30.3
solvent	39.9	37.4
Ramachandran favored (%)	97	98
Ramachandran outliers (%)	0	0
R.m.s deviations		
Bond lengths (Å)	0.007	0.007
Bond angles (°)	1.27	1.27

*Values in parentheses are for highest-resolution shell.

Table A.3 *Continued*

PDB Code	bsNOS-7 4D3T	H128S bsNOS-7 4D3U
Data Collection		
Wavelength (Å)	0.97945	0.97891
Space group	$P2_12_12$	$P2_12_12$
Cell dimensions		
a, b, c (Å)	80.42 94.91 62.86	80.93 94.73 62.03
α, β, γ (°)	90 90 90	90 90 90
Total Observations	344120 (12494)	172015
Unique Observations	69173 (3171)	33624
Resolution (Å)	37.02 - 1.55 (1.58 - 1.55)	37.65 - 1.98 (2.03 - 1.98)
R_{merge}	0.039 (2.151)	0.038 (1.303)
R_{PIM}	0.029 (1.697)	0.027 (0.950)
$CC_{1/2}$	0.999 (0.601)	1.000 (0.657)
$I / \sigma I$	15.0 (0.7)	20.1 (1.0)
Completeness (%)	98.3 (92.5)	99.2 (97.1)
Multiplicity	5.0 (3.9)	5.1 (4.9)
Wilson B-factor	26.72	36.44
Refinement		
Resolution (Å)	1.55	1.98
No. reflections	68910	26173
R_{work}	0.1782	0.1662
R_{free}	0.1998	0.2083
No. of atoms	3364	3206
macromolecules	2941	2937
ligands	114	100
solvent	309	169
Average B-factor	42.9	48.4
macromolecule	42.3	48.5
ligands	40.7	46.7
solvent	49.5	47.3
Ramachandran favored (%)	97	98
Ramachandran outliers (%)	0	0
R.m.s deviations		
Bond lengths (Å)	0.006	0.008
Bond angles (°)	1.25	1.32

*Values in parentheses are for highest-resolution shell.

Table A.3 *Continued*

PDB Code	I218V bsNOS-7 4D3V
Data Collection	
Wavelength (Å)	0.999746
Space group	$P2_12_12$
Cell dimensions	
a, b, c (Å)	80.55 94.94 62.13
α, β, γ (°)	90 90 90
Total Observations	212567 (9899)
Unique Observations	39483 (2495)
Resolution (Å)	49.20 - 1.88 (1.92 - 1.88)
R_{merge}	0.073 (0.917)
R_{PIM}	0.045 (0.810)
$CC_{1/2}$	0.998 (0.515)
$I / \sigma I$	18.7 (1.5)
Completeness (%)	99.9 (99.7)
Multiplicity	5.4 (4.0)
Wilson B-factor	30.17
Refinement	
Resolution (Å)	1.88
No. reflections	39297
R_{work}	0.1724
R_{free}	0.209
No. of atoms	3318
macromolecules	2940
ligands	106
solvent	272
Average B-factor	45.1
macromolecule	44.8
ligands	44.1
solvent	48.5
Ramachandran favored (%)	98
Ramachandran outliers (%)	0
R.m.s deviations	
Bond lengths (Å)	0.007
Bond angles (°)	1.3

*Values in parentheses are for highest-resolution shell.

Table A.4 Data collection, processing and refinement statistics of the NOS inhibitor complexes reported in Chapter 4.

PDB Code	bsNOS-**19** 4D7H	bsNOS-**32** 4D7J
Data Collection		
Wavelength (Å)	0.976484	0.918370
Space group	$P2_12_12$	$P2_12_12$
No. unique reflections	32128 (2261)	70341 (3408)
Cell dimensions		
a, b, c (Å)	80.9 94.7 62.8	80.5 94.8 62.8
α, β, γ (°)	90 90 90	90 90 90
Resolution (Å)	49.62 - 2.02 (2.07 - 2.02)	37.06 - 1.55 (1.58 - 1.55)
R_{merge}	0.128 (0.570)	0.052 (2.522)
R_{PIM}	0.078 (0.530)	0.033 (1.599)
$CC_{1/2}$	0.997 (0.834)	1.000 (0.528)
$I / \sigma I$	10.1 (1.6)	18.0 (0.6)
Completeness (%)	99.5 (97.5)	99.8 (99.8)
Redundancy	5.2 (3.0)	6.5 (6.7)
Refinement		
Resolution (Å)	49.62 - 2.02 (2.092 - 2.02)	37.061 - 1.550 (1.605 - 1.55)
No. reflections used	31936	70050
Completeness (%)	98.8	99.45
R_{work}	0.1849 (0.2734)	0.173 (0.3612)
R_{free}	0.2377 (0.3350)	0.2035 (0.3715)
No. of atoms	3257	3468
macromolecules	2952	2950
ligands	101	121
solvent	204	397
Average B-factor	41.4	28.7
macromolecules	41.4	27.7
ligands	42.8	29.5
solvent	41.9	36.4
R.m.s deviations		
Bond lengths (Å)	0.007	0.007
Bond angles (°)	1.177	1.195

*Values in parentheses are for highest-resolution shell.

Table A.4 *Continued*

PDB Code	I218V bsNOS-**32** 4D7I	nNOS-**32** 4D7O
Data Collection		
Wavelength (Å)	0.999746	0.9999
Space group	$P2_12_12$	$P2_12_12_1$
No. unique reflections	48394 (2575)	90851 (3910)
Cell dimensions		
a, b, c (Å)	80.6 95.0 61.6	51.8 110.6 165.2
α, β, γ (°)	90 90 90	90 90 90
Resolution (Å)	48.94 - 1.96 (2.01 - 1.96)	1.78 (1.81 - 1.73)
R_{merge}	0.135 (1.518)	0.061 (0.662)
R_{PIM}	0.096 (1.074)	0.030 (0.385)
$CC_{1/2}$	0.992 (0.558)	0.999 (0.834)
$I / \sigma I$	7.3 (1.0)	26.4 (1.2)
Completeness (%)	99.6 (100.0)	99.0 (87.1)
Redundancy	4.3 (4.4)	4.9 (3.3)
Refinement		
Resolution (Å)	48.94 - 1.96 (2.03 - 1.96)	92.07 - 1.78 (1.826 - 1.78)
No. reflections used	34419	90785
Completeness (%)	99.23	98.86
R_{work}	0.1893 (0.3501)	0.1794 (0.289)
R_{free}	0.2352 (0.3622)	0.2092 (0.294)
No. of atoms	3253	7283
macromolecules	2940	6673
ligands	92	179
solvent	221	431
Average B-factor	41.1	38.1
macromolecules	41.2	38.5
ligands	34.5	26.1
solvent	42.9	38
R.m.s deviations		
Bond lengths (Å)	0.008	0.01
Bond angles (°)	1.19	1.311

*Values in parentheses are for highest-resolution shell.

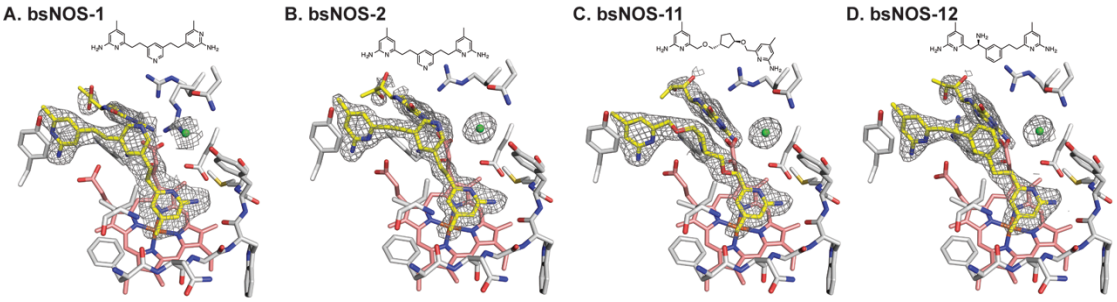

Fig. A.1 Active site view of bsNOS with inhibitors that induce an alternate conformation in Y357. Inhibitors and H4B are colored yellow and the heme is colored salmon. The 2Fo-Fc maps are shown at 1 σ for A) **1,** B) **2**, C) **11**, and D) **12**.

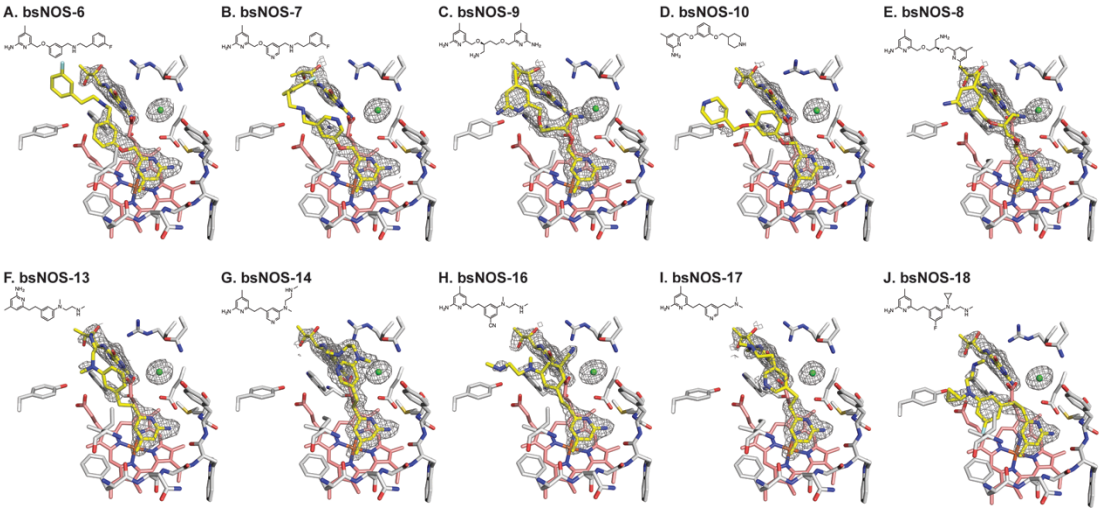

Figure A.2. Crystal structures of aminopyridine based inhibitors bound to bsNOS. The 2Fo-Fc map for inhibitor is shown at 1.0σ for inhibitors colored yellow.

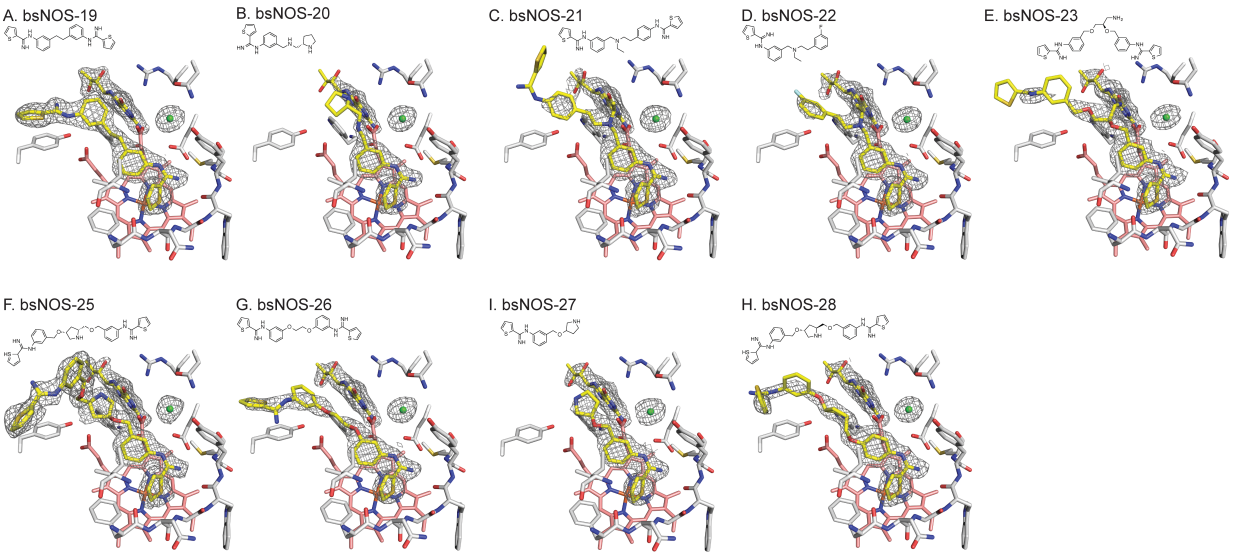

Figure A.3. Crystal structures of thiophencarboximidamide based inhibitors bound to bsNOS. The 2Fo-Fc map for inhibitor, H_4B and a chlorine ion are shown at 1σ for inhibitors colored yellow.

Table A.5 Data collection, processing and refinement statistics of the NOS inhibitor complexes reported in Chapter 5.

PDB Code	bsNOS-1 4UG5	bsNOS-2 4UG6
Data Collection		
Wavelength (Å)	1.000	1.000
Space group	$P2_12_12$	$P2_12_12$
Cell dimensions		
a, b, c (Å)	80.29 94.92 61.2	81.46 95.435 63.35
α, β, γ (°)	90 90 90	90 90 90
Total Observations	69706 (7450)	224463 (10655)
Unique Observations	20017 (2053)	45754 (2674)
Resolution (Å)	37.50 - 2.35 (2.44 - 2.35)	38.11 - 1.81 (1.85 - 1.81)
R_{merge}	0.044 (0.140)	0.264 (1.209)
R_{PIM}	0.042 (0.132)	0.166 (1.062)
$CC_{1/2}$	0.998 (0.991)	0.945 (0.602)
$I / \sigma I$	10.2 (3.0)	5.4 (1.1)
Completeness (%)	99.7 (99.8)	100.0 (99.9)
Multiplicity	3.5 (3.6)	4.9 (4.0)
Wilson B-factor	37.183	8.8
Refinement		
Resolution (Å)	36.974 - 2.352	38.115 - 1.81
No. reflections used	14223	45658
R_{work}	0.2102	0.1915
R_{free}	0.2706	0.2337
No. of atoms	3083	3345
macromolecules	2949	2941
ligands	87	107
solvent	47	297
Average B-factor	37.2	20.7
macromolecule	37.4	20
ligands	39.3	22.1
solvent	25.2	22.8
Ramachandran favored (%)	96	97
Ramachandran outliers (%)	0.28	0.28
R.m.s deviations		
Bond lengths (Å)	0.002	0.018
Bond angles (°)	0.834	1.706

*Values in parentheses are for highest-resolution shell.

Table A.5 *Continued*

PDB Code	bsNOS-3 4UG7	bsNOS-4 4UG8
Data Collection		
Wavelength (Å)	1.000	0.979
Space group	$P2_12_12$	$P2_12_12$
Cell dimensions		
a, b, c (Å)	80.444 95.046 62.947	80.55 95.19 62.77
α, β, γ (°)	90 90 90	90 90 90
Total Observations	231180 (10545)	166622 (10031)
Unique Observations	48479 (2710)	38817 (2428)
Resolution (Å)	49.57 - 1.76 (1.79 - 1.76)	37.09 - 1.88 (1.92 - 1.88)
R_{merge}	0.046 (0.110)	0.069 (2.099)
R_{PIM}	0.028 (0.087)	0.054 (1.766)
$CC_{1/2}$	0.999 (0.984)	0.998 (0.543)
$I / \sigma I$	20.0 (6.5)	9.8 (0.7)
Completeness (%)	99.8 (98.9)	97.6 (96.3)
Multiplicity	4.8 (3.9)	4.3 (4.1)
Wilson B-factor	21.1	29.198
Refinement		
Resolution (Å)	40.917 - 1.760	37.092 - 1.888
No. reflections used	48431	31894
R_{work}	0.1643	0.1869
R_{free}	0.1894	0.228
No. of atoms	3351	3279
macromolecules	2954	2941
ligands	107	95
solvent	290	243
Average B-factor	31.6	38
macromolecule	30.9	37.6
ligands	31.3	41.7
solvent	38.2	41.2
Ramachandran favored (%)	98	97
Ramachandran outliers (%)	0	0
R.m.s deviations		
Bond lengths (Å)	0.008	0.007
Bond angles (°)	1.283	1.194

*Values in parentheses are for highest-resolution shell.

Table A.5 *Continued*

PDB Code	bsNOS-5 4UG9	bsNOS-6 4UGA
Data Collection		
Wavelength (Å)	0.979	1.000
Space group	$P2_12_12$	$P2_12_12$
Cell dimensions		
a, b, c (Å)	80.38 94.98 62.78	80.54 94.44 63.05
α, β, γ (°)	90 90 90	90 90 90
Total Observations	219475 (10448)	194246 (9340)
Unique Observations	42473 (2570)	38650 (2442)
Resolution (Å)	37.87 - 1.84 (1.88 - 1.84)	37.80 - 1.90 (1.94 - 1.90)
R_{merge}	0.099 (0.960)	0.076 (0.549)
R_{PIM}	0.063 (0.835)	0.048 (0.480)
$CC_{1/2}$	0.996 (0.513)	0.998 (0.803)
$I / \sigma I$	13.1 (1.1)	12.2 (2.7)
Completeness (%)	100.0 (99.5)	100.0 (99.9)
Multiplicity	5.2 (4.1)	5.0 (3.8)
Wilson B-factor	24.231	26.669
Refinement		
Resolution (Å)	37.874 - 1.841	37.797 - 1.900
No. reflections used	33032	38463
R_{work}	0.163	0.1776
R_{free}	0.2079	0.2112
No. of atoms	3352	3311
macromolecules	2941	2941
ligands	80	88
solvent	331	282
Average B-factor	20	30.6
macromolecule	19.3	29.9
ligands	18.9	38
solvent	26.7	36.5
Ramachandran favored (%)	98	98
Ramachandran outliers (%)	0	0
R.m.s deviations		
Bond lengths (Å)	0.007	0.008
Bond angles (°)	1.242	1.205

*Values in parentheses are for highest-resolution shell.

Table A.5 *Continued*

PDB Code	bsNOS-7 4UGB	bsNOS-8 4UGC
Data Collection		
Wavelength (Å)	0.979	1.000
Space group	$P2_12_12$	$P2_12_12$
Cell dimensions		
a, b, c (Å)	80.6 95.05 63.08	80.66 94.78 62.81
α, β, γ (°)	90 90 90	90 90 90
Total Observations	191114 (12833)	227269 (9799)
Unique Observations	38015 (2495)	45231 (2620)
Resolution (Å)	37.96 - 1.91 (1.95 - 1.91)	37.83 - 1.80 (1.84 - 1.80)
R_{merge}	0.086 (2.108)	0.085 (0.490)
R_{PIM}	0.062 (1.548)	0.054 (0.428)
$CC_{1/2}$	0.999 (0.522)	0.998 (0.821)
$I / \sigma I$	9.9 (0.6)	12.0 (2.4)
Completeness (%)	99.4 (99.4)	99.9 (99.6)
Multiplicity	5.0 (5.1)	5.0 (3.7)
Wilson B-factor	34.731	18.62
Refinement		
Resolution (Å)	37.958 - 1.912	43.968 - 2.087
No. reflections used	29922	29263
R_{work}	0.1799	0.1556
R_{free}	0.2278	0.1995
No. of atoms	3320	3378
macromolecules	2941	2941
ligands	88	91
solvent	291	346
Average B-factor	36.8	23.5
macromolecule	35.9	22.4
ligands	53.1	26.7
solvent	41.7	31.5
Ramachandran favored (%)	98	97
Ramachandran outliers (%)	0	0
R.m.s deviations		
Bond lengths (Å)	1.065	0.005
Bond angles (°)	0.005	1.14

*Values in parentheses are for highest-resolution shell.

Table A.5 *Continued*

PDB Code	bsNOS-9 4UGD	bsNOS-10 4UGE
Data Collection		
Wavelength (Å)	1.127	1.000
Space group	$P2_12_12$	$P2_12_12$
Cell dimensions		
a, b, c (Å)	80.57 94.59 63.18	80.56 94.58 62.9
α, β, γ (°)	90 90 90	90 90 90
Total Observations	146671 (8316)	104832 (8496)
Unique Observations	31648 (2297)	27187 (2177)
Resolution (Å)	37.86 - 2.03 (2.08 - 2.03)	34.22 - 2.14 (2.20 - 2.14)
R_{merge}	0.097 (0.374)	0.128 (0.829)
R_{PIM}	0.060 (0.316)	0.118 (0.748)
$CC_{1/2}$	0.995 (0.815)	0.991 (0.584)
$I / \sigma I$	9.6 (3.1)	6.7 (1.4)
Completeness (%)	99.4 (99.1)	99.9 (100.0)
Multiplicity	4.6 (3.6)	3.9 (3.9)
Wilson B-factor	22.54	21.628
Refinement		
Resolution (Å)	37.862 - 2.030	34.219 - 2.140
No. reflections used	31589	23572
R_{work}	0.2134	0.1905
R_{free}	0.2433	0.2335
No. of atoms	3180	3186
macromolecules	2941	2941
ligands	92	85
solvent	150	160
Average B-factor	22	32.8
macromolecule	21.9	32.6
ligands	26.7	44.9
solvent	20	30.4
Ramachandran favored (%)	98	97
Ramachandran outliers (%)	0	0.28
R.m.s deviations		
Bond lengths (Å)	0.003	0.003
Bond angles (°)	0.968	0.932

*Values in parentheses are for highest-resolution shell.

Table A.5 *Continued*

PDB Code	bsNOS-11 4UGF	bsNOS-12 4UGG
Data Collection		
Wavelength (Å)	0.979	1.127
Space group	$P2_12_12$	$P2_12_12$
Cell dimensions		
a, b, c (Å)	80.16 96.06 63.09	80.5 94.97 62.94
α, β, γ (°)	90 90 90	90 90 90
Total Observations	231068 (10866)	106268 (6862)
Unique Observations	45204 (2665)	20270 (1828)
Resolution (Å)	49.58 - 1.81 (1.85 - 1.81)	49.58 - 2.35 (2.44 - 2.35)
R_{merge}	0.116 (1.280)	0.098 (0.351)
R_{PIM}	0.075 (1.108)	0.062 (0.294)
$CC_{1/2}$	0.994 (0.557)	0.993 (0.901)
$I / \sigma I$	9.1 (1.1)	7.7 (2.0)
Completeness (%)	100.0 (99.8)	98.3 (91.5)
Multiplicity	5.1 (4.1)	5.2 (3.8)
Wilson B-factor	20.165	28.494
Refinement		
Resolution (Å)	44.057 - 1.810	49.583 - 2.356
No. reflections used	45106	17716
R_{work}	0.1791	0.1967
R_{free}	0.2061	0.2469
No. of atoms	3366	3142
macromolecules	2941	2941
ligands	97	94
solvent	328	107
Average B-factor	30.5	29.6
macromolecule	29.9	29.5
ligands	31.9	38.1
solvent	35.8	24.1
Ramachandran favored (%)	98	97
Ramachandran outliers (%)	0	0
R.m.s deviations		
Bond lengths (Å)	0.009	0.007
Bond angles (°)	1.358	1.174

*Values in parentheses are for highest-resolution shell.

Table A.5 *Continued*

PDB Code	bsNOS-13 4UGH	bsNOS-14 4UGY
Data Collection		
Wavelength (Å)	0.979	1.000
Space group	$P2_12_12$	$P2_12_12$
Cell dimensions		
a, b, c (Å)	80.54 94.79 62.78	80.6 95.06 62.95
α, β, γ (°)	90 90 90	90 90 90
Total Observations	183432 (9558)	216160 (9248)
Unique Observations	32454 (2386)	45372 (2615)
Resolution (Å)	37.83 - 1.99 (2.05 - 1.99)	37.93 - 1.80 (1.84 - 1.80)
R_{merge}	0.088 (0.611)	0.050 (0.176)
R_{PIM}	0.050 (0.481)	0.033 (0.152)
$CC_{1/2}$	0.998 (0.761)	0.999 (0.970)
$I / \sigma I$	13.9 (2.2)	17.0 (4.9)
Completeness (%)	97.3 (98.4)	99.8 (98.5)
Multiplicity	5.7 (4.0)	4.8 (3.5)
Wilson B-factor	31.862	17.071
Refinement		
Resolution (Å)	37.826 - 1.994	37.931 - 1.801
No. reflections used	26314	45202
R_{work}	0.1623	0.155
R_{free}	0.2079	0.188
No. of atoms	3320	3404
macromolecules	2941	2941
ligands	83	89
solvent	296	374
Average B-factor	29	24
macromolecule	28.3	23.1
ligands	35.1	19
solvent	34.3	32.4
Ramachandran favored (%)	97.5	97
Ramachandran outliers (%)	0.00	0.28
R.m.s deviations		
Bond lengths (Å)	0.007	0.011
Bond angles (°)	1.202	1.55

*Values in parentheses are for highest-resolution shell.

Table A.5 *Continued*

PDB Code	bsNOS-15 4UGI	bsNOS-16 4UGJ
Data Collection		
Wavelength (Å)	1.000	0.979
Space group	$P2_12_12$	$P2_12_12$
Cell dimensions		
a, b, c (Å)	80.44 95.01 63.03	80.48 94.66 62.76
α, β, γ (°)	90 90 90	90 90 90
Total Observations	227679 (9749)	306760 (16699)
Unique Observations	45386 (2630)	46671 (2590)
Resolution (Å)	49.61 - 1.80 (1.84 - 1.80)	37.03 - 1.78 (1.82 - 1.78)
R_{merge}	0.083 (0.690)	0.069 (1.998)
R_{PIM}	0.053 (0.598)	0.043 (1.278)
$CC_{1/2}$	0.998 (0.669)	0.999 (0.554)
$I / \sigma I$	12.4 (1.4)	13.6 (0.9)
Completeness (%)	99.9 (99.3)	99.9 (99.4)
Multiplicity	5.0 (3.7)	6.6 (6.4)
Wilson B-factor	24.306	27.9
Refinement		
Resolution (Å)	40.906 - 1.801	37.032 - 1.78
No. reflections used	45330	46583
R_{work}	0.1683	0.1779
R_{free}	0.2038	0.2106
No. of atoms	3355	3258
macromolecules	2941	2941
ligands	101	85
solvent	313	232
Average B-factor	33.4	40.1
macromolecule	32.6	39.6
ligands	34.2	45.3
solvent	41	44.1
Ramachandran favored (%)	98	97
Ramachandran outliers (%)	0	0
R.m.s deviations		
Bond lengths (Å)	0.007	0.011
Bond angles (°)	1.232	1.407

*Values in parentheses are for highest-resolution shell.

Table A.5 *Continued*

PDB Code	bsNOS-17 4UGK	bsNOS-18 4UGL
Data Collection		
Wavelength (Å)	0.980	0.979
Space group	$P2_12_12$	$P2_12_12$
Cell dimensions		
a, b, c (Å)	80.77 94.76 62.09	80.74 94.78 63.06
α, β, γ (°)	90 90 90	90 90 90
Total Observations	329028 (15443)	290499 (17704)
Unique Observations	60757 (2918)	44089 (2607)
Resolution (Å)	37.67 - 1.62 (1.65 - 1.62)	37.89 -1.82 (1.86 - 1.82)
R_{merge}	0.040 (1.708)	0.071 (1.994)
R_{PIM}	0.028 (1.207)	0.045 (1.241)
$CC_{1/2}$	1.000 (0.562)	0.999 (0.575)
$I / \sigma I$	17.7 (0.8)	17.1 (1.0)
Completeness (%)	99.7 (98.2)	99.9 (100.0)
Multiplicity	5.4 (5.3)	6.6 (6.8)
Wilson B-factor	28.416	25.497
Refinement		
Resolution (Å)	33.854 - 1.623	37.886 - 1.820
No. reflections used	50949	44012
R_{work}	0.1672	0.1752
R_{free}	0.1953	0.2042
No. of atoms	3353	3329
macromolecules	2941	2941
ligands	82	92
solvent	330	296
Average B-factor	29.8	39.4
macromolecule	29.2	38.6
ligands	27.7	47
solvent	35.6	45.2
Ramachandran favored (%)	98	98
Ramachandran outliers (%)	0	0
R.m.s deviations		
Bond lengths (Å)	0.007	0.008
Bond angles (°)	1.293	1.266

*Values in parentheses are for highest-resolution shell.

Table A.5 *Continued*

PDB Code	bsNOS-19 4UGM	bsNOS-20 4UGN
Data Collection		
Wavelength (Å)	1.000	1.000
Space group	$P2_12_12$	$P2_12_12$
Cell dimensions		
a, b, c (Å)	80.53 95.05 62.89	80.65 94.94 62.92
α, β, γ (°)	90 90 90	90 90 90
Total Observations	167356 (8637)	112169 (8459)
Unique Observations	29294 (2218)	29306 (2246)
Resolution (Å)	49.57 - 2.09 (2.15 - 2.09)	49.61 - 2.09 (2.14 - 2.09)
R_{merge}	0.09 (0.428)	0.057 (0.232)
R_{PIM}	0.054 (0.374)	0.049 (0.200)
$CC_{1/2}$	0.996 (0.841)	0.998 (0.923)
$I / \sigma I$	14.6 (2.9)	13.4 (4.3)
Completeness (%)	99.9 (99.6)	99.7 (99.9)
Multiplicity	5.7 (3.9)	3.8 (3.8)
Wilson B-factor	29.821	19.589
Refinement		
Resolution (Å)	40.929 - 2.090	43.968 - 2.087
No. reflections used	29329	29263
R_{work}	0.1906	0.1556
R_{free}	0.235	0.1995
No. of atoms	3180	3320
macromolecules	2941	2941
ligands	91	95
solvent	148	284
Average B-factor	37.4	29.5
macromolecule	37.5	29
ligands	33.3	26.1
solvent	38.3	36.1
Ramachandran favored (%)	97	98
Ramachandran outliers (%)	0.28	0
R.m.s deviations		
Bond lengths (Å)	0.008	0.005
Bond angles (°)	1.307	1.14

*Values in parentheses are for highest-resolution shell.

Table A.5 *Continued*

PDB Code	bsNOS-21 4UGO	bsNOS-22 4UGX
Data Collection		
Wavelength (Å)	1.000	1.000
Space group	$P2_12_12$	$P2_12_12$
Cell dimensions		
a, b, c (Å)	80.41 94.94 62.97	80.59 94.93 62.85
α, β, γ (°)	90 90 90	90 90 90
Total Observations	73212 (7592)	216360 (9985)
Unique Observations	19831 (2057)	40955 (2460)
Resolution (Å)	49.58 - 2.38 (2.47 - 2.38)	37.88 - 1.86 (1.90-1.86)
R_{merge}	0.080 (0.294)	0.100 (1.141)
R_{PIM}	0.072 (0.258)	0.065 (0.997)
$CC_{1/2}$	0.995 (0.939)	0.997 (0.545)
$I / \sigma I$	10.9 (4.2)	11.1 (1.3)
Completeness (%)	99.4 (99.6)	99.4 (98.5)
Multiplicity	3.7 (3.7)	5.3 (4.1)
Wilson B-factor	18.585	22.909
Refinement		
Resolution (Å)	43.946 - 2.380	37.875 - 1.860
No. reflections used	19795	40897
R_{work}	0.156	0.1634
R_{free}	0.2121	0.1996
No. of atoms	3247	3315
macromolecules	2941	2952
ligands	101	100
solvent	205	263
Average B-factor	23.6	37.2
macromolecule	23.3	36.8
ligands	29.7	35.1
solvent	24.6	42.2
Ramachandran favored (%)	96	98
Ramachandran outliers (%)	0.28	0
R.m.s deviations		
Bond lengths (Å)	0.007	0.012
Bond angles (°)	1.31	1.5

*Values in parentheses are for highest-resolution shell.

Table A.5 *Continued*

PDB Code	bsNOS-23 4UGP	bsNOS-24 4UGQ
Data Collection		
Wavelength (Å)	1.000	1.000
Space group	$P2_12_12$	$P2_12_12$
Cell dimensions		
a, b, c (Å)	80.53 94.65 63.0	80.83 94.75 63.37
α, β, γ (°)	90 90 90	90 90 90
Total Observations	170731 (9522)	147095 (9150)
Unique Observations	44904 (2604)	42211 (2605)
Resolution (Å)	37.84 - 1.80 (1.84 - 1.80)	37.94 - 1.85 (1.89 - 1.85)
R_{merge}	0.122 (0.697)	0.091 (1.070)
R_{PIM}	0.105 (0.594)	0.081 (0.937)
$CC_{1/2}$	0.988 (0.771)	0.992 (0.581)
$I / \sigma I$	5.7 (1.3)	8.7 (1.9)
Completeness (%)	99.3 (99.1)	99.8 (99.9)
Multiplicity	3.8 (3.7)	3.5 (3.5)
Wilson B-factor	13.856	22.744
Refinement		
Resolution (Å)	37.838 - 1.801	37.944 - 1.850
No. reflections used	44842	42099
R_{work}	0.1834	0.1672
R_{free}	0.2199	0.2001
No. of atoms	3307	3308
macromolecules	2941	2952
ligands	103	109
solvent	263	247
Average B-factor	36.4	33.8
macromolecule	35.8	33.3
ligands	42.1	35.3
solvent	40.9	39.4
Ramachandran favored (%)	98	97
Ramachandran outliers (%)	0	0.28
R.m.s deviations		
Bond lengths (Å)	0.007	0.01
Bond angles (°)	1.265	1.424

*Values in parentheses are for highest-resolution shell.

Table A.5 *Continued*

PDB Code	bsNOS-25 4UGR	bsNOS-26 4UGS
Data Collection		
Wavelength (Å)	1.000	0.979
Space group	$P2_12_12$	$P2_12_12$
Cell dimensions		
a, b, c (Å)	80.34 95.22 63.0	80.3 94.72 62.84
α, β, γ (°)	90 90 90	90 90 90
Total Observations	111007 (8357)	176503 (9287)
Unique Observations	29082 (2192)	33357 (2402)
Resolution (Å)	37.98 - 2.09 (2.14 - 2.09)	37.82 - 1.99 (2.05 - 1.99)
R_{merge}	0.067 (0.233)	0.079 (0.408)
R_{PIM}	0.061 (0.212)	0.048 (0.333)
$CC_{1/2}$	0.996 (0.960)	0.996 (0.442)
$I / \sigma I$	9.8 (3.5)	10.2 (2.2)
Completeness (%)	99.1 (98.4)	99.8 (98.5)
Multiplicity	3.8 (3.8)	5.3 (3.9)
Wilson B-factor	14.933	29.881
Refinement		
Resolution (Å)	37.984 - 2.087	37.823 - 1.994
No. reflections used	29061	33239
R_{work}	0.1622	0.1862
R_{free}	0.2117	0.2312
No. of atoms	3424	3270
macromolecules	2949	2941
ligands	105	93
solvent	370	236
Average B-factor	16.3	30.6
macromolecule	15	30.1
ligands	13.8	35.7
solvent	27.9	34.4
Ramachandran favored (%)	98	97
Ramachandran outliers (%)	0	0.28
R.m.s deviations		
Bond lengths (Å)	0.01	0.012
Bond angles (°)	1.39	1.445

*Values in parentheses are for highest-resolution shell.

Table A.5 *Continued*

PDB Code	bsNOS-27 4UGT	bsNOS-28 4UGU
Data Collection		
Wavelength (Å)	1.127	1.000
Space group	$P2_12_12$	
Cell dimensions		
a, b, c (Å)	80.71 94.8 62.05	80.3 95.01 63.08
α, β, γ (°)	90 90 90	90 90 90
Total Observations	120949 (8803)	227635 (10033)
Unique Observations	31320 (2282)	45321 (2626)
Resolution (Å)	51.92 - 2.03 (2.08 - 2.03)	49.61 - 1.80 (1.84 - 1.80)
R_{merge}	0.057 (0.643)	0.056 (0.303)
R_{PIM}	0.050 (0.550)	0.035 (0.259)
$CC_{1/2}$	0.998 (0.648)	0.999 (0.926)
$I / \sigma I$	11.8 (1.6)	16.7 (3.5)
Completeness (%)	99.6 (99.7)	99.9 (99.1)
Multiplicity	3.9 (3.9)	5.0 (3.8)
Wilson B-factor	32.001	19.797
Refinement		
Resolution (Å)	51.918 - 2.030	40.887 - 1.801
No. reflections used	31269	45267
R_{work}	0.1979	0.156
R_{free}	0.234	0.1876
No. of atoms	3124	3124
macromolecules	2932	2932
ligands	88	88
solvent	104	104
Average B-factor	48.9	48.9
macromolecule	49.2	49.2
ligands	46.5	46.4
solvent	41.9	41.9
Ramachandran favored (%)	97	97
Ramachandran outliers (%)	0.28	0.28
R.m.s deviations		
Bond lengths (Å)	0.003	0.01
Bond angles (°)	1.004	1.487

*Values in parentheses are for highest-resolution shell.

Table A.5 *Continued*

PDB Code	bsNOS Y357F-Arginine 4UGV	bsNOS Y357F-4 4UGW
Data Collection		
Wavelength (Å)	1.12709	1
Space group	$P2_12_12$	$P2_12_12$
Cell dimensions		
a, b, c (Å)	80.65 94.42 61.92	80.52 94.77 61.59
α, β, γ (°)	90 90 90	90 90 90
Total Observations	172810 (8929)	143369 (9142)
Unique Observations	33503 (2304)	37791 (2402)
Resolution (Å)	37.54 - 1.98 (2.03 - 1.98)	37.56 - 1.90 (1.94 - 1.90)
R_{merge}	0.139 (0.704)	0.071 (0.558)
R_{PIM}	0.085 (0.626)	0.061 (0.478)
$CC_{1/2}$	0.996 (0.751)	0.996 (0.862)
$I / \sigma I$	8.3 (1.4)	8.1 (1.7)
Completeness (%)	100.0 (99.5)	99.8 (99.8)
Multiplicity	5.2 (3.9)	3.8 (3.8)
Wilson B-factor	30.982	28.674
Refinement		
Resolution (Å)	37.543 - 1.985	37.556 - 1.901
No. reflections used	24995	28157
R_{work}	0.1771	0.1548
R_{free}	0.2271	0.2009
No. of atoms	3289	3283
macromolecules	2952	2940
ligands	66	95
solvent	271	248
Average B-factor	25.7	31.2
macromolecule	25.5	30.9
ligands	18.7	31.8
solvent	29.9	35.1
Ramachandran favored (%)	97	98
Ramachandran outliers (%)	0	0
R.m.s deviations		
Bond lengths (Å)	0.005	0.012
Bond angles (°)	1.03	1.1551

*Values in parentheses are for highest-resolution shell.